Signal Processing Design and Performance Enhancement Techniques for Non-Orthogonal Multiple Access (NOMA)

By

Muhammad Waseem Akhtar

00000202566

Supervisor

Dr. Syed Ali Hassan

Department of Electrical Engineering

A thesis submitted in partial fulfillment of the requirements for the degree

of Doctor of Philosophy in Electrical Engineering (PhD EE)

In

School of Electrical Engineering and Computer Science,

National University of Sciences and Technology (NUST),

Islamabad, Pakistan.

(April, 2021)

Thesis Acceptance Certificate

Certified that final copy of PhD thesis written by **Mr. Muhammad Waseem Akhtar**, Registration No **00000202566**, of **School of Electrical Engineering and Computer Science** (SEECS) has been vetted by undersigned, found complete in all respects as per NUST Statutes/Regulations, is free of plagiarism, errors and mistakes and is accepted as partial fulfillment for award of PhD degree. It is further certified that necessary amendments as pointed out by GEC members of the scholar have also been incorporated in the said thesis.

Signature: _____

Name of Supervisor: **Dr. Syed Ali Hassan**

Date: _____

Signature (HOD): _____

Date: _____

Signature (Dean/Principal): _____

Date: _____

Approval

It is certified that the contents and form of the thesis entitled "**Signal Processing Design and Performance Enhancement Techniques for Non-Orthogonal Multiple Access (NOMA)**" submitted by **Muhammad Waseem Akhtar** have been found satisfactory for the requirement of the degree.

Advisor: **Dr. Syed Ali Hassan**

Signature: _____

Date: _____

Committee Member 1: **Dr. Hassaan Khaliq Qureshi**

Signature: _____

Date: _____

Committee Member 2: **Dr. Fahd Ahmed Khan**

Signature: _____

Date: _____

Committee Member 3 (External): **Dr. Adil Masood Siddiqui**

Signature: _____

Date: _____

Dedication

Dedicated

to

my family.

Certificate of Originality

I hereby declare that this submission is my own work and to the best of my knowledge it contains no materials previously published or written by another person, nor material which to a substantial extent has been accepted for the award of any degree or diploma at NUST SEECS or at any other educational institute, except where due acknowledgement has been made in the thesis. Any contribution made to the research by others, with whom I have worked at NUST SEECS or elsewhere, is explicitly acknowledged in the thesis.

I also declare that the intellectual content of this thesis is the product of my own work, except for the assistance from others in the project's design and conception or in style, presentation and linguistics which has been acknowledged.

Author Name: **Muhammad Waseem Akhtar**

Signature: _____

Date: _____

Acknowledgment

First and foremost I offer the gratitude to Allah Almighty who bestowed me with all the wisdom, strength and ability to carry out this work. Then I am thankful to my supervisor Dr. Syed Ali Hassan for all his cooperation, guidance, encouragement and the confidence he showed in me during the course of this research work.

I have had the good fortune of finding these great mentors: Dr. Syed Ali Hassan, Dr. Sajid Saleem, and Dr. Haejoon Jung, who gave me the useful advice at the right time. Despite their busy schedules, their ability to always remain upbeat enabled me with a balanced perspective that will always remain.

Finally, I want to thank my family, to whom I owe a lot. To my late father, Khair Ullah Khan, who has always been a source of strength and motivation for me. To my mother, who made an untold number of sacrifices for the entire family and, in particular, for me to continue my education. And lastly, the one person who made it all possible was my wife. She's been a consistent source of inspiration and care. Therefore, immense gratitude and overwhelming thanks are owed to her, for I am confident that this research would never have been done without her understanding. I'll thank all of you.

Abstract

With the tremendous increase in the number of mobile devices, and a plethora of multimedia services, there is a demand for the development of a new access schemes that can have properties of high capacity and spectral efficiency, low latency, and capabilities to accommodate a massive number of devices. Non-orthogonal multiple access (NOMA) is proposed as a promising access technology for beyond fifth generation (B5G) and sixth generation (6G) communication systems having all the desired properties. Unlike orthogonal multiple access (OMA), the same physical resource (e.g., frequency and time) but with different power is allocated to multiple users in NOMA, which greatly increases spectral efficiency. The combination of non-orthogonal multiple access (NOMA) and cooperative communications can be a suitable solution for fifth generation (5G) and beyond 5G (B5G) wireless systems with massive connectivity, because it can improved fairness compared to the non-cooperative NOMA. This thesis offers a comprehensive approach to this recently emerging technology, from the fundamental concepts of NOMA, to its combination with space-time block codes (STBC) to the cooperate with users with weak channel conditions, as well as analysis of the effect of practical impairments such as timing offsets, imperfect successive interference cancellation (SIC) and imperfect channel state information (CSI). We derive closed-form expressions of the received signals in the presence of such realistic

impairments and then use them to evaluate outage probability. Further, we provide intuitive insights into the impact of each impairment on the outage performance through asymptotic analysis at high transmit signal-to-noise ratio (SINR). We also compare the complexity of STBC-CNOMA with existing cooperative NOMA protocols for a given number of users.

In addition, to meet the highly diverse quality-of-service (QoS) requirements of Internet of Things (IoT) devices, we propose a novel Q-learning-based self-organizing and self-optimizing multiple access technique for radio resource allocation in NOMA systems. We optimize the sum-rate and spectral efficiency (SE) of the overall network by using a Q-learning algorithm that assigns optimal bandwidth and power to the users with the same range of data rate requirements. Simulation results show that the proposed algorithm can significantly enhance the overall system throughput and SE, while satisfying heterogeneous QoS requirements.

Contents

List of Figures

List of Tables

Chapter 1

Introduction

An exponential increase in the number of connecting devices is driving the researchers to design robust access schemes for future-generation wireless systems that can accommodate a massive number of devices and provide high data rates [1, 2]. Wireless data traffic is increasing sharply with the growing demand for mobile Internet. Also, a tremendous number of mobile users would result in the shrinkage of cell sizes to support the maximum number of users with existing capacity. Therefore, the new technologies such as small cells, macro-extension relays, and macro-extension radio remote heads (RRHs) are attractive solutions to enhance the system capacity because signal-to-interference-plus-noise-ratio (SINR) can be considerably enhanced by reducing the distance between the base station (BS) or access point (AP) and the mobile users [3]. Furthermore, a robust access technique is also required to cater to the demands of mobile devices and IoT networks.

1.1   Overview

Next-generation communication systems aim to achieve high spectral and energy efficiency, low latency, and massive connectivity because of extensive growth in the number of Internet-of-Things (IoT) devices. These IoT devices will realize advanced services such as smart traffic, environment monitoring, and control, virtual reality (VR)/virtual navigation, telemedicine, digital sensing, high definition (HD), and full HD video transmission in connected drones and robots. IoT devices are predicted to reach 25 billion by the year 2025 [4], and therefore, it is very challenging for the existing multiple access techniques to accommodate such a massive number of devices. Even fifth generation (5G) communication systems, which are being rolled out in the world at the moment, cannot support such a high number of IoT devices. Third generation partnership project (3GPP) is already working on the development of 5G standard and has identified massive machine type communication (mMTC), ultra-reliable and low latency communication (URLLC), and enhanced mobile broad band (eMBB) as three main use cases for 5G in its Release 13 (R13) [5].

It seems like the need for the massive transfer of wireless data is never met. Wireless communication networks have overcome 3G and are welcoming the 4G era after more than 30 years of exponential growth. A typical 5G communication system can support at most 50,000 IoTs and/or narrowband IoT (NB-IoT) devices per cell [5]. While the data transfer speed is 1000 times higher than that of the first generation wireless communication networks, there are still significant obstacles to the proliferation of data transfer and customer needs [6, 7, 8].

From 2G (circuit plus packet switching) to 4G (all IP), the cellular-based network infrastructure concept helps mobile communications to achieve

tremendous performance [9, 10, 11, 12, 13]. Today, wireless networks have developed into muti-radio access technology (RAT) and heterogeneous network connectivity infrastructure. However, this architecture is getting more and more inept to face the plethora of application in modern digital communication systems. And conventional deployment of single-RAT base stations becomes an intolerable burden on operators for the expense, service, and maintenance [9, 14, 15, 16, 17, 18]. Some state-of-the-art methods, such as cloudification and softwarization, are also increasingly being implemented into cellular networks, which draws great interest in both academia and industry.

In the industry, thousands of sensors are installed and hundreds of sensors in homes are deployed. It is very difficult to connect all these sensors through wires [19], and a huge volume of data can be produced by all these devices. These devices are both smart and intelligent, able to make smart decisions, and have less computational power [20, 21, 22, 23, 24, 25, 26]. Therefore, we need to offload the data from cloud to edge and device end. In terms of cloud/fog, we need to move the process close to end devices to reduce the processing delay. For a better QoS, we need to put the workload closer to the edge.

It is difficult to install the hardware equipment which provides all of the mentioned functionalities. By realizing the functionalities by underlying networks, softwarization and virtualization have emerged as the two most demanding paradigms for B5G/6G networks [27].

Softwarization is the term used for the set of interfaces and protocols which can allow the network to be configured in software by decoupling the control and user plane. The user plan usually consists of a set of distributed and stateless routing tables at which packet switching is performed at a very

high speed. These tables are updated by the centralized control plan which maintains the end-to-end routing information for multiple services. Data and control management operations are exchanged between the service consumer and the SDN provider [28]. SDN provider ultimately forwards the required service to the service consumer. These services are controlled by the service consumer by taking acting on these virtual resources.

In 5G wireless networking, two critical problems have arisen: spectral performance and energy efficiency [20, 29, 30, 31, 32, 33]. For 5G multi-tier networks where subscribers at various levels have different channel connectivity priorities, the current wireless networking architectures and technology will not be able to solve these two problems at the same time. Cellular broadband networks of the 5G are seen as a potential response to the high requirements for traffic volume driven by the growth and deployment of broadband services. A combination of network speeds of varying sizes, communication powers, backhaul links, and radio connectivity systems reached by unparalleled quantities of intelligent and heterogeneous wireless applications was anticipated to be 5G wireless networks. In multi-tier and heterogeneous 5G networks, how to assure infrastructure capability under varying conditions would be a primary research problem. For 5G wireless networks applications, it is easy to remember that perhaps the increase in transceiver energy will rise both bandwidth (by detecting more available channels), and SNR (by improving transmission power), resulting in increased channel performance [22, 34, 35, 36, 37, 38, 39, 40]. Recent research efforts have been dedicated to improving energy performance for a traditional wireless network, particularly energy efficiency hardware and devices, energy-efficient communication strategies, the construction of energy-aware network architectures and protocols, energy-friendly network architectures and protocols, Technology and

devices, and sources of clean energy [41, 42, 43, 44, 45, 46]. Interest in wireless networks of alternative energy sources, including thermal, vibration, solar, acoustic, wind, and even atmospheric radio power, which are used to mitigate energy costs or possibly adverse environmental impacts caused by Carbon dioxide emissions, has recently increased considerably.

Non-orthogonal multiple access (NOMA) is considered to be one of the most promising techniques for fifth-generation (5G) and beyond 5G (B5G) wireless systems to meet the heterogeneous demands on low latency, high reliability, massive connectivity, improved fairness, and high throughput [47]. The key principle behind NOMA is to exploit non-orthogonal resource allocation among multiple users at the cost of increased receiver complexity, which is required for separating the non-orthogonal signals [48]. In contrast to orthogonal multiple access (OMA), multiple users in NOMA are assigned the same physical resource (e.g., frequency and time) but with different power, which significantly enhances spectral efficiency.

Fig. 1.1 depicts a comparative analysis of the network architecture of 5G and 6G. The 6G core network is shown to have upgraded to the basic 5G core network based on intelligence, high computational power, and high capacity. By integrating BSs/APs, satellites, and UAVs, the access network is upgraded similarly. There is a vertical hand-off in 6G in addition to the horizontal as in that of 5G. Besides, fog computing and MEC are an integral component of the 6G network infrastructure, that reduces latency and bandwidth utilization for regularly needed services by a massive number of devices on the user plan.
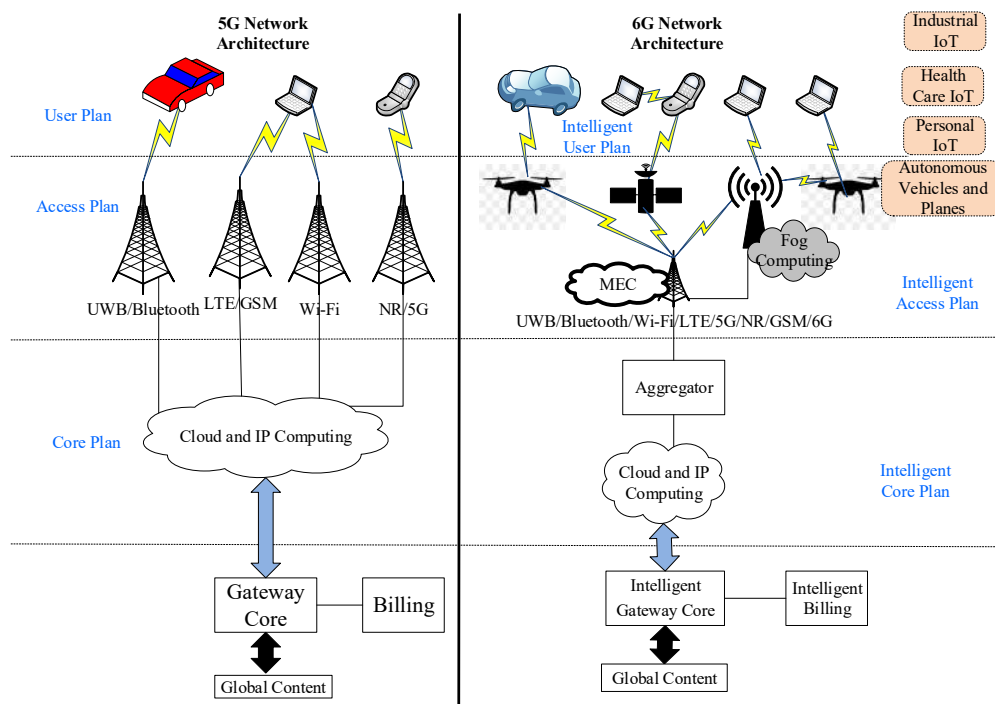
Figure 1.1: A comparative analysis between 5G and 6G network architecture.

1.2 Technical limitations in implementation of Cooperative NOMA scheme

1.2.1 Imperfect SIC

Despite their effectiveness, the aforementioned NOMA schemes combined with cooperative communications incur an excessive number of successive interference cancellations (SIC) executed at user terminals as compared to the non-cooperative NOMA [36]. When it comes to the IoT networks with limited capabilities (e.g., computational resources and power), users may suffer from prohibitively large energy consumption due to the excessive number of SIC. The average number of SIC is increased exponentially with the increase in the total number of users in the network. Also, the inter-users interfer-

ence is increased with the increase in the total number of users. Therefore, to maintain an optimum level of SINR at each user, a maximum number of users per each band has to be limited.

1.2.2 Imperfect Timing Synchronization

In STBC-aided cooperative NOMA, the users are randomly distributed in the coverage area of the base station (BS). Owing to this nature of user distribution, the received signal at the receiving user is not completely synchronized, which ultimately degrades the SINR level at each receiver.

1.2.3 Imperfect Channel State Information

Another impairment in the real-time transmission is the imperfect channel state information (ipCSI). In reality, ideal CSI is typically difficult to obtain because of channel estimation errors, limited feedback, and quantization errors. In this work, we will also study the effect of ipCSI on the STBC-aided cooperative NOMA scheme.

1.3 Motivation and Objectives

Motivated by the advantage of NOMA, various aspects of NOMA have been actively investigated, engaging industry, standardization bodies, and academia. Further, as noted in [49], NOMA can be flexibly combined with various existing and emerging wireless technologies. In particular, the combination of NOMA and cooperative communications can be a suitable solution for the Internet-of-Things (IoT) networks with massive connectivity, because it can provide higher spectral efficiency, lower energy consumption, and improved fairness compared to the non-cooperative NOMA [50]. Our main

contributions can be summarized as follows.

- Enhance the spectral efficiency in the B5G/6G networks.

- Enhance the power efficiency in the B5G/6G networks.

- Enhance the coverage probability of the network.

- Analyze the impact of timing offset in the STBC-aided cooperative NOMA network.

- Analyze the impact of imperfect SIC on the STBC-aided cooperative NOMA network.

- Analyze the impact of imperfect CSI on the STBC-aided cooperative NOMA network.

1.4   The Problem Statement

Non-orthogonal multiple access (NOMA) is known to be an effective solution to support a large number of devices. However, the performance of users/devices can be severely degraded because of strong interference from other users. A pioneer work on the cooperative NOMA system is proposed in [51] to maximize the SINR of the weak users. However, owing to the high number of successive interference cancellations performed at each user, the complexity of NOMA grows exponentially with the increase in the number of users. To overcome this issue, while enhancing the SINR of the weak user, an STBC-based cooperative NOMA scheme is proposed in [52]. Some challenges need to be addressed in the STBC-CNOMA systems in practical scenarios. For instance, distributed nature of terminals and their mobility

causes the timing offsets, which is especially severe in virtual antenna array-based approaches including distributed STBC [53, 54]. In addition, reliability performance of NOMA can be significantly degraded by imperfect SIC, and imperfect CSI [55, 56, 57], as reported in [58]. However, the existing studies on STBC-CNOMA assume the ideal case without considering such realistic impairments [36] [59]. For this reason, in this work, to better evaluate STBC-CNOMA, we investigate the impacts of the timing offsets, imperfect SIC, and imperfect CSI on its performance.

Also, communication networks beyond the fifth generation (B5G) and sixth generation (6G) are required to support a vast range of Internet-of-things (IoT) applications with highly diverse quality-of-service (QoS) requirements. Therefore, to ensure the flexible data rate of users in next-generation communication networks, a reliable scheme needs to be designed.

1.5 Thesis Outlines

The organization of this thesis is as follows

- **Chapter 2** gives a review of the literature and knowledge used in this thesis. It gives an overview of the previous technologies used in 1G through 5G. Then it describes the basic principle of NOMA followed by the different cooperative NOMA schemes introduced in the literature. An overview of machine learning techniques is given with emphasis on Q learning.

- **Chapter 3** analyzes the impact of timing offset on the performance of STBC-aided cooperative NOMA. The outage probability and the complexity analysis of STBC-aided NOMA are compared with state-of-the-art cooperative schemes in NOMA is discussed in this chapter.

- **Chapter 4** described the impact of imperfect successive interference cancellation (SIC) on the performance of STBC-aided cooperative NOMA.

- **Chapter 5** analyses the impact of imperfect channel state information in STBC-aided cooperative NOMA.

- **Chapter 6** presents the ergodic capacity analysis of STBC-aided cooperative NOMA.

- **Chapter 7** presents a Q-learning approach for the QoS-aware NOMA system in the downlink. This chapter presents a novel intelligent approach to optimize the system performance by optimizing the radio resource allocation to each user ensuring the QoS of each user.

- **Chapter 8** presents the main conclusions and future research avenues in the domain of this thesis.

Chapter 2

Literature Review

2.1 Introduction

The initial stage of the wireless communication system is the development
of the advanced mobile phone system (AMPS). Global systems for mo-
bile (GSM) and general packet radio systems (GPRS) family is developed in
2G wireless systems. Code-division multiple access (CDMA) family shifted
the wireless systems from 2G to the 3G. OFDM with the integration of
turbo codes and MIMO systems are the key technology for 4G communi-
cation systems. 5G communication systems brought some new technologies
such as cloud/fog/edge computing, massive MIMO, SDN, mmWave, and
sub mmWave (NR) along with low-density parity-check (LDPC) and polar
codes. ML, AI, blockchain, THz communication, orbital angular momentum
multiplexing (OAM Mux), spatial Modulation (SM)-MIMO and intelligent
re-configurable reflecting surfaces are the new technological domains in 6G.

Fig. 2.1 gives an overview of the evolution of the wireless generation,
with timelines, from 1G to 6G with respect to applications, KPIs, network
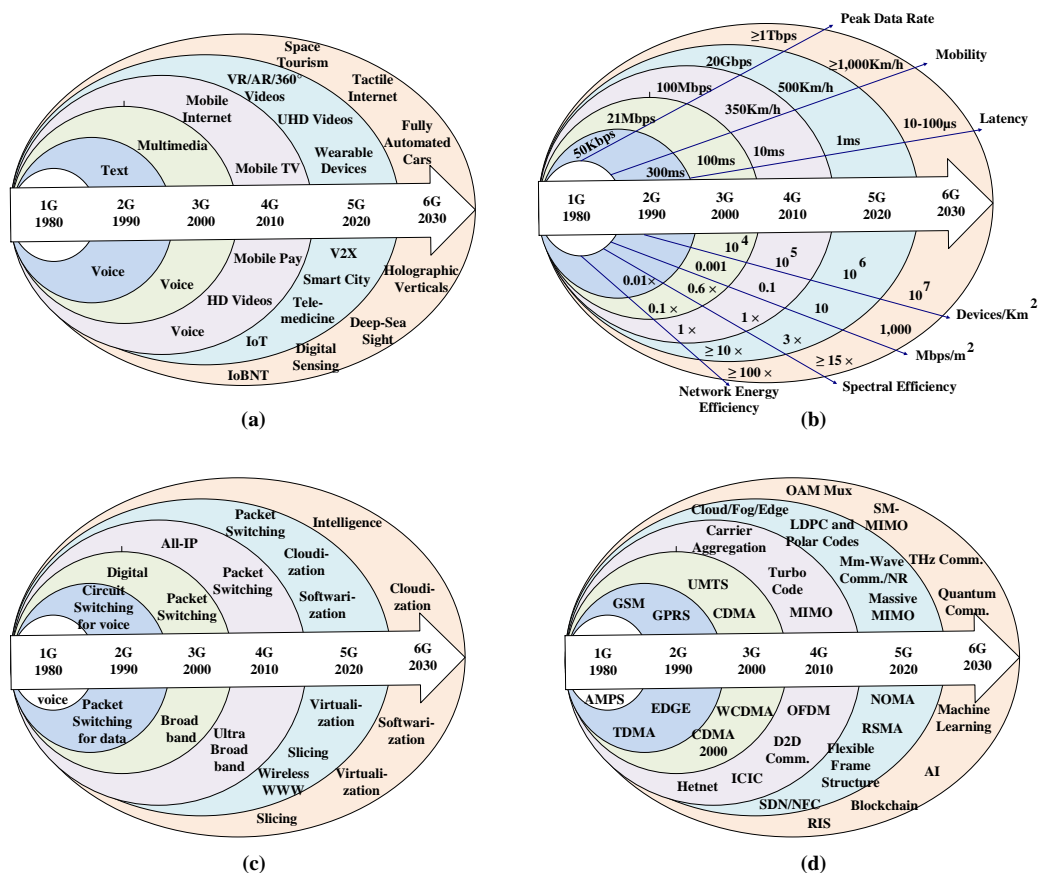
Figure 2.1: Evolution of wireless communication, with timeline, from 1G to 6G based on (a) Applications (b) KPIs (c) Network characteristics and (d) Technological development.

characteristics, and technology. Fig. 2.1(a) shows that a major leap in the application is observed with 4G. 4G introduced mobile Internet, mobile TV, and HD videos. AR/ VR, ultra-HD (UHD) videos, wearable devices, vehicle-to-infrastructure (V2X), smart city, telemedicine, and IoTs concepts are introduced in 5G. 6G is projected to have applications such as space tourism, Tactile Internet, fully automated cars, holographic verticals, deep-sea sight, digital sensing, and Internet-of-bio-Nano-things (IoBNT). Fig. 2.1(b) shows

that how KPIs are changing with the evolution of wireless generations from 1G to 6G.

Fig. 2.1(c) shows the evolution of the network characteristics with wireless generations. All Internet protocol (IP) and the ultra-broadband concept is introduced in 4G. The concepts of cloudification, softwarization, slicing, virtualization, and wireless worldwide web (WWW) are introduced in 5G. Integration of intelligence with cloudification, softwarization, slicing, and virtualization will be introduced in 6G communication systems. Fig. 2.1(d) depicts the evolution of technologies with the development of wireless communication generations. The initial stage of the wireless communication system is the development of the advanced mobile phone system (AMPS). Global systems for mobile (GSM) and general packet radio systems (GPRS) family is developed in 2G wireless systems. Code-division multiple access (CDMA) family shifted the wireless systems from 2G to the 3G. OFDM with the integration of turbo codes and MIMO systems are the key technology for 4G communication systems. 5G communication systems brought some new technologies such as cloud/fog/edge computing, massive MIMO, SDN, mmWave, and sub mmWave (NR) along with low-density parity-check (LDPC) and polar codes. ML, AI, blockchain, THz communication, orbital angular momentum multiplexing (OAM Mux), spatial Modulation (SM)-MIMO and intelligent re-configurable reflecting surfaces are the new technological domains in 6G.

2.2   Basic Principle of NOMA

Previous orthogonal multiple access (OMA) technologies, i.e., time division multiple access (TDMA), frequency division multiple access (FDMA), and code division multiple access (CDMA) were applied in 2G, 3G, and 4G wire-
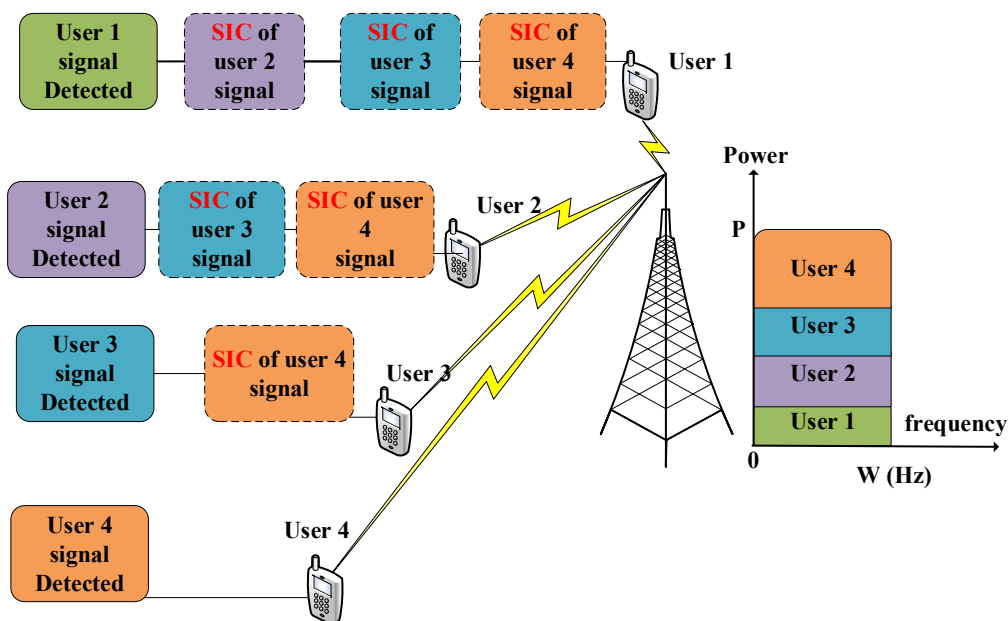
Figure 2.2: A Representation of NOMA System with 4 users.

less communication systems. NOMA, on the other hand, introduces a new dimension for multiplexing the user that is the power domain. In NOMA systems, users are distributed in the power domain as per their channel conditions. As shown in Fig. 2.2, the user with the highest channel gains is termed as the strongest user, whereas the user with the least channel gains is termed as the weakest user. The weakest user is assigned the maximum power, while the minimum power is given to the strongest user. At the receiver sides, the strong user first applies the successive interference cancellation (SIC) to detect the messages of the weak users and then subtract it from the composite NOMA signal and finally detects its own message.

2.3   Cooperative NOMA Schemes

To enhance the SINR level at the weak user, the concept of a cooperative NOMA scheme was introduced. The complete transmission in the cooperative NOMA scheme is accomplished in two steps. The first step is the direct NOMA scheme, in which a composite NOMA signal is transmitted to all users. The second step is the cooperative NOMA phase, in which the amplify-and-forward (AF) or decode-and-forward (DF) relays transmit the signal to the destination The user at the receiving end (i.e., destination) apply different signal combining schemes such as maximal ratio combining (MRC), selective combining (SC), etc., to combine the received signals. In [60], cooperative NOMA is combined with simultaneous wireless information and power transfer (SWIPT) to improve energy efficiency through energy harvesting. Further, in [61], full-duplex relaying-based NOMA schemes are introduced to reduce the number of time slots required to relay weak users' messages. Similarly, cooperation among users employing full-duplex device-to-device (D2D) communication is discussed in [62], where the outage performance of weak users is enhanced with the assistance of the full-duplex relaying by strong users. Also, the authors in [63] propose a two-stage relay selection scheme for cooperative NOMA, which also provides lower outage rates.

2.3.1   Conventional Cooperative NOMA (CCN)

In one of the pioneering studies on the NOMA schemes that incorporates the principles of cooperative communications, the authors in [51] propose *cooperative NOMA*, which is subsequently referred to as conventional cooperative NOMA (CCN). In this scheme, *strong* users with better channel conditions

support *weak* users with worse channel conditions by serving as relays, which increases the reliability of the weak users through diversity gain.

2.3.2   Decode-and-forward Relays-aided cooperative NOMA

Relay-assisted cooperative communication can significantly improve the coverage of systems due to the use of spatial diversity and the combat against channel fading. In decode-and-forward (DF) relaying, the relays firstly encode the incoming message to extract their own messages and then re-encode the message and re-send it to the destination. NOMA techniques adopting cooperative relaying systems are also extensively studied. For example, in [64], the authors propose an algorithm called a cooperative relaying system using NOMA (CRS-NOMA), in which a decode-and-forward (DF) relay is adopted. Also, assuming a single DF relay and two far users, the outage performances of different relaying schemes are investigated in [65].

2.3.3   Amplify-and-forward Relays-aided cooperative NOMA

Apart from the DF technique, amplify-and-forward (AF) relays amplify the received signal linearly and forward that to the destination without decoding. AF relaying is also advantageous on DF relaying in terms of complexity and power consumption. NOMA using an amplify-and-forward (AF) protocol is investigated in [66].

2.4   Machine Learning

Integrating artificial intelligence with wireless communication is a hot research topic nowadays. Because of the exponential increase in the number of
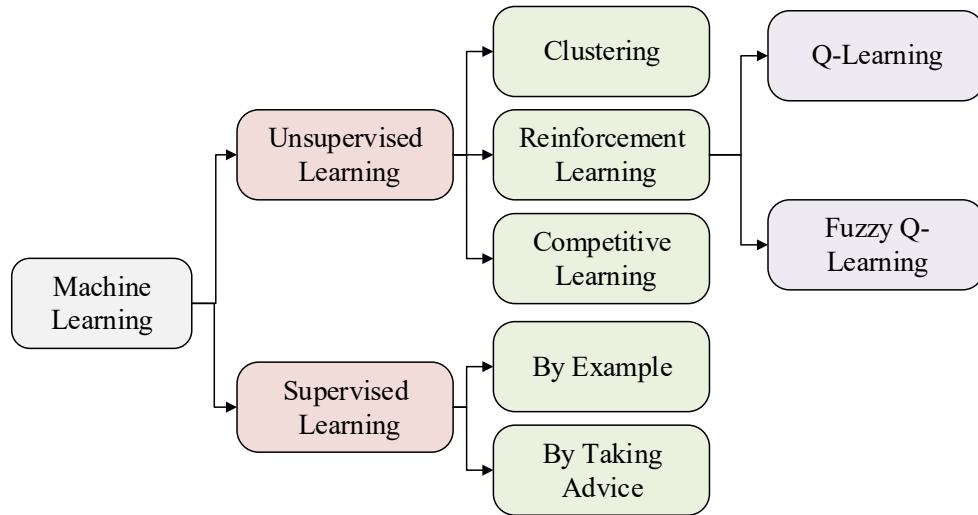
Figure 2.3: A tree diagram of machine learning algorithms.

wireless devices, and a plethora of applications, the resource allocation problem is getting more challenging than ever before. Therefore, using machine learning for resource allocation in future wireless communication networks is an attractive choice. In this section, we study the application of reinforcement learning especially Q-learning for resource allocation in future wireless communication networks.

2.4.1   Q Learning

Q-learning is a sub-class of reinforcement learning in which the agent learns to improve with experience. The agent takes the action in the environment initially on a random basis, and learns to act optimally with time. The process through which the agent learns from the environment is called exploration, while the process through which it implies the intelligent actions learned in the exploration phase is called exploitation. The elements of a

Q-learning algorithm are

- State A state is a representation of current situation. For a wireless communication system, a state may be the key performance indicator (KPI) of the network. It can be the SINR, sumrate, or spectral efficiency of the network.

- Action The agent takes some actions to achieve the goal. In a wireless communication system, action can be the assignment of power, bandwidth, or both. The Q-value represents that how an action is good in a certain state.

- Policy A policy is the way the agent behaves in an environment. A policy is built on the Q-values for all state-action pairs during the exploration phase.

The procedure of the Q-learning algorithm is described as follows

- Observes the state $s \in \mathbb{S}$ of the network.

- Based on the current state observed, take an action $a \in \mathbb{A}$.

- As a result of action a, the system generates a new transition and moves to state $s' \in \mathbb{S}$.

- Observe the new state $s' \in \mathbb{S}$ due to assignment of an action a.

- Take the immediate reward as in (7.11), which is fed to the agent.

- Change the action, $a \in \mathbb{A}$, according to the new state s'.

- Transition from state $s \rightarrow s'$ leads the change in the Q-value which is required to be updated as in the Q-table.

- Repeat the process until optimization is achieved.

2.5 Chapter Summary

In this chapter, we discussed the evolution of mobile communication systems from 1G-to-5G, and the requirements of B5G/6G communication systems. Further, we studied the NOMA and cooperative NOMA schemes followed by perspective machine learning algorithms especially the Q-learning algorithm and its potential applications in NOMA.

Chapter 3

STBC-Aided Cooperative NOMA with Timing Offsets

3.1 Introduction

We discuss the problem of timing offset in space-time block code (STBC)-assisted cooperative NOMA protocols in this chapter, which benefit from diversity advantage with a reduced SIC number. A lot of research is carried out on the STBC-based cooperation process in the literature. For instance, the conventional Alamouti (i.e., 2×1) STBC-based NOMA system is investigated in [67], which uses two antennas at the BS and a single antenna at each user. This scheme doubles the diversity order as compared to that of conventional NOMA. Furthermore, in [68], the authors propose an Alamouti STBC-based CRS-NOMA protocol for a network with source, relay, and destination, which are equipped with two transmit antennas, two transmit and one receive antennas, and one receive antenna, respectively. It shows higher sum capacity and lower outage probability compared to the conventional

CRS-NOMA in [64]. Instead of using the co-located (or real) antenna array, the authors in [36, 59] propose a new cooperative NOMA with a *distributed* STBC (i.e., STBC-CNOMA) for the virtual antenna array created by a group of single-antenna users, which can be readily applied to the IoT networks. In their proposed scheme, STBC-CNOMA, they employ 2×2 distributed STBC on the NOMA system, in which two strong users act as DF relays and transmit the messages of the weak users through a 2×2 STBC. They show that STBC-CNOMA can achieve higher throughput with a smaller number of SIC compared to the CCN in [51].

Notation: $\mathbb{E}[\cdot]$ and $\mathbb{V}\text{ar}[\cdot]$ denote the statistical expectation and variance, respectively. Also, $|\cdot|$ denotes the absolute value of a scalar quantity. Also, the definitions of the variables used in our analysis are provided in Table 3.1.

3.2   System Model

We consider an STBC-based downlink NOMA system as shown in Fig. 3.1. Base station (BS) transmits the superimposed signal to all users in its coverage area. We assume the channel between the BS and the users and that between any two users to be a flat fading Rayleigh channel, as in [51] and [64]. In general, the users near the BS experience a strong channel to the BS, henceforth referred to as the *strong users*. Similarly, the users lying at the cell edge have weak channel conditions, and they are considered as *weak users*. The user with the weakest channel conditions is assigned the maximum power, whereas the user with the strongest channel conditions is assigned the lowest power. Without loss of generality, it is assumed that the users are aligned as per descending order of their channel condition, i.e., $|h_1| \geq |h_2| \geq \cdots \geq |h_k| \geq \cdots \geq |h_K|$, where $|h_k|$ is the channel coefficient

Table 3.1: Table of Notations

Symbol	Definition
h_k	Channel gain from BS to the kth user
$g_{k,j}$	Channel gain between the kth and the jth user
$\gamma_{k,noma}$	SINR at the kth user to detect its own signal in direct NOMA phase
$\gamma_{k,ccn}$	SINR at the kth user for conventional cooperative NOMA case [51]
γ_k	SINR at the kth user with perfect timing synchronization, perfect SIC (pSIC), and perfect CSI (pCSI)
γ_k^{η}	SINR at the kth user with perfect timing synchronization, imperfect SIC (ipSIC), and perfect CSI (pCSI)
γ_k^{ε}	SINR at the kth user with imperfect timing synchronization, perfect SIC (pSIC), and perfect CSI (pCSI)
$\gamma_k^{\varepsilon,\eta}$	SINR at the kth user with imperfect timing synchronization, imperfect SIC (ipSIC), and perfect CSI (pCSI)
γ_k^{χ}	SINR at the kth user with perfect timing synchronization, perfect SIC (pSIC), and imperfect CSI (ipCSI)
γ_{th}	SINR threshold
Υ	Rate threshold
p_k	Power received at the kth user from BS
p_s	Mean power received by the user during STBC cooperation phase
$\xi_{k,t}$	Noise received at the kth user during time slot t of the STBC cooperation phase
$r_{k,t}$	Received signal at the kth user during time slot t of the STBC cooperation phase
λ_h	Fading parameter for exponentially distributed variable A
λ_i	Fading parameter for hypo-exponentially distributed variable B
λ_η	Fading parameter for exponentially distributed variable F
λ_g	Fading parameter for Gamma distributed variable Z
$\mathrm{erf}(.)$	Error function
$\mathbf{Ei}(x)$	Exponential integral of x and $\mathbf{Ei}(x) = \int_{-\infty}^{x} \frac{e^t}{t} dt$

from BS to the kth user and K is the total number of users. We consider User 1, U_1, as the strongest user and User K, U_K, as the weakest user, where $\{U_1, U_2, \ldots, U_k, \ldots, U_K\}$ is the set of all users.
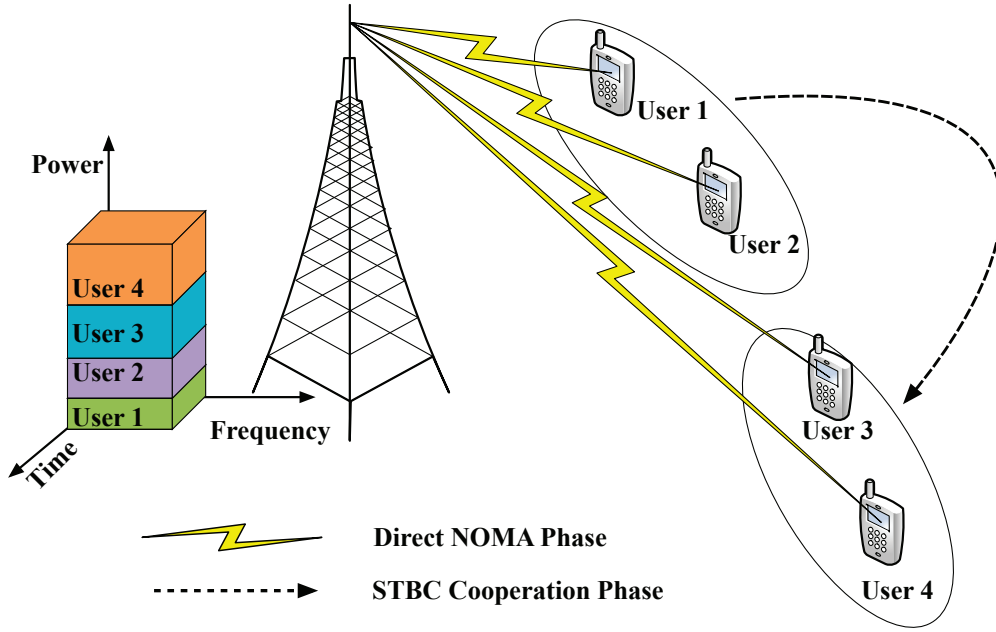
Figure 3.1: An example illustration of downlink STBC-CNOMA with four users.

Transmission from BS to the users takes place in two phases. In the first phase, called the *direct NOMA phase*, BS sends the superimposed signal to all users. The weakest user extracts its own signal by considering the signals for all the other users as noise. Other users employ SIC to cancel the interference from the weak users and treat the signals for other strong users as noise. In the second phase, referred to as *cooperative NOMA phase*, the first two strongest users, U_1 and U_2, make an STBC pair and transmit the messages of the next two users, U_3 and U_4, by a distributed 2×2 STBC transmission. This process of 2×2 STBC continues until the weakest user U_K is reached.
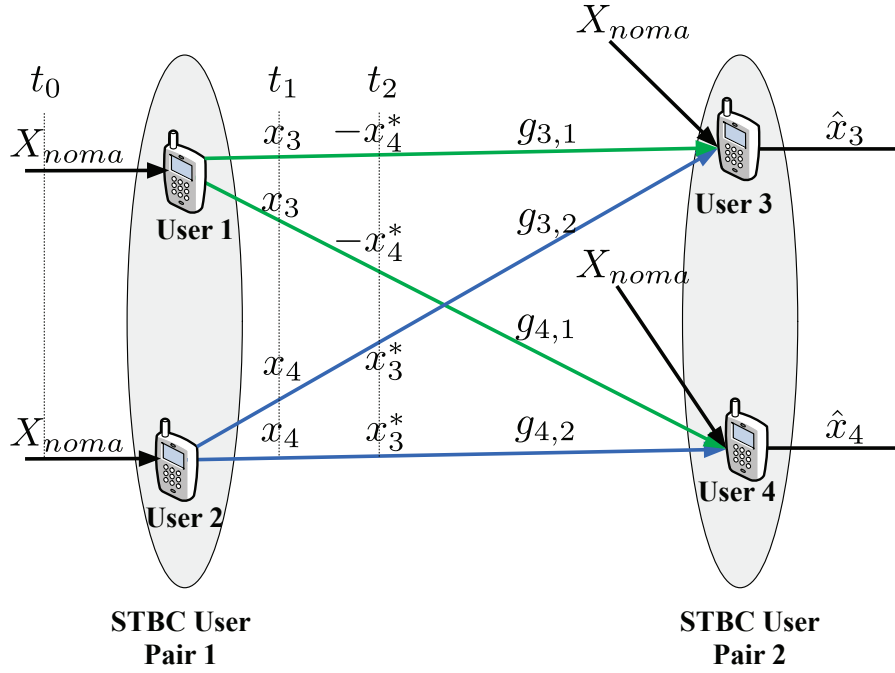
Figure 3.2: Cooperation mechanism in the STBC-CNOMA network with two STBC user pairs.

3.2.1 Direct NOMA Phase

As shown in Fig. 3.2, the direct NOMA phase is accomplished in the first time slot, when the BS transmits the superimposed signal to all of the K users. The kth user, such that $1 \leq k < K$, detects the message of the ith user, where $i > k$, then applies SIC to subtract it from the superimposed signal and finally detects its own message.

3.2.2 STBC-based Cooperative Transmission Phase

The second phase of the proposed transmission is the STBC-based cooperative transmission phase. Users are paired as per their channel conditions, i.e., the first two strongest users make the first user pair followed by U_3 and U_4 making the second user pair until U_{K-1} and U_K making the Mth user

pair, where $M = K/2$ and K is even. For the case K is odd, U_{K-2} and U_{K-1} construct the Mth user pair, where $M = \frac{K-1}{2}$. In this phase, all of the users cooperate with each other by employing a distributed 2×2 STBC transmission. However, at the receiving STBC users' pair, we use 2×1 STBC reception for the detection of the symbols [69]. Each receiving STBC user receives two symbols, one for itself and the other for its neighbor. Thus, an STBC user keeps the decoded symbol for itself, while the other symbol for its neighbor is discarded. In the first time slot, t_0, BS transmits the composite NOMA signal to all users in its coverage area. Since the first two strongest users have decoded the messages for all the other users, therefore, they can contribute to the STBC cooperation by transmitting the information for the next two users in the next two time slots. Therefore, during the second and third time slots, t_1 and t_2, U_1 and U_2 transmit to the users U_3 and U_4 using Alamouti code. Similarly, in the two following time slots, U_3 and U_4 transmit the STBC signal to U_5 and U_6 and this process continues till U_K receives its message. Assuming The SINR at each user of the receiving STBC pair, with perfect timing synchronization and perfect SIC, is given by

$$\gamma_k = \frac{|h_k|^2 p_k}{\sum\limits_{i=1}^{k-1} |h_k|^2 p_i + \sigma^2} + \frac{(|g_{k,k-\iota-1}|^2 + |g_{k,k-\iota-2}|^2)p_s}{\sigma^2}, \qquad (3.1)$$

where $2 < k \leq K$, $p_k = \Phi_k P_{NOMA}$ is the power assigned to the kth user, Φ_k is the power coefficient for the kth user, P_{NOMA} is the power assigned to the composite NOMA signal and p_s is the fraction of power transmitted from the transmitting users' pair in STBC cooperation. Also, $\iota \in \{0, 1\}$ denotes the first and the second user of the 2×2 STBC receiving pair, respectively. In case of conventional cooperative NOMA [51], each strong user, U_i, for any $i < k$ will cooperate with the weak user, U_k, by means of decode and forward

relay. Assuming maximum-ratio combining (MRC), as in [51], the SINR at each user in this case is given by

$$\gamma_{k_{ccn}} = \frac{|h_k|^2 p_k}{\sum\limits_{i=1}^{k-1} |h_k|^2 p_i + \sigma^2} + \sum_{j=1}^{k-1} \frac{|g_{k,k-j}|^2 q_{k,k-j}}{\sum\limits_{i=1}^{k-1} |g_{k,k-j}|^2 q_{k,k-i} + \sigma^2}, \tag{3.2}$$

where $\gamma_{k_{ccn}}$ is the SINR at the kth user for conventional cooperative NOMA and $q_{k,k-j}$ is the power transmitted from the $(k-j)^{th}$ user to the kth user in the cooperation phase.

3.3   Synchronization Error

Fig. 3.2 shows an STBC-based downlink NOMA network for two user pairs. During the first time slot t_o, each user receives the composite NOMA signal X_{noma} from the base station. Since U_1 and U_2 are located in close vicinity of the BS, they decode their own messages in addition to the messages of U_3 and U_4 and send these to U_3 and U_4 through STBC transmission. In other words, U_1 and U_2 send x_3 and x_4 to U_3 and U_4 during time slot t_1. During next time slot t_2, U_1 and U_2 send $-x_4^*$ and x_3^*, respectively, to U_3 and U_4. Thus, the STBC receiving user pair U_3 and U_4 can detect their respective messages.

Fig. 3.3 illustrates the timing diagram with different synchronization conditions. Fig. 3.3(a) depicts the STBC mechanism at the receiver with perfect timing synchronization. The symbols from both users U_1 and U_2 of STBC pair arrive at the receiver at the same time instant, where T is the symbol duration.

On the other hand, Fig. 3.3(b) shows the STBC transmission with timing offset of $\tau = \varepsilon_2 T$. For the perfect timing synchronization, $\varepsilon_2 = 0$, and $\varepsilon_2 =$
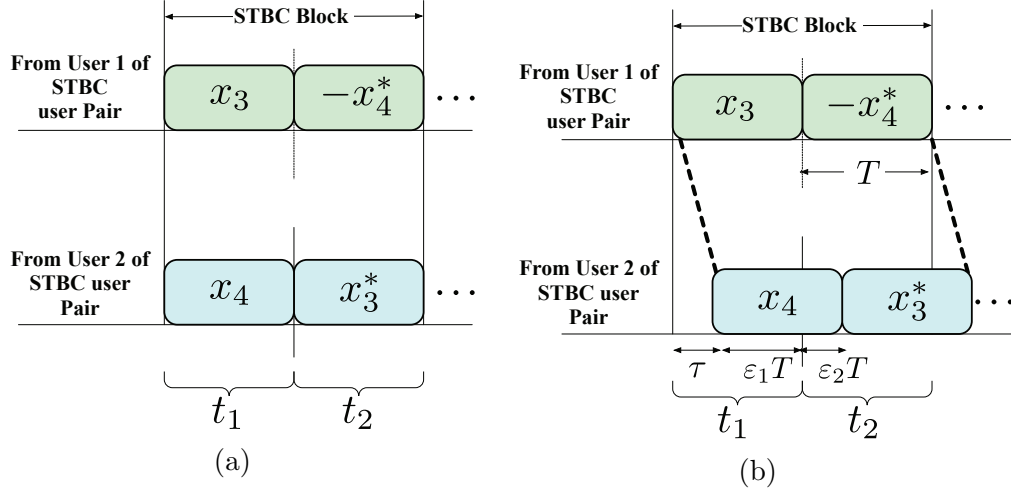
Figure 3.3: Timing diagram of the received signals. (a) Perfect timing synchronization, (b) Imperfect timing synchronization with $\tau = \varepsilon_2 T$.

1 indicates the timing offset of one symbol time. In this case, the symbols from U_1 and U_2 does not arrive simultaneously and there is a substantial inter-symbol-interference (ISI) experienced by the STBC receiving user pair, which causes the decrease in the SINR. The STBC block used by U_1 and U_2 is given by

$$S = \begin{bmatrix} x_3 & -x_4^* \\ x_4 & x_3^* \end{bmatrix}. \tag{3.3}$$

Thus, if U_4 is not perfectly synchronized, as shown in Fig. 3.3(b), the receiver equations for U_3 or U_4 of STBC receiving pair at time slots t_1 and t_2 are given as

$$r_{3,1} = g_{3,1}x_3 + g_{3,2}\varepsilon_1 x_4 + \xi_{3,1}, \tag{3.4}$$

$$r_{3,2} = -g_{3,1}x_4^* + g_{3,2}\varepsilon_1 x_3^* + g_{3,2}\varepsilon_2 x_4 + \xi_{3,2}, \tag{3.5}$$

$$r_{4,1} = g_{4,1}x_3 + g_{4,2}\varepsilon_1 x_4 + \xi_{4,1}, \tag{3.6}$$

$$r_{4,2} = -g_{4,1}x_4^* + g_{4,2}\varepsilon_1 x_3^* + g_{4,2}\varepsilon_2 x_4 + \xi_{4,2}, \tag{3.7}$$

where $r_{k,t}$ and $\xi_{k,t}$ are the received signal and the additive noise observed at the kth user during time slot t, respectively. The received signals after combiner at User 3 and User 4 are given by

$$\tilde{v}_3 = g_{3,1}^* r_{3,1} + g_{3,2} r_{3,2}^*, \qquad (3.8)$$

$$\tilde{v}_4 = g_{4,2}^* r_{4,1} - g_{4,1} r_{4,2}^*, \qquad (3.9)$$

which can be expanded as

$$\tilde{v}_3 = (|g_{3,1}|^2 + \varepsilon_1 |g_{3,2}|^2)x_3 + (\varepsilon_1 - 1)g_{3,1}^* g_{3,2} x_4 + \varepsilon_2 |g_{3,2}|^2 x_4^* + g_{3,1}^* \xi_{3,1} + g_{3,2} \xi_{3,2}^*, \qquad (3.10)$$

$$\tilde{v}_4 = (|g_{4,1}|^2 + \varepsilon_1 |g_{4,2}|^2)x_4 + (1 - \varepsilon_1)g_{4,1} g_{4,2}^* x_3 - \varepsilon_2 g_{4,1} g_{4,2}^* x_4^* + g_{4,2}^* \xi_{4,1} - g_{4,1} \xi_{4,2}^*. \qquad (3.11)$$

As a result, assuming MRC of the received signals in both direct NOMA and STBC phases, the SINRs of U_3 and U_4 can be obtained as (3.12) and (3.13), respectively. We note that if timing synchronization is perfect (i.e., $\varepsilon_1 = 1$ and $\varepsilon_2 = 0$), the corresponding SINRs in (3.12) and (3.13) are reduced into (3.1). Furthermore, generalizing this four-user example to a larger number of users (e.g., $K = 6, 8, ...$), in the presence of the synchronization error, the mathematical expressions of the SINR of the mth and the nth users can be derived as (3.14) and (3.15), respectively, for any $m \in \{3, 5, 7, \ldots, K-1\}$ and $n \in \{4, 6, 8, \ldots, K\}$.

3.4 Outage Probability Analysis

In this section, we analyze the outage performance under the three practical impairments: timing error, imperfect SIC, and channel estimation error. Be-

cause the last user (i.e., User K) has the weakest channel gain and also suffers from the impairments, it has the worst outage probability compared to the other users, as shown in [36, 59]. For this reason, we focus on the outage performance of User K (e.g., User 4 in the four-user example in the previous section), which will set a benchmark for the other users with stronger channel gains.

An outage event occurs when a user cannot achieve the reliable SINR to detect the signal. Following [36] and [59], the outage probability of any user

$$
\gamma_3^\varepsilon = \frac{|h_3|^2 p_3}{\sum\limits_{i=1}^{2} |h_3|^2 p_i + \sigma^2} + \frac{(|g_{3,1}|^2 + \varepsilon_1 |g_{3,2}|^2)^2 p_s}{|(\varepsilon_1 - 1)g_{3,1}^* g_{3,2} + \varepsilon_2 g_{3,2} g_{3,2}^*|^2 p_s + (|g_{3,1}|^2 + |g_{3,2}|^2)\sigma^2}.
$$
(3.12)

$$
\gamma_4^\varepsilon = \frac{|h_4|^2 p_4}{\sum\limits_{i=1}^{3} |h_4|^2 p_i + \sigma^2} + \frac{(|g_{4,1}|^2 + \varepsilon_1 |g_{4,2}|^2)^2 p_s}{|(1 - \varepsilon_1)g_{4,1} g_{4,2}^* - \varepsilon_2 g_{4,1} g_{4,2}^*|^2 p_s + (|g_{4,1}|^2 + |g_{4,2}|^2)\sigma^2}.
$$
(3.13)

$$
\gamma_m^\varepsilon = \frac{|h_m|^2 p_m}{\sum\limits_{i=1}^{m-1} |h_m|^2 p_i + \sigma^2} +
$$
$$
\frac{(|g_{m,m-2}|^2 + \varepsilon_1 |g_{m,m-1}|^2)^2 p_s}{|(\varepsilon_1 - 1)g_{m,m-2}^* g_{m,m-1} + \varepsilon_2 g_{m,m-2} g_{m,m-2}^*|^2 p_s + (|g_{m,m-2}|^2 + |g_{m,m-1}|^2)\sigma^2}.
$$
(3.14)

$$
\gamma_n^\varepsilon = \frac{|h_n|^2 p_n}{\sum\limits_{i=1}^{n-1} |h_n|^2 p_i + \sigma^2} +
$$
$$
\frac{(|g_{n,n-3}|^2 + \varepsilon_1 |g_{n,n-2}|^2)^2 p_s}{|(1 - \varepsilon_1)g_{n,n-3} g_{n,n-2}^* - \varepsilon_2 g_{n,n-3} g_{n,n-2}^*|^2 p_s + (|g_{n,n-3}|^2 + |g_{n,n-2}|^2)\sigma^2}.
$$
(3.15)

k (for $k \leq K$) is defined as

$$P_{out} = \mathbb{P}(\gamma_k < \gamma_{th}) = \int_0^{\gamma_{th}} f_\Gamma(\gamma_k)d\gamma_k, \qquad (3.16)$$

where γ_{th} is the SINR threshold and $f_\Gamma(\gamma_k)$ is the probability density function (PDF) of SINR received at the kth user with perfect SIC, perfect timing synchronization, and perfect CSI, which is derived in (3.1). We can also use the SINR derived in the previous section as in (3.14)-(5.9) for different cases in order to find their respective outage probabilities. Similarly, the rate outage (i.e., capacity outage) probability is defined as

$$\tilde{P}_{out} = \mathbb{P}[\gamma_k < 2^\Upsilon - 1], \qquad (3.17)$$

where $\Upsilon = \log_2(1 + \gamma_{th})$ is the rate threshold.

In order to find the outage probability using (3.16), we need the PDF of SINR for different cases. Therefore, as the SINR expressions in (3.14)-(5.9) contain random variables, we consider the following mathematical manipulation and define some composite random variables for finding the PDF of SINRs for different cases.

We redefine the variables used in (3.14)-(5.9) as $A = |h_k|^2 p_k$, $B = \sum_{i=1}^{I} |h_k|^2 p_i$, $C = |g_{k,k-2}|^2 p_s$, $D = |g_{k,k-3}|^2 p_s$, $F = |g_\eta|^2 p_\eta$, $C_\chi = |A_\chi|^2 p_s$ and $D_\chi = |B_\chi|^2 p_s$, where $|h_k|^2$, $|g_\eta|^2$, $|g_{k,k-2}|^2$, $|g_{k,k-3}|^2$, $|A_\chi|^2$ and $|B_\chi|^2$ follow the exponential distribution with parameters ζ_h, ζ_η, $\zeta_{g_{k,k-2}}$, $\zeta_{g_{k,k-3}}$, ζ_{a_χ} and ζ_{b_χ}, respectively. The variables A, C, D, F, C_χ and D_χ also follow the exponential distributions with parameters λ_h, $\lambda_{g_{k,k-2}}$, $\lambda_{g_{k,k-3}}$, λ_η, λ_{a_χ} and λ_{b_χ}, respectively. We assume that $\lambda_{g_{k,k-2}} = \lambda_{g_{k,k-3}} = \lambda_g$ and $\lambda_{a_\chi} = \lambda_{b_\chi} = \lambda_\chi$, where disparate path losses with large-scale fading are compensated by appropriate power control at the relaying users, as in [70]. The variable B follows the

hypo-exponential distribution with parameters λ_i, where $i \in (1, 2, 3, \ldots, I)$ is a set of interfering users and $I = k - 1$. We denote $\lambda_h = \frac{1}{p_k \zeta_h}$, $\lambda_i = \frac{1}{p_i \zeta_i}$, $\lambda_g = \frac{1}{p_s \zeta_g}$, $\lambda_\eta = \frac{1}{p_\eta \zeta_\eta}$ and $\lambda_\chi = \frac{1}{p_\chi \zeta_\chi}$, where p_η and p_χ is the power of interfering signal (IS) due to imperfect SIC and power of IS due to imperfect CSI, respectively.

In the following five lemmas and five propositions, we treat different combinations of the three impairments. In the lemmas, we derive the exact outage probabilities based on $\tilde{P}_{out}$ in (3.17). The probability distributions of the SINRs in each case can be found in its proof. Further, in the propositions, which correspond to each of the five lemmas, we provide the asymptotic outage probabilities in the high transmit SNR regime using $\tilde{P}_{out}$ in (3.17), which provide intuitive insights into the impacts of the impairments.

For mathematical notations used to derive the lemmas, please refer to Table 3.2.

Table 3.2: Mathematical Notations

Mathematical Notations used in Corollaries and Appendices
$\psi_1 = \prod_{j=1}^{I} \lambda_j,\ \psi_1^{\eta} = \lambda_h \lambda_{\eta} \prod_{j=1}^{I} \lambda_j,\ \psi_2 = \sum_{i=1}^{I} \prod_{\substack{j=1,\\ j \neq i}}^{I} \lambda_j,\ \psi_2^{\eta} = \lambda_{\eta} + \psi_2$
$\psi_3 = \sum_{i=1}^{I} log[\lambda_i] \prod_{\substack{j=1,k=1,\\ j \neq i, j \neq k,\\ i \neq k}}^{I} (\lambda_j - \lambda_k),\ \psi_4 = \lambda_h \psi_a,$ $$\psi_3^{\eta} = \sum_{j=1}^{I} log[\lambda_i] \prod_{\substack{j=1,k=1,\\ i \neq j, i \neq k,\\ j \neq k}}^{I} (\lambda_j - \lambda_k) + log[\lambda_{\eta}] \prod_{\substack{j=1,k=1,\\ i \neq j, i \neq k,\\ j \neq k}}^{I} (\lambda_j - \lambda_k)$$
$$\psi_4^{\eta} = \lambda_h \sum_{j=1}^{I} log[\lambda_i] \prod_{j=1,k=1,k>j}^{I} (\lambda_j - \lambda_k)(\lambda_j - \lambda_{\eta}),$$ $$\psi_6 = \sum_{i=1}^{I} log[\lambda_i] \prod_{\substack{j=1,k=1,\\ j \neq i, i \neq k,\\ k>j}}^{I} (\lambda_j - \lambda_k),$$
$$\psi_7 = \prod_{\substack{j=1,k=1,\\ k>j}}^{I} (\lambda_j - \lambda_k)^2,\ \psi_8 = \sum_{i=1}^{I} \lambda_i log[\lambda_i] \prod_{\substack{j=1,k=1,\\ j \neq i, i \neq k,\\ k>j}}^{I} (\lambda_j - \lambda_k),$$
$$\psi_7^{\eta} = \sum_{i=1}^{I} log[\lambda_i] \prod_{\substack{j=1,k=1,\\ i \neq j, i \neq k,\\ i \neq \eta, k>j}}^{I} (\lambda_j - \lambda_k)(\lambda_j - \lambda_{\eta}) + log[\lambda_{\eta}] \prod_{\substack{j=1,k=1,\\ i \neq j, i \neq k,\\ i \neq \eta, k>j}}^{I} (\lambda_j - \lambda_k),$$
$$\psi_8^{\eta} = \psi_8 + \lambda_{\eta} log(\lambda_{\eta}) \prod_{j=1, j \neq \eta}^{I} (\lambda_j - \lambda_{\eta}),\ \psi_9 = \lambda_h^2 \psi_7,$$
$$\psi_9^{\eta} = \lambda_h^2 \psi_b \prod_{\substack{j=1,\eta=1,\\ \eta>j}}^{I} (\lambda_j - \lambda_{\eta})^2,\ \psi_{10} = \sum_{i=1}^{I} e^{\lambda_i} \prod_{\substack{j=1,k=1,\\ j \neq i, i \neq k,\\ k>j}}^{I} (\lambda_j - \lambda_k) E_i(-\lambda_i),$$ $$\psi_{10}^{\eta} = \lambda_h^2 \psi_8^{\eta}$$
$$\psi^I = \sum_{i=1}^{I} \sum_{j>i}^{I} \cdots \sum_{s>\cdots>j>i}^{I} \lambda_s \ldots \lambda_j \lambda_i,$$ $$\psi_a = \prod_{\substack{j=1,k=1,\\ k>j}}^{I} (\lambda_j - \lambda_k), \psi_b = \prod_{\substack{j=1,k=1,\\ k>j}}^{I} (\lambda_j - \lambda_k)^2$$

First, we consider the outage probability in the absence of any impairments, which can serve as a baseline to quantify the impact of the imperfections, in the following lemma.

Lemma 1 . *The outage probability for the perfect timing, perfect SIC, and perfect CSI is given as*

$$P_{out} = \frac{1}{\lambda_g^2 \lambda_h^2} \sum_{i=1}^{I} \left[\mho e^{-\frac{\lambda_i + \lambda_h \gamma_{th}}{\lambda_g \lambda_h}} \left(\lambda_i (\lambda_i + \lambda_h \gamma_{th}) \mathrm{Ei} \left(\frac{\lambda_i}{\lambda_g \lambda_h} \right) \right. \right.$$
$$\left. - \lambda_i (\lambda_i + \lambda_h \gamma_{th}) \mathrm{Ei} \left(\frac{\gamma_{th} \lambda_h + \lambda_i}{\lambda_g \lambda_h} \right) + \lambda_g \lambda_h e^{\frac{\lambda_i}{\lambda_g \lambda_h}} \right.$$
$$\left. \left. \left(\left(e^{\gamma_{th}/\lambda_g} - 1 \right) (\lambda_g \lambda_h + \lambda_i) - \lambda_h \gamma_{th} \right) \right) \right], \tag{3.18}$$

where γ_{th} is the SINR threshold and $\mho = \sum_{i=1}^{I} \frac{\prod_{i=1}^{I} \lambda_i}{\prod_{j=1, i \neq j}^{I} (\lambda_j - \lambda_i)}$.

Proof

See Appendix A.

Since the exact outage expression derived in Lemma 1 is complicated and does not yield to easy interpretation, we consider the asymptotic behavior of the rate outage given in (3.17), when the transmit SNR, which is denoted by SNR, is high enough in the following proposition.

Proposition 1 . *As SNR $\to \infty$, the rate outage probability for the perfect timing synchronization, perfect SIC, and perfect CSI becomes*

$$\lim_{\mathtt{SNR} \to \infty} \tilde{P}_{out} \sim \frac{\lambda_h g(\mathtt{SNR})}{\Phi_k - \sum_{i=1}^{k-1} \Phi_i (2^\Upsilon - 1)} + 2\lambda_g^2 [g(\mathtt{SNR})]^2, \tag{3.19}$$

where $g(\mathtt{SNR}) = \frac{2^\Upsilon - 1}{\mathtt{SNR}}$, λ_h, and λ_g are the parameters of exponential RVs A and C, respectively (as explained in Section 3.4).

Proof

See Appendix B.

Based on this ideal case, we will investigate how each impairment impacts the outage probability.

Proposition 2 . *As* $\mathtt{SNR} \to \infty$*, the rate outage probability for the perfect timing synchronization, imperfect SIC, and perfect CSI becomes*

$$\lim_{\mathtt{SNR}\to\infty} \tilde{P}_{out}^{\eta} \sim \tilde{g}(\mathtt{SNR}) + 2\lambda_g^2[g(\mathtt{SNR})]^2, \tag{3.20}$$

where $\tilde{g}(\mathtt{SNR}) = \dfrac{\lambda_h g(\mathtt{SNR})}{\Phi_k - (\Phi_\eta + \sum\limits_{i=1}^{k-1} \Phi_i)(2^{\Upsilon}-1)}$ and Φ_η is the coefficient of power received due to ipSIC.

Proof

See Appendix D.

Compared to the ideal case in (3.19), we observe that the adverse effect of Φ_η introduced by the imperfect SIC is to increase the outage probability.

Lemma 2 . *The outage probability for the imperfect timing synchronization, perfect SIC, and perfect CSI is given as*

$$P_{out}^{\varepsilon} = \frac{1}{\Gamma(\alpha)} \left[\left(-\frac{1}{\beta^2}\right)^{-\alpha} \beta^{-\alpha} \left((-1)^{\alpha} \left(\frac{1}{\beta}\right)^{\alpha} \delta(\gamma_{th}) \right. \right.$$
$$\left. \left. + \left(-\frac{1}{\beta}\right)^{\alpha}\right) \left(\Gamma(\alpha) - \Gamma\left(\alpha, \frac{\gamma_{th}}{\beta}\right)\right) \right], \tag{3.21}$$

where α and β are given in (E.4).

Proof

See Appendix E.

Proposition 3 . *As* $\mathtt{SNR} \to \infty$, *the rate outage probability for the imperfect timing synchronization (*$0 < \varepsilon_1 < 1$*), perfect SIC, and perfect CSI becomes*

$$\lim_{\mathtt{SNR} \to \infty} \tilde{P}^\varepsilon_{out} \sim \frac{\lambda_h g(\mathtt{SNR})}{\Phi_k - \sum\limits_{i=1}^{k-1} \Phi_i (2^\Upsilon - 1)} + g^\varepsilon(\mathtt{SNR}). \tag{3.22}$$

where $g^\varepsilon(\mathtt{SNR}) = 2\varepsilon_1 \lambda_g^2 \left(\frac{2^\Upsilon - 1}{\mathtt{SNR}} \right)^2$.

Proof

See Appendix F.

From this proposition, it is clear that the second term in (3.19) quantifies the effect of the timing error on the outage probability.

Lemma 3 . *The outage probability for the imperfect timing synchronization, imperfect SIC, and perfect CSI is given as*

$$P^{\varepsilon,\eta}_{out} = \frac{1}{\Gamma(\theta)} \left[\left(-\frac{1}{\phi^2} \right)^{-\theta} \phi^{-\theta} \left((-1)^\theta \left(\frac{1}{\phi} \right)^\theta \delta(\gamma_{th}) \right. \right.$$
$$\left. \left. + \left(-\frac{1}{\phi} \right)^\theta \right) \left(\Gamma(\theta) - \Gamma\left(\theta, \frac{\gamma_{th}}{\phi} \right) \right) \right], \tag{3.23}$$

where the values of θ *and* ϕ *are given in (G.1).*

Proof

See Appendix G.

We note that Lemmas 1, 2, and 3 are special cases of this lemma. The following asymptotic analysis provides the corresponding limiting rate outage for $\mathtt{SNR} \to \infty$.

Proposition 4 . *As* SNR $\rightarrow \infty$, *the rate outage probability for the imperfect timing synchronization, imperfect SIC, and perfect CSI becomes*

$$\lim_{\text{SNR}\rightarrow\infty} \tilde{P}_{out}^{\varepsilon,\eta} \sim \tilde{g}(\text{SNR}) + g^{\varepsilon}(\text{SNR}). \tag{3.24}$$

Proof

See Appendix H.

In fact, this result in (3.24) is in line with the composite degradations found in Propositions 2 and 3. In the following lemma and proposition, we will investigate the impact of the imperfect CSI.

Since the outage rates are obtained in closed-form expressions in the five lemmas, it is possible to estimate how the outage performance of the STBC-CNOMA scheme changes as various system parameters change. Also, the asymptotic analysis in the propositions provides insights into how the rate outage is degraded by the three imperfections. Our analysis in the lemmas and propositions will be validated by comparing with simulation results.

3.5   Simulation Results

In this section, we present numerical and simulation results and validate our analysis in the previous sections. We consider a downlink NOMA system with one BS and K users. As in [36, 51, 64], we assume that the channels between the BS and each user, and inter-users are flat fading Rayleigh channels. The noise power spectral density is considered as -174 dBm/Hz. The rate threshold Υ is set to be 2 bits per channel use (BPCU). Each user is considered as stationary. The parameters ζ_h, ζ_η, $\zeta_{g_{k,k-2}}$, $\zeta_{g_{k,k-3}}$ ζ_χ are considered to be unity. Symbol duration T is also considered as unity for the simplicity. For the STBC-CNOMA scheme, the transmit power at the BS (i.e., P_{NOMA})
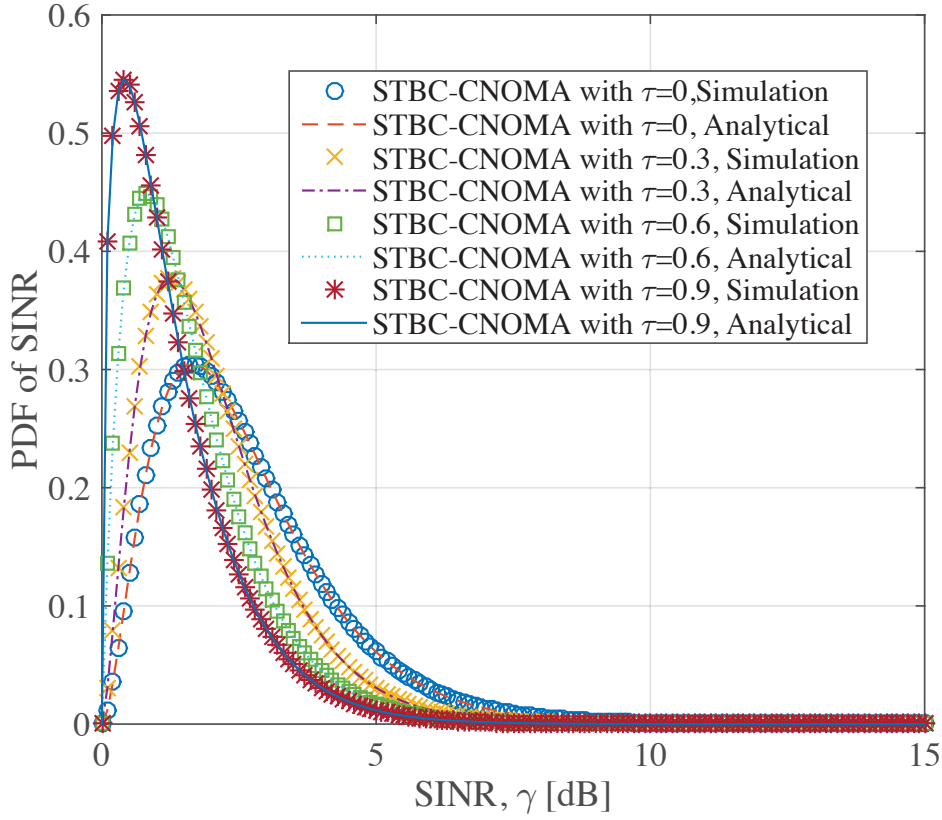
Figure 3.4: The SINR PDFs for the perfect SIC, perfect CSI, and variable timing offsets, when $K = 4$.

is considered as 45 dBm, whereas the power transmitted during STBC co-operation phase (i.e., p_s) is considered as half of the power transmitted from the BS. Power coefficients for simulations with $K = 4$ are $\Phi_1 = 0.1$, $\Phi_2 = 0.2$, $\Phi_3 = 0.3$, and $\Phi_4 = 0.4$ for $k \in \{1, 2, 3, 4\}$, respectively. It is to be noted that we assume the same total power budget for all of the schemes in the simulation for the fair comparison.

Similarly, Fig. 3.6 shows the analytical and simulation results for the performance of STBC-CNOMA with different timing offsets for the perfect CSI and imperfect SIC of -5 dBs, when $K = 4$. In this case, Fig. 3.6 show the great correlation between the simulation and analytical results based
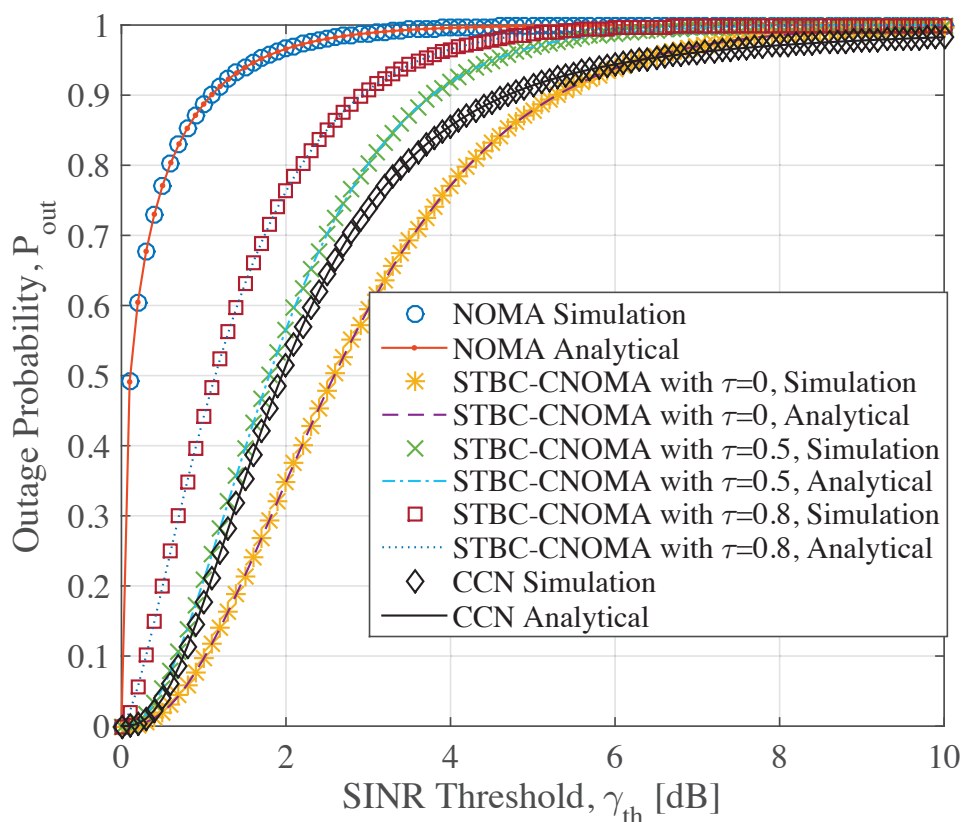
Figure 3.5: Outage probability performance for the perfect SIC, perfect CSI, and variable timing offsets, when $K = 4$.

on Lemma 4. Also, as shown in the figures, we observe that the outage probability increases sharply, as τ and the SIC imperfection increase.

Fig. 3.4 provides the comparison of simulation and analytical results for the SINR PDFs for different timing offsets, assuming $K = 4$ with the perfect SIC and CSI. It can be noticed that the simulation results closely match the analytical results for various timing offsets $\tau \in \{0, 0.3, 0.6, 0.9\}$. Thus, as an essential component for further performance analysis, the SINR PDFs derived in Section VI have been validated. Also, as expected, as the timing offset increases, the mean of the distribution approaches zero. In other words,
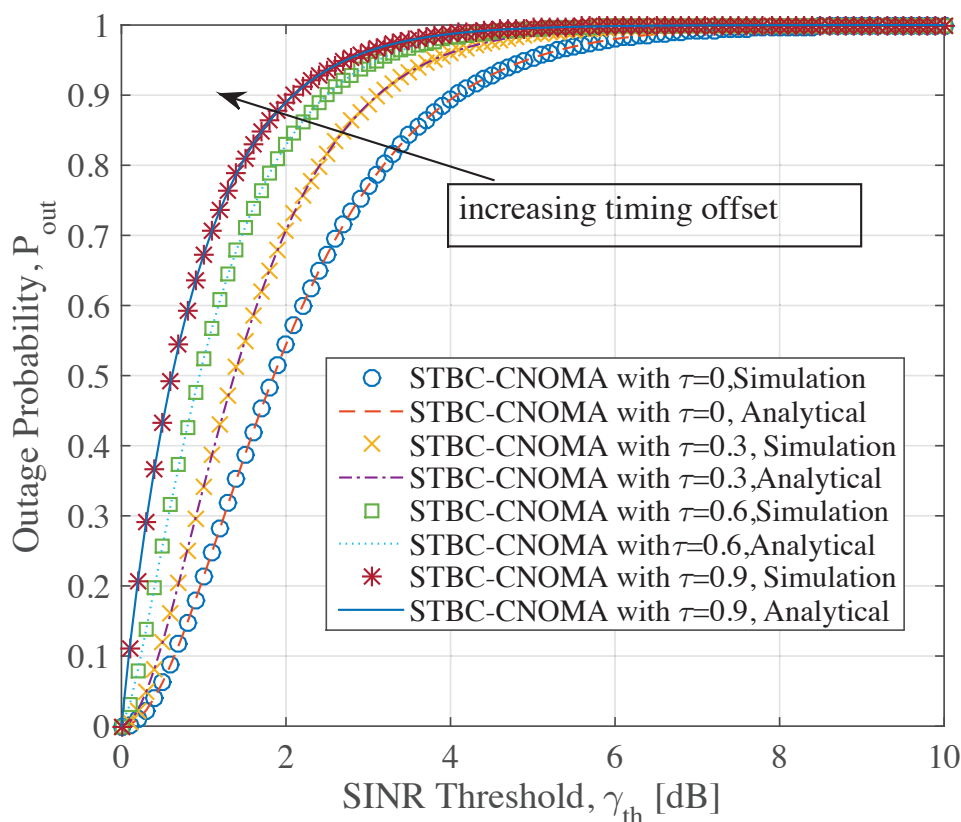
Figure 3.6: Outage probability performance with $K = 4$ for the imperfect SIC $=-5$ dBs, perfect CSI, and variable timing offsets.

the average SINR of the user decreases, as the timing offset τ increases, which means that the outage probability of the user is an increasing function of τ.

In Fig. 3.5, we compare the outage probabilities of NOMA, CCN, and STBC-CNOMA for $\tau = \{0, 0.5, 0.8\}$ and $K = 4$. In the figure, the horizontal axis represents the SINR threshold γ_{th}. The simulation and analytical results show a great correlation with each other, which validates Lemmas 1 and 3. Further, in the figure, we observe that the outage probability of NOMA is the highest for a given γ_{th}, because it is a non-cooperative scheme that does not provide diversity gain. It is also noted that STBC-CNOMA outperforms
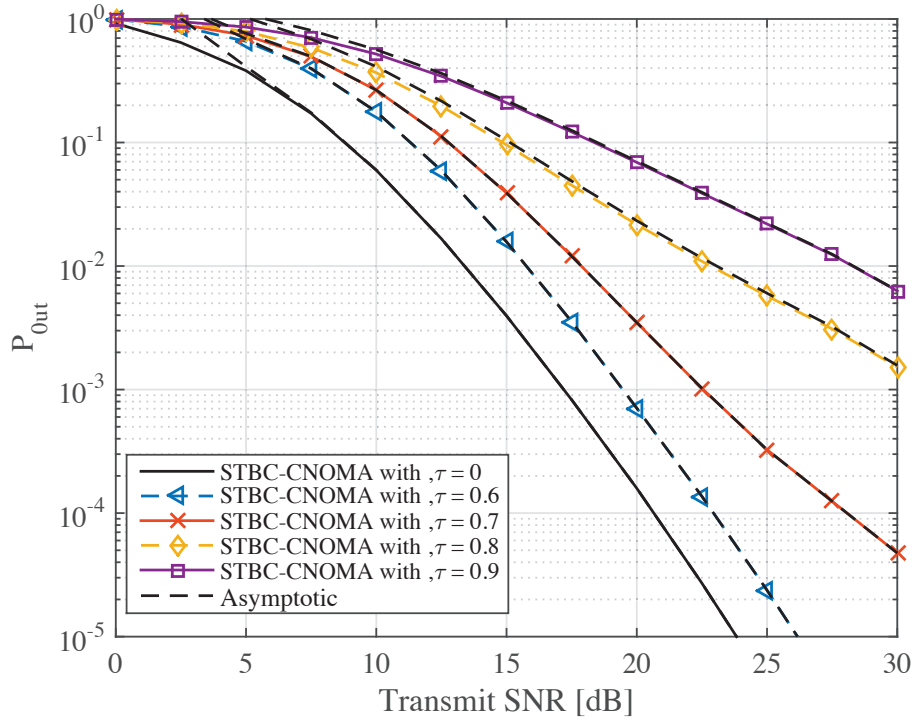
Figure 3.7: Rate outage probability of User 4 in STBC-CNOMA at $\tau = \{0, 0.6, 0.7, 0.8, 0.9\}$, perfect CSI, and perfect SIC.

the CCN for the low SINR thresholds. Also, the performance of the STBC-CNOMA with $\tau = 0.5$ is similar to that of CCN for an SINR threshold of up to 2 dB. Fig. 3.5 also demonstrates that the outage probability of the STBC-CNOMA approaches to that of NOMA with the timing offset, τ approaching 1. Therefore, for the low SINR threshold and $\tau < 0.5$, STBC-CNOMA is still an attractive scheme. Similarly, Fig. 3.6 shows the analytical and simulation results for the performance of STBC-CNOMA with different timing offsets for the perfect CSI and imperfect SIC of -5 dBs, when $K = 4$. In this case, Fig. 3.6 show the great correlation between the simulation and analytical results based on Lemma 4. Also, as shown in the figures, we observe that the outage probability increases sharply, as τ and the SIC

imperfection increase. Fig. 3.7 presents a comparative analysis of the rate outage performance as a function of the transmit SNR, SNR, of User 4 for STBC-CNOMA with the perfect SIC and different values of timing offsets. We assume that the rate threshold is 2 bits per channel use (BPCU) and there are 4 users (i.e., $K = 4$) in the system. Also, the dotted lines correspond to the asymptotic rate outage probabilities. The results show that the rate outage degrades with the increase in the timing offset τ, which is in line with the previous simulation results. The user has the best outage performance for $\varepsilon_1 = 1$, i.e., when there is no timing offset. However, in case that the users are not perfectly synchronized, the orthogonality of the received symbols is compromised, which leads to performance degradation. The user with $\tau = 1$ experiences an outage probability close to that of non-cooperative NOMA. We also observe the asymptotic analysis curves based on Propositions 1 and 3, which show good agreement with both simulation and original analytical results in the high SNR regime.

3.6 Summary

In this chapter, we provided the theoretical framework to incorporate the impairments of timing error with outage performance. We derived the closed-form expressions of the outage probabilities for the different combinations of the three impairments. Further, the complexity of STBC-CNOMA has been compared with existing cooperative NOMA protocols such as CCN, CRS-NOMA, CRS-STBC-NOMA, and CRS-NOMA-ND in terms of the total number of SIC. Through both analysis and simulation, we show that STBC-CNOMA can be an attractive solution for systems with a higher number of users or devices and having low power constraints. The simulation results also

have shown that for a small number of users (i.e., $K \leq 4$) STBC-CNOMA without any imperfection outperforms CCN until the SINR threshold exceeds a certain value. Even with moderate timing offset $\tau < 0.5$, we have observed that the outage performance degradation of STBC-CNOMA relative to CCN is not significant.

Chapter 4

STBC-Aided Cooperative NOMA with Imperfect SIC

4.1 Introduction

To meet the rising demand for high spectral efficiency, energy efficiency, and capacity for 3rd generation (3G) and 4th generation (4G) mobile communication networks such as Long-Term Evolution (LTE) and LTE-Advanced, the 3rd Generation Partnership Group (3GPP) has specified several solutions. The use of orthogonal multiple access (OMA) approaches to achieve good system-level throughput is one of these solutions. However, researchers are still working on the continued development of 4G through 5th generation (5G) mobile communication networks and beyond (future radio access (FRA)) with the growing amount of mobile traffic and the inclusion of technology such as the Internet of Things (IoT). Researchers are investigating options for new multiple access methods to go beyond 5G and further develop radio access technologies. Non-orthogonal multiple access (NOMA),

which is considered to be a promising approach for achieving improved device efficiency than the present one, is one of these newly suggested strategies.

To extract user information at the receiver, NOMA employs SIC. In SIC, the UE receiver can concurrently extract two or more signals. The message of the strong user is decoded after subtracting the messages of weak users from the composite signal. It is necessary to know the decoding order at the UE to perform SIC in downlink NOMA. This order is, in short, defined by the increasing channel gain of UEs from a corresponding BS. The UE with high channel gain, known as the strong user, decodes the low channel gain signal based on this order. The objective of this research is to include the performance of SIC under the imperfect conditions in downlink STBC-aided NOMA, thereby offering a more realistic analysis of SIC's.

4.2   System Model

We consider an STBC-based downlink NOMA system as given in section 3.2. The channel between the BS and the users, as well as the channel between any two users, is considered a flat fading Rayleigh channel. Without losing generality, users who are close to the BS have a strong channel to the BS, and are therefore referred to as strong users. Users near the cell edge, on the other hand, have poor channel conditions and are thus classified as weak users. The user with the weakest channel conditions is given the most power, while the user with the strongest channel conditions is given the least. User 1, U_1, is the strongest user, and User K, U_K, is the weakest, where $\{U_1, U_2, U_3, \ldots, U_K\}$ is the range of all users. Furthermore, in the presence of the imperfect SIC, the mathematical expressions of the SINR of the mth and n^{th} users can be derived as (4.1) and (4.2), respectively, for any $m \in \{3, 5, 7, \ldots, K-1\}$ and

$n \in \{4, 6, 8, \ldots, K\}$ for any $m \in \{3, 5, 7, ; K - 1\}$. The SINRs at the mth and the nth users are given by

$$\gamma_m^\eta = \frac{|h_m|^2 p_m}{\eta |g_\eta|^2 p_\eta + \sum_{i=1}^{m-1} |h_m|^2 p_i + \sigma^2} + \frac{(|g_{m,m-1}|^2 + |g_{m,m-2}|^2) p_s}{\sigma^2}, \qquad (4.1)$$

and

$$\gamma_n^\eta = \frac{|h_n|^2 p_n}{\eta |g_\eta|^2 p_\eta + \sum_{i=1}^{n-1} |h_n|^2 p_i + \sigma^2} + \frac{(|g_{n,n-2}|^2 + |g_{n,n-3}|^2) p_s}{\sigma^2}, \qquad (4.2)$$

respectively.

Therefore, in the presence of both the synchronization error and imperfect SIC, the SINRs of the mth and the nth users can be derived as (4.3) and (4.4),

$$\gamma_m^{\varepsilon,\eta} = \frac{|h_m|^2 p_m}{\eta |g_\eta|^2 p_\eta + \sum_{i=1}^{m-1} |h_m|^2 p_i + \sigma^2} +$$
$$\frac{(|g_{m,m-2}|^2 + \varepsilon_1 |g_{m,m-1}|^2)^2 p_s}{|(\varepsilon_1 - 1)g_{m,m-2}^* g_{m,m-1} + \varepsilon_2 g_{m,m-2} g_{m,m-2}^*|^2 p_s + (|g_{m,m-2}|^2 + |g_{m,m-1}|^2)\sigma^2}. \qquad (4.3)$$

$$\gamma_n^{\varepsilon,\eta} = \frac{|h_n|^2 p_n}{\eta |g_\eta|^2 p_\eta + \sum_{i=1}^{n-1} |h_n|^2 p_i + \sigma^2} +$$
$$\frac{(|g_{n,n-3}|^2 + \varepsilon_1 |g_{n,n-2}|^2)^2 p_s}{|(1 - \varepsilon_1)g_{n,n-3} g_{n,n-2}^* - \varepsilon_2 g_{n,n-3} g_{n,n-2}^*|^2 p_s + (|g_{n,n-3}|^2 + |g_{n,n-2}|^2)\sigma^2}. \qquad (4.4)$$

respectively, where $m \geq 3$ and $n \geq 4$ can be any odd and even numbers, respectively. In addition, it is to be noted that $\eta = 0$ and $\eta = 1$ represent the perfect and imperfect SIC employed at that user, respectively. It is noted that the SIC imperfection and timing error do not affect each other.
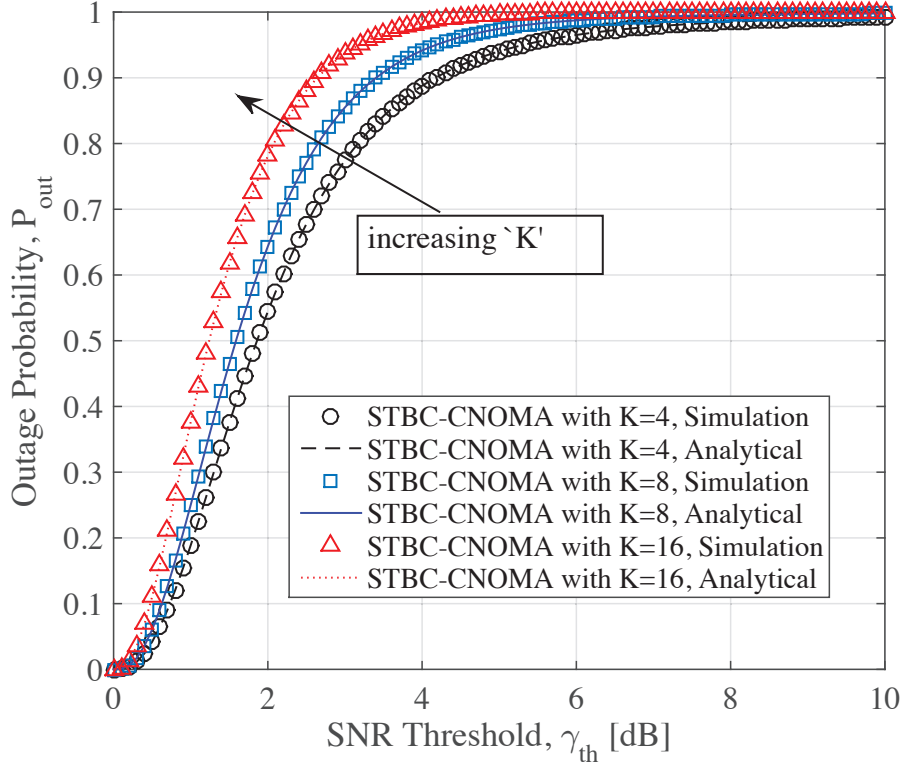
Figure 4.1: Outage probability performance for the perfect timing, perfect CSI, and imperfect SIC $= -5$dBs, when $K \in \{4, 8, 16\}$.

Lemma 4 . *The outage probability for the perfect timing synchronization, imperfect SIC, and perfect CSI is given as*

$$
P_{out}^{\eta} = \sum_{i=1}^{I} \left[\frac{1}{\lambda_g^3 \lambda_h^2 (\lambda_i - \lambda_\eta)} \left[\mho \left\{ \lambda_g e^{-\frac{\lambda_\eta + \lambda_i + \lambda_h \gamma_{th}}{\lambda_g \lambda_h}} \left[e^{\frac{\lambda_i}{\lambda_g \lambda_h}} \left\{ \right. \right. \right. \right. \right.
$$

$$
\lambda_\eta \lambda_i (\lambda_\eta + \lambda_h \gamma_{th}) \text{Ei} \left(\frac{\lambda_\eta}{\lambda_g \lambda_h} \right) - \lambda_\eta \lambda_i \left(\lambda_\eta + \lambda_h \gamma_{th} \right)
$$

$$
\text{Ei} \left(\frac{\gamma_{th} \lambda_h + \lambda_\eta}{\lambda_g \lambda_h} \right) + \lambda_g \lambda_h^2 (\lambda_\eta - \lambda_i)(\lambda_g + \gamma_{th}) e^{\frac{\lambda_\eta}{\lambda_g \lambda_h}} \right\}
$$

$$
+ \lambda_\eta \lambda_i \left(-e^{\frac{\lambda_\eta}{\lambda_g \lambda_h}} \right) (\lambda_i + \lambda_h \gamma_{th}) \text{Ei} \left(\frac{\lambda_i}{\lambda_g \lambda_h} \right)
$$

$$
+ \lambda_\eta \lambda_i e^{\frac{\lambda_\eta}{\lambda_g \lambda_h}} (\lambda_i + \lambda_h \gamma_{th}) \text{Ei} \left(\frac{\gamma_{th} \lambda_h + \lambda_i}{\lambda_g \lambda_h} \right) \right] + \lambda_g^3 \lambda_h^2 (\lambda_i - \lambda \eta) \right\} \right] \right]. \quad (4.5)
$$
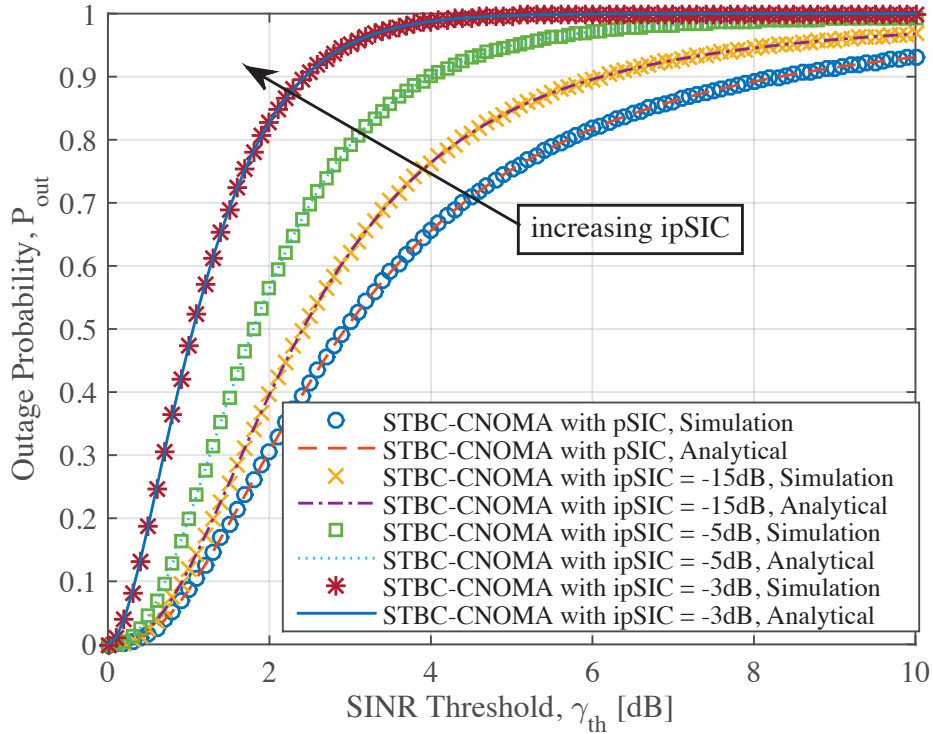
Figure 4.2: Outage probability of User 4 in STBC-CNOMA with the imperfect SIC, perfect timing synchronization, and perfect CSI.

Proof

See Appendix C.

4.3   Numerical Results

In this section, we provide the simulation results based on the analysis in Section 4.2. Fig 4.2 depicts the outage probability with different levels of the SIC imperfection. Fig 4.2 show the great correlation between the simulation and analytical results based on Lemma 4. Also, as shown in the figures, we observe that the outage probability increases sharply, as τ and the SIC im-
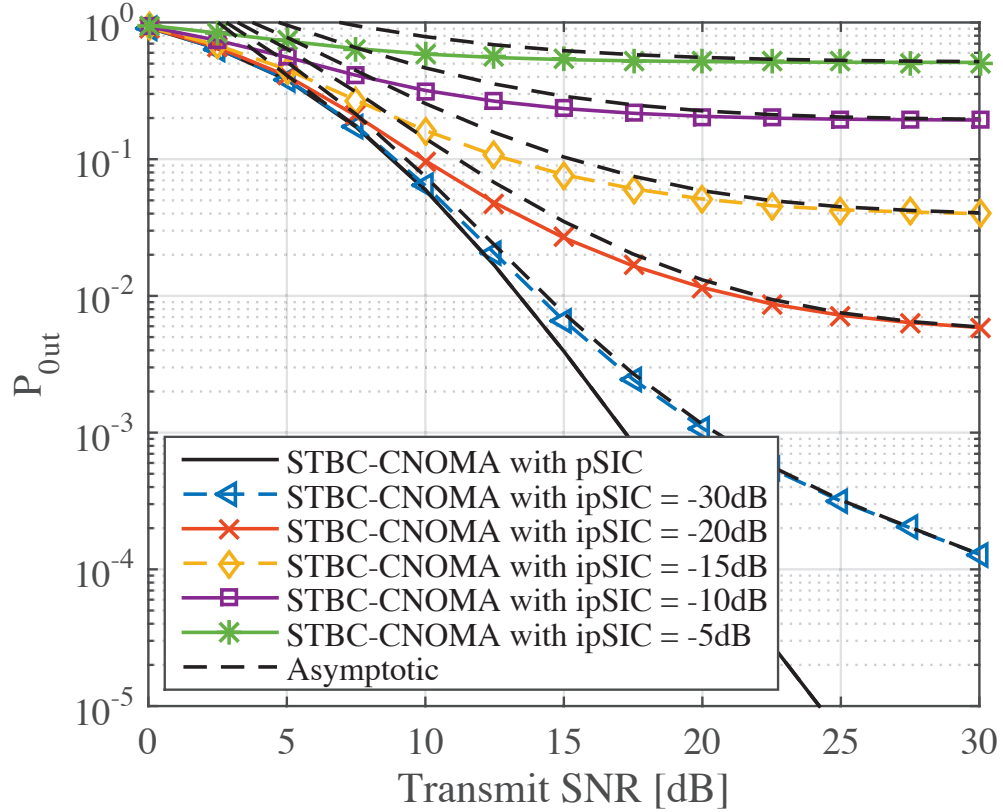
Figure 4.3: Rate outage probability of User 4 in STBC-CNOMA with the perfect timing synchronization, perfect CSI, and imperfect SIC.

perfection increase. Fig. 4.3 shows the rate outage probability of User 4 with the perfect timing synchronization, perfect CSI, and imperfect SIC. In the figure, we can find that the performance of User 4 degrades significantly with the increasing impact of imperfect SIC even with perfect timing synchronization. This implies that even if the system is perfectly synchronized but with imperfect SIC, its performance is not reliable. Fig. 4.5 gives a snapshot of the rate outage probability of User 4 with the imperfect SIC and timing offset τ of 0.5. As expected, the figure shows that the outage probability of User 4 degrades severely with the increasing effect of imperfect SIC. A small
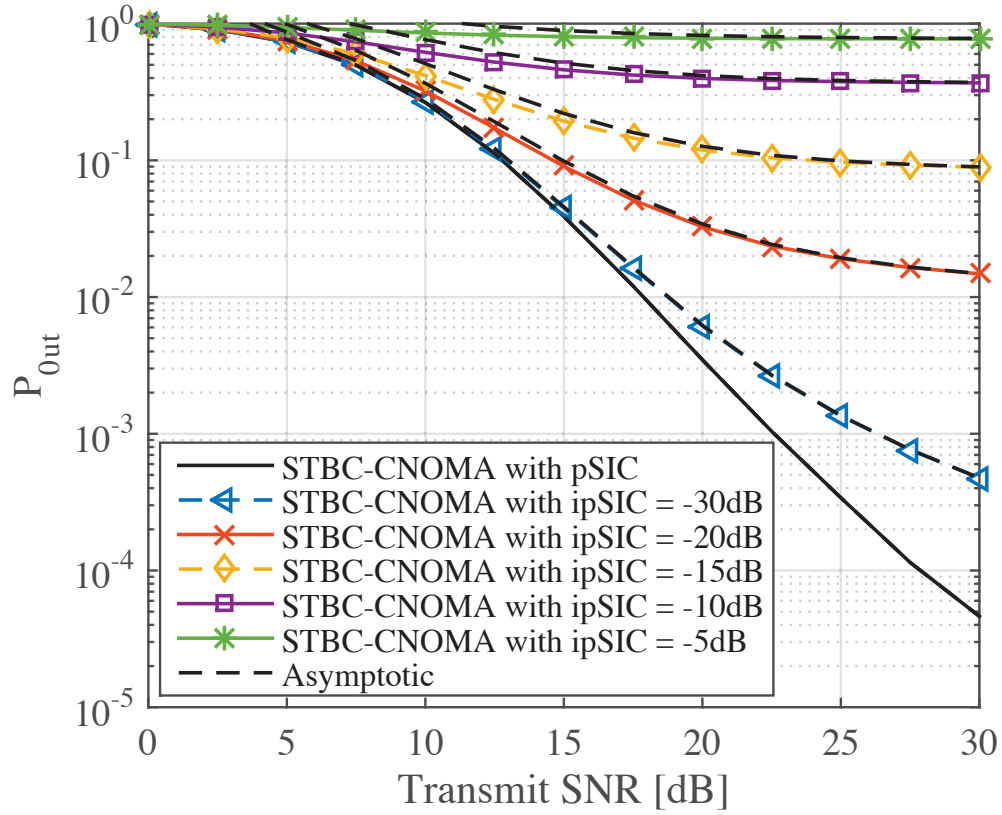
Figure 4.4: Rate outage probability of User 4 in STBC-CNOMA with the timing offset of 0.7, perfect CSI, and imperfect SIC.

increase in the intensity of imperfect SIC leads to a higher degradation in the performance of the system. Furthermore, in both Figs. 4.3 and 4.5, as SNR increases, we observe the asymptotic analysis curves show the almost identical results as the simulation and exact analysis, which validates Propositions 2 and 4. Fig. 4.4 illustrates the rate outage probability with the timing offset τ of 0.7 and the imperfect SIC. As expected, the rate outage probability in Fig. 4.4 is higher compared to Fig. 4.5, which corresponds to $\tau = 0.5$, for the same SIC condition.

Fig. 4.1 shows both analytical and simulation results of the outage performance of the STBC-CNOMA with the total number of users $K \in \{4, 8, 16\}$.
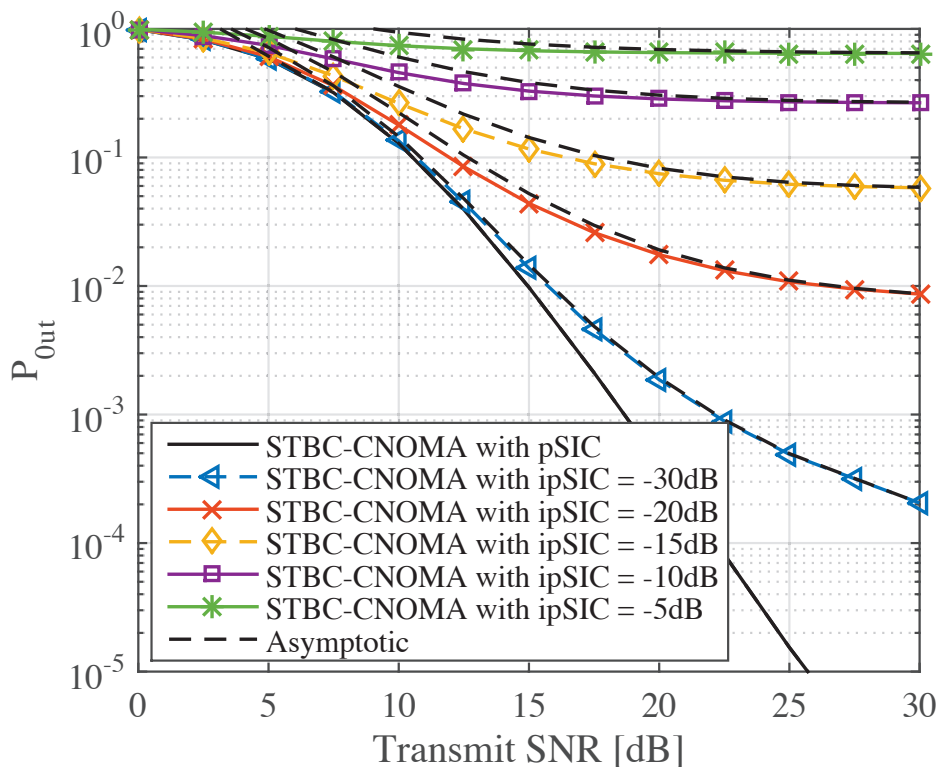
Figure 4.5: Rate outage probability of User 4 in STBC-CNOMA with the timing offset of 0.5, perfect CSI, and imperfect SIC.

In the figure, we observe the outage performance degradation with the increasing number of users. Further, it is noted that there is not much difference in the outage performance as K exceeds 8. In other words, in the absence of any imperfection, the outage performance of STBC-CNOMA is not much degraded with the increasing number of users. Also, the analytical and simulation results closely match, which validates Lemma 2.

4.4   Summary

In this chapter, we have provided the theoretical framework to SIC imperfection with outage performance. We have derived the closed-form expressions of the outage probabilities for ipSIC. We have observed that the impact of the imperfect SIC on the outage performance of STBC-CNOMA is more significant compared to those of the timing offset and the imperfect CSI. Therefore, considering the smaller number of SIC in STBC-CNOMA compared to the other cooperative NOMA protocols, we can conclude that STBC-CNOMA is an effective solution to achieve high reliability for the same SIC imperfection condition.

Chapter 5

STBC-Aided Cooperative NOMA with Imperfect CSI

5.1 Introduction

Most of the existing works in the open NOMA literature need perfect CSI knowledge. The presumption of perfect CSI, in practice, may not be available at transmitters, since a substantial device overhead would be required to achieve perfect CSI, especially in a wireless network with a large number of users. Also, there will be an increasing need for mobile networks for 5G, such as users in high-speed trains, where perfect CSI at the constantly evolving channel due to the rapidly varying channel conditions. Inspired by these practical constraints, we emphasize the use of imperfect CSI, which is critical for analysis in the STBC-aided cooperative NOMA. Also, we equate STBC-aided NOMA's performance with partial CSI, which offers a precise roadmap for realizing NOMA's efficiency improvements in practice. In this chapter, we consider a single-cell NOMA downlink with uniformly distributed

co-users with imperfect channel state information at each user.

5.2   System Model

We assume a cellular network with a single base station (BS) and U users in its coverage area. Each user is equipped with a single antenna. Let $\mathfrak{u} \in \{1, 2, 3, \ldots, U\}$ is the set of all users. The user 1, u_1, is assumed the nearest user to the BS and thereby is termed as the strongest user. The user U, u_U, is the farthest user from the BS and is termed as the weakest user. G_1 represents the STBC transmitting user's pair, whereas G_2 represents the STBC receiving user's pair. Each user in G_2 receives two signals. One from the BS, which is through the direct NOMA phase and contains a composite NOMA signal and the other from users in G_1. As shown in Figure 5.1, the channel between the BS and the uth user is represented by g_u, whereas $h_j \ \forall j \in \{1, 2\}$ is the channel between the 2nd user of G_2 and j^{th} user in G_1, respectively. Similarly, $f_j \ \forall j \in \{1, 2\}$ is the channel between the 1st user of G_2 and j^{th} user in G_1, respectively. The channel between the BS and each user and between two users is considered as a flat fading Rayleigh channel.

The transmission is completed in two phases. The first phase is the direct NOMA phase, in which the BS broadcasts the following composite NOMA signal to all users

$$m_{noma} = \sum_{u=1}^{U} \sqrt{q_u} m_u, \tag{5.1}$$

where $q_u = a_u Q_{noma}$ is the power transmitted from the BS to the uth user, a_u is the power coefficient assigned to u^{th} user, Q_{noma} is the power assigned to the composite NOMA signal and m_u is the information message for the uth user. In this work, we are mainly interested in determining the SER performance of the weakest user, i.e., u_U, from a fairness perspective. Therefore, we set
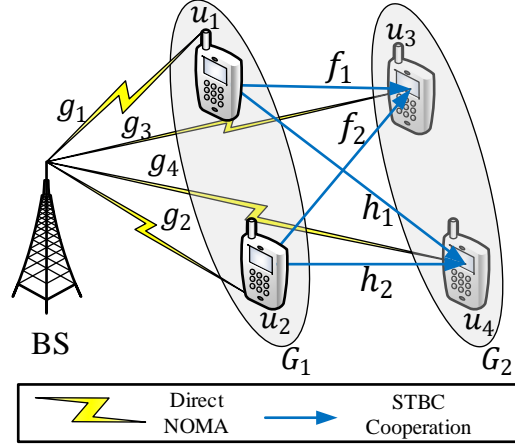
Figure 5.1: System model for Alamouti-coded cooperative communication in downlink NOMA for $U = 4$.

the performance of the weakest user as a threshold for other users. As shown in Figure 5.1, u_U receives two types of independent signals, one through direct NOMA phase and other through STBC cooperation phase given as

$$y_{U,DN} = g_U \sum_{u=1}^{U} \sqrt{q_u} m_u + n_u, \tag{5.2}$$

and

$$y_{U,STBC} = (|h_1|^2 + |h_2|^2) m_U + h_2^* n_1 - h_1 n_2^*, \tag{5.3}$$

respectively. where g_U is the channel between the BS and user U, q_u is the power assigned to the user u, m_u is the message of user u, and n_u is additive white Gaussian noise (AWGN) at user u in the time slot $t = 0$. The notations h_1 and h_2 represents the AWGN channel between U^{th} user and 1st, and 2nd users of STBC transmitting pair, respectively.

At the receiver side, the strongest user detects its own message by apply-

ing SIC to the messages of the weak users. It is to be noted that the strong users can detect the messages of the weak users. Therefore, the strong users can act as relays to re-transmit the messages of the weak user. In the second phase, that is the Alamouti cooperation phase, two the strong users cooperate with the two weak users by means of Alamouti transmission as shown in Figure 5.1. After applying maximal ratio combining (MRC), the SINR at each user for $2 < u \leq U$ is given by

$$\gamma_u = \frac{|g_u|^2 q_u}{\sum\limits_{i=1}^{u-1} |g_u|^2 q_i + \sigma^2} + \frac{(\alpha_1^2 + \alpha_2^2)q_s}{\sigma^2}, \tag{5.4}$$

$$= \gamma_g + \gamma_{h_1} + \gamma_{h_2}, \tag{5.5}$$

where $\alpha_1^2 = |h_1|^2$ and $\alpha_2^2 = |h_2|^2$. Further, $\gamma_g = \frac{|g_u|^2 q_u}{\sum_{j=1}^{u-1} |g_u|^2 q_j + \sigma^2}$, $\gamma_{h_1} = \frac{\alpha_1^2 q_u}{\sigma^2}$ and $\gamma_{h_2} = \frac{\alpha_1^2 q_u}{\sigma^2}$. Also, q_s is the power transmitted by the STBC transmitting users' pair in cooperation phase.

For imperfect CSI, let us assume user user 4 in Fig. 5.1 as the kth user, and $j \in \{1, 2\}$ are the first and second STBC transmitting users. we consider $\hat{h}_{k,j} = h_{k,j} + \omega_j$, where $\hat{h}_{k,j}$ is the estimate of $h_{k,j}$ and $h_{k,j}$ is the channel between k^{th} and j^{th} user. ω_j is the channel estimation error and it is assumed to be complex Gaussian random variable (RV) with zero mean and variance of σ_ω^2. The RV $\hat{h}_{k,j}$ are complex Gaussian with zero mean and variance $\sigma_{\hat{g}}^2 = \sigma_g^2 + \sigma_\omega^2$. Also, the correlation coefficient between the estimated channel and the real channel is $\rho = \sigma_g^2/(\sigma_g^2 + \sigma_\omega^2)$. We can write that $h_{k,j} = \rho\hat{h}_{k,j} + \varrho_{k,j}$, where $\varrho_{k,j}$ are independent complex Gaussian RVs with zero mean and variance $\sigma_\varrho^2 = \sigma_g^2\sigma_\omega^2/(\sigma_g^2 + \sigma_\omega^2)$ [55, 56]. By putting the value $h_{k,j} = \rho\hat{h}_{k,j} + \varrho_{k,j}$

into (3.8) and (3.9) [71], we get

$$
\tilde{v}_3^\chi = [(\varrho_{3,1} + h_{3,1}\rho)(\varrho_{3,1} + \rho h_{3,1})^* + (\varrho_{3,2} + h_{3,2}\rho)(\varrho_{3,2} + \rho h_{3,2})^*]x_3
$$
$$
+ \xi_{3,1}(\varrho_{3,1} + \rho h_{3,1})^* + \xi_{3,2}^*(\varrho_{3,2} + h_{3,2}\rho), \tag{5.6}
$$

and

$$
\tilde{v}_4^\chi = [(\varrho_{4,2} + h_{4,2}\rho)(\varrho_{4,2} + \rho h_{4,2})^* + (\varrho_{4,1} + h_{4,1}\rho)(\varrho_{4,1} + \rho h_{4,1})^*]x_4
$$
$$
\xi_{4,1}(\varrho_{4,2} + \rho h_{4,2})^* - \xi_{4,2}^*(\varrho_{4,1} + h_{4,1}\rho), \tag{5.7}
$$

respectively. Assuming the MRC of the received signals at each user for direct NOMA and STBC cooperation phase, and solving (5.6)-(5.7) for the SINRs, we obtain (5.8) and (5.9), respectively. The equations for received SINR with imperfect CSI are given as

$$
\gamma_m^\chi = \frac{|g_m|^2 p_m}{\sum\limits_{i=1}^{m-1} |g_m|^2 p_i + \sigma^2} + \frac{(|\varrho_{m,m-2} + h_{m,m-2}\rho|^2 + |\varrho_{m,m-1} + h_{m,m-1}\rho|^2)p_s}{\sigma^2}.
$$
$$\tag{5.8}$$

$$
\gamma_n^\chi = \frac{|g_n|^2 p_n}{\sum\limits_{i=1}^{n-1} |g_n|^2 p_i + \sigma^2} + \frac{(|\varrho_{n,n-3} + h_{n,n-3}\rho|^2 + |\varrho_{n,n-2} + h_{n,n-2}\rho|^2)p_s}{\sigma^2}. \tag{5.9}
$$

Lemma 5 . *The outage probability for the perfect timing synchronization, perfect SIC, and imperfect CSI is given as*

$$
P_{out}^\chi = \frac{1}{\lambda_\chi^2 \lambda_h^2} \sum_{i=1}^{I} \left[\mho e^{-\frac{\lambda_i + \lambda_h \gamma_{th}}{\lambda_\chi \lambda_h}} \left(\lambda_i(\lambda_i + \lambda_h \gamma_{th}) \mathrm{Ei}\left(\frac{\lambda_i}{\lambda_\chi \lambda_h} \right) \right.\right.
$$
$$
\left. - \lambda_i(\lambda_i + \lambda_h \gamma_{th}) \mathrm{Ei}\left(\frac{\gamma_{th}\lambda_h + \lambda_i}{\lambda_\chi \lambda_h} \right) + \lambda_\chi \lambda_h e^{\frac{\lambda_i}{\lambda_\chi \lambda_h}} \right.
$$
$$
\left.\left. \left(\left(e^{\gamma_{th}/\lambda_\chi} - 1\right)(\lambda_\chi \lambda_h + \lambda_i) - \lambda_h \gamma_{th} \right) \right) \right]. \tag{5.10}
$$

Proof

See Appendix I.

Proposition 5 . *As* $\mathtt{SNR} \to \infty$, *the outage probability for the perfect timing synchronization, perfect SIC, and imperfect CSI becomes*

$$\lim_{\mathtt{SNR}\to\infty} \tilde{P}_{out}^{\chi} \sim \frac{\lambda_h g(\mathtt{SNR})}{\Phi_k - \sum\limits_{i=1}^{k-1} \Phi_i(2^{\Upsilon} - 1)} + 2\lambda_{\chi}^2[g(\mathtt{SNR})]^2, \qquad (5.11)$$

where $\lambda_{\chi} = 1/\sigma_{\chi}^2 = 1/(\sigma_{\varrho}^2 + \rho^2\sigma_g^2)$.

Proof

See Appendix J.

5.3 Complexity Analysis

In this section, we will compare the complexity of STBC-aided cooperative NOMA (STBC-CNOMA) with other cooperative NOMA techniques in terms of the number of SIC performed, which is widely used to evaluate the computational complexity of NOMA as in [60, 61, 72, 73, 74]. We consider five different NOMA schemes: conventional cooperative NOMA (CCN) [51], cooperative relay systems using NOMA (CRS-NOMA) [64], CRS-NOMA novel design (CRS-NOMA-ND) [75], cooperative relay selection by using STBC (CRS-STBC-NOMA) [68], and lastly STBC-CNOMA. We note that this is the first extensive comparison of the five schemes, which quantifies the total number of SIC performed for a given number of users K.

The total number of SIC performed by CCN is given by

$$SIC_{ccn} = \sum_{j=0}^{K-2} \left[\sum_{i=1}^{K-1-j} (K - (i + j)) \right]. \tag{5.12}$$

Also, the total number of SIC performed by CRS-NOMA, which uses a half-duplex relay between the source and each user, is given by

$$SIC_{crs-noma} = \sum_{j=1}^{K} j. \tag{5.13}$$

Also, the total number of SIC performed by CRS-STBC-NOMA, which has a two-phase communication from the source to each user by means of 2×1 STBC, is given by

$$SIC_{crs-stbc-noma} = \sum_{j=1}^{K} 4j. \tag{5.14}$$

In this scheme, the source is equipped with two transmit antennas, and each relay is equipped with one receive antenna and two transmit antennas, whereas each user is equipped with one receive antenna.

On the other hand, the total number of SIC performed by CRS-NOMA-ND is given by

$$SIC_{crs-noma-nd} = \sum_{j=1}^{K} 2j. \tag{5.15}$$

In this scheme, two sources transmit two symbols to two users through superposition coding, and each user decodes its symbol by MRC and SIC. Whereas, the total number of SIC performed by STBC-CNOMA is given by

$$SIC_{stbc-cnoma} = \sum_{i=1}^{K-1} (K - i). \tag{5.16}$$

It is noted that (5.12) and (5.16) show that for a larger number of users, the complexity of CCN increases due to higher number of SIC. Whereas, the number of SIC is not increased in cooperation phase of STBC-CNOMA. Therefore, it achieves the diversity gain of STBC codes and maintains the number of SIC same as that of conventional direct NOMA scheme.

Table 5.1: A comparison of time slots required and number of transmissions for different cooperative NOMA schemes.

Algorithm	No. of Time Slots	No. of Transmissions
CCN [51]	K	K
CRS-NOMA [64]	K	K
CRS-NOMA-ND [75]	K	K
CRS-STBC-NOMA [68]	$2K$	$4K$
STBC-CNOMA	$K-1$	$2K-3$

In Table 5.1, we compare the number of time slots required for the complete transmission in various cooperative schemes for even $K \geq 4$. As shown in the table, STBC-CNOMA requires $K-1$ time slots for the complete transmission. Therefore, saving one time slot as compared to that of in CCN and CRS-NOMA. This time slot can be utilized in other types of signaling, which makes STBC-CNOMA a more efficient scheme. In addition, in the last column of Table 5.1, we compare the number of transmissions, which indicates the communication overhead. As shown in the table, CRS-STBC-NOMA has the largest number of transmissions. Due to the STBC phase, we can find out that STBC-CNOMA also requires more number of transmissions compared to the other three schemes for any $K \geq 4$.
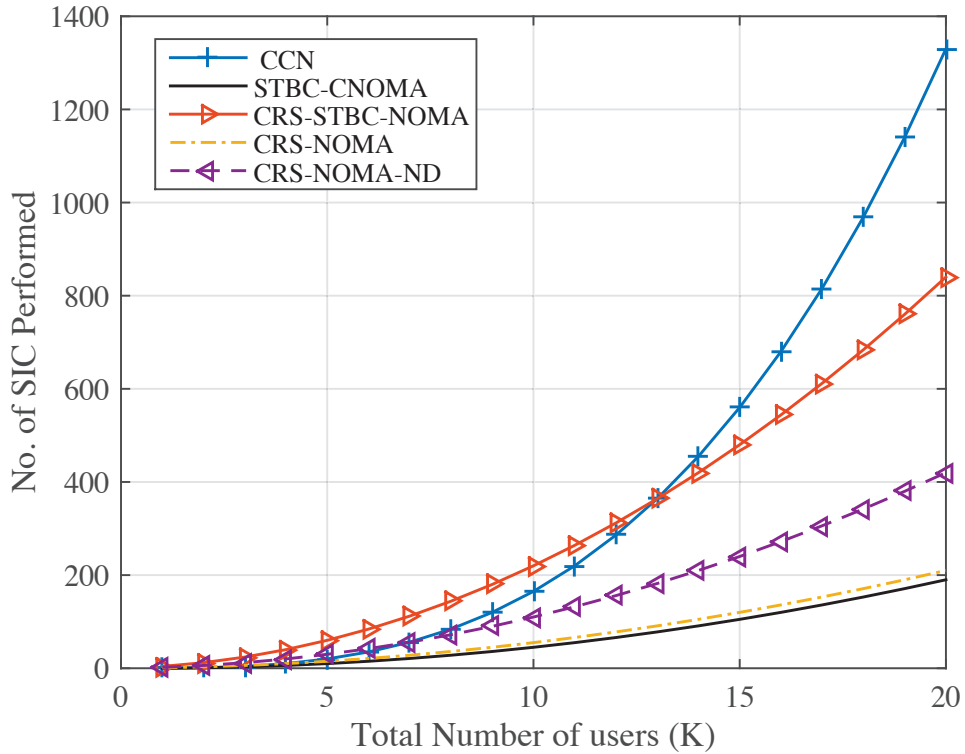
Figure 5.2: A comparison of number of SIC performed in different flavors of cooperative NOMA.

5.4   Numerical Results

In this section, we simulate the analytical results as shown in Section 5.2 and Section 5.3. Further, the complexity of STBC-CNOMA has been compared with existing cooperative NOMA protocols such as CCN, CRS-NOMA, CRS-STBC-NOMA, and CRS-NOMA-ND in terms of the total number of SIC. Through both analysis and simulation, we show that STBC-CNOMA can be an attractive solution for systems with a higher number of users or devices and having low power constraints. The simulation results also have shown that for a small number of users (i.e., $K \leq 4$) STBC-CNOMA without any imperfection outperforms CCN until the SINR threshold exceeds a certain
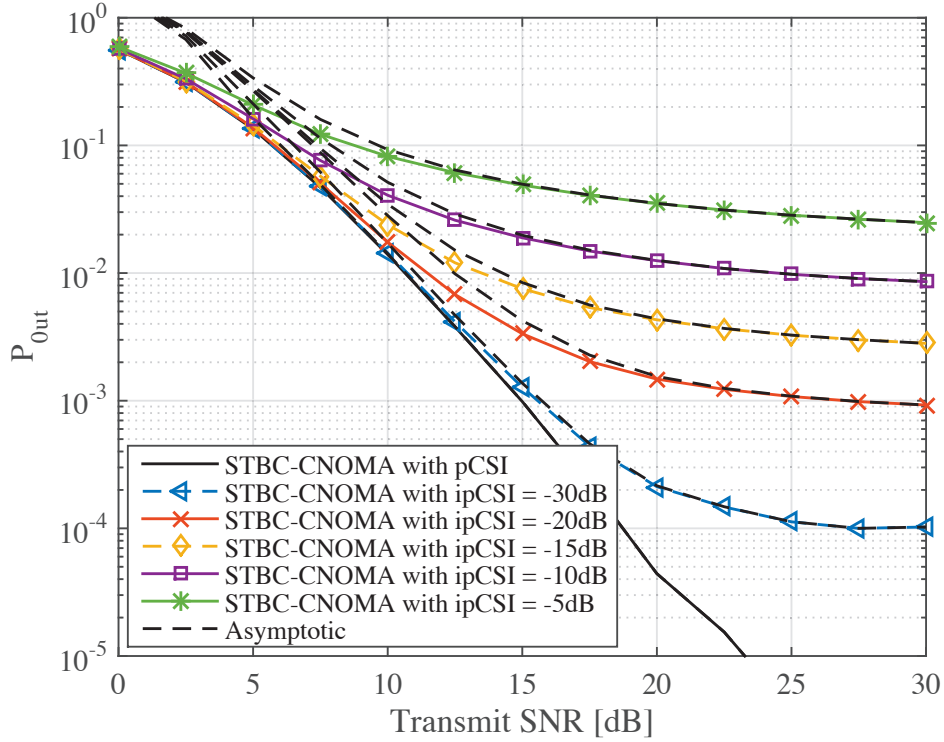
Figure 5.3: Rate outage probability of User 4 in STBC-CNOMA with the perfect timing synchronization, perfect SIC, and imperfect CSI.

value. Even with moderate timing offset $\tau < 0.5$, we have observed that the outage performance degradation of STBC-CNOMA relative to CCN is not significant. On the other hand, the impact of the imperfect SIC on the outage performance of STBC-CNOMA is more significant compared to those of the timing offset and the imperfect CSI. Therefore, considering the smaller number of SIC in STBC-CNOMA compared to the other cooperative NOMA protocols, we can conclude that STBC-CNOMA is an effective solution to achieve high reliability for the same SIC imperfection condition. Lastly, Fig. 5.2 shows the complexity comparison in Section V. As shown in the figure, it is obvious that the CCN becomes computationally expensive for a higher number of users due to its exponential increase in the number of SIC to

be performed. On the other hand, STBC-CNOMA has substantially reduced the number of SIC. For example, when the total number of users is 6, the CCN requires 35 SIC whereas, in STBC-CNOMA, the number of SIC required is 15, making a 57% reduction in the number of SIC performed. This reduction of SIC increases to 72.72 % and 83.17% as the number of users increases to 10 and 18, respectively. We can say that the CRS-STBC-NOMA has the worst performance in terms of complexity for low and medium numbers of users. But, for a higher number of users, i.e., $K > 13$, conventional cooperative NOMA has the worst performance in terms of complexity. The proposed scheme, STBC-CNOMA, outperforms all of the other schemes in terms of the numbers of SIC performed, which is desirable in hardware-limited networks.

Fig. 5.3 shows the effect of the channel estimation error (i.e., CSI imperfection) on the rate outage performance of STBC-CNOMA. In the figure, we first observe that the analytical results indicated by the solid lines have an excellent correlation with the corresponding simulation results, which are indicated by the different markers. In addition, the dotted lines, which correspond to the asymptotic analysis, approach the solid lines and markers, as SNR increases. Thus, both Lemma 5 and Proposition 5 have been validated. Also, in the figure, the performance degrades rapidly with the increase in the magnitude of the imperfection in the channel estimation. By comparing the results in Figs. 5.3, it is observed that the impact of the imperfect SIC is greater compared to that of the imperfect CSI. This is because the SIC imperfection degrades the SINR performance in the direct NOMA phase as well as in cooperative NOMA phase because accurate detection of weak users' symbols in the direct NOMA phase depends on the level of perfection in SIC. The imperfection in the detected weak users' symbols leads to a decrease in SINR in the cooperative NOMA phase.

5.5   Summary

In this chapter, we have provided the theoretical framework to CSI imperfection with outage performance. We have derived the closed-form expressions of the outage probabilities for ipCSI. We have observed that the impact of the imperfect CSI on the outage performance of STBC-CNOMA is more significant compared to those of the timing offset and the imperfect CSI. Therefore, considering the smaller number of CSI in STBC-CNOMA compared to the other cooperative NOMA protocols, we can conclude that STBC-CNOMA is an effective solution to achieve high reliability for the same CSI imperfection condition.

Chapter 6

Ergodic Capacity of STBC-Aided Cooperative NOMA

6.1 Introduction

The demand for massive connectivity and low latency in the beyond fifth-generation (B5G) and the sixth-generation (6G) systems has motivated the researcher to develop more efficient multiple access schemes. In the previous generations (i.e., 1G to 4G), orthogonal multiple access (OMA) schemes were used. For example, orthogonal frequency division multiple access (OFDMA) was employed as the key technology in the fourth generation (4G). However, the issues of high peak-to-average power ratio (PAPR) and cyclic prefix, which carries no extra information, make OFDM less attractive for future systems. Therefore, non-orthogonal multiple access (NOMA) is proposed as a promising access technology for beyond 5G/6G systems due to its capabil-

ities to accommodate a massive number of devices, high data rates, and low latency [76, 77, 78].

In a NOMA system, multiple users can access the same resource block (i.e., frequency and time) simultaneously, and users are differentiated in the power domain, where the user with the strongest channel condition (the strongest user) is allocated the least power, whereas the farthest user (the weakest user) is assigned highest power level. On the receiver side, the strongest user decodes its message after subtracting the messages of the weak users from the composite NOMA signal by applying successive interference cancellations (SICs). However, the challenge of the exponential increase in the number of SIC for a higher number of users limits the achievable performance of NOMA.

Several cooperation schemes for NOMA are proposed for the performance improvements of the weak users [79, 80, 81, 82]. A two-stage relay selection scheme is proposed in [79] for the cooperation in NOMA users. The authors in [80] propose cooperation from all strong users for the weakest user. The scheme substantially improves the data rate of the weak user, but at the cost of a higher number of SICs. The article [81] addresses the physical layer security issues for the cooperative NOMA by considering both amplify-and-forward (AF) and decode-and-forward (DF) schemes, whereas the performance of single relay selection with imperfect channel state information (CSI) over fading channel is studied in [83]. NOMA with novel concept of backscatter communication is studied in [84].

Space-time-block-code (STBC)-based cooperative NOMA termed as STBC-NOMA is proposed in [85], which exploits the diversity feature of STBC codes while the number of SIC operations is minimized during the STBC cooperation phase. In this way, the sum rates of the overall system are im-

proved, and outage probability is reduced as compared to the conventional NOMA scheme [86]. However, all of the existing works on STBC-NOMA assume perfect SIC, which cannot be guaranteed in practice. Therefore, in this chapter, we evaluate the system under consideration with imperfect SIC implementations. More specifically, we study the ergodic rate performance of the STBC-NOMA under imperfect SIC (ipSIC) conditions and compare its performance with conventional cooperative NOMA (CCN) [87] and non-cooperative NOMA schemes [88].

6.2   System Model

The principle of NOMA is based on exploiting the broadcast nature of the channel, where each user utilizes the same frequency, time, and code, whereas the users are differentiated in the power domain. We consider a downlink NOMA system with a base station (BS) and L users in its coverage area, as shown in Fig.6.1. The User 1, l_1, is assumed nearest to the BS, and thereby has the strongest channel g_1, whereas the user L is the farthest user from the BS and has the weakest channel g_L. Each user is equipped with a single antenna. As per the NOMA principle, the strongest user, l_1, is assigned the least power, whereas the weakest user, l_L, is allocated the maximum power. The complete transmission consists of two phases. The first phase is the direct NOMA phase, in which the following composite NOMA signal is broadcasted to all of the users,

$$s_{noma} = \sum_{l=1}^{L} \sqrt{q_l} s_l, \qquad (6.1)$$

Table 6.1: Alamouti Code-Aided Cooperative NOMA Communication Protocol for 4 Users

Timing		Transmitter	Receiver
Phase 1 (Direct NOMA) :	t_o	BS: Broadcasts s_{noma} to all users l_l	l_l : Receives s_{noma} from BS
Phase 2 (Alamouti Coop.) :	t_1	l_1 : Transmits s_3 to l_3 and l_4 l_2 : Transmits s_4 to l_3 and l_4	l_3 : Receives s_3 from l_1 and l_2 l_4 : Receives s_4 from l_1 and l_2
	t_2	l_1 : Transmits $-s_4^*$ to l_3 and l_4 l_2 : Transmits s_3^* to l_3 and l_4	l_3 : Receives $-s_4^*$ from l_1 and l_2 l_4 : Receives s_3^* from l_1 and l_2

where $q_l = a_l q_{noma}$ is the power transmitted from the BS to the lth user, a_l is the power coefficient assigned to l^{th} user, q_{noma} represents the power of composite NOMA signal and s_l is the information message for the lth user. A stronger user can detect the signals of weak users and decode its own message by applying the SIC. We can say that the strongest user, l_1, detects the messages of all other users to decode its own message. Therefore, stronger users can cooperate with weaker users to increase their SINR.

6.2.1 Received Signal Model

As shown in Table 6.1, the received signal at the lth user, in the first time slot, t_0, during the direct NOMA phase is given by

$$y_l = g_l \sum_{l=1}^{L} \sqrt{q_l} s_l + n_l, \tag{6.2}$$
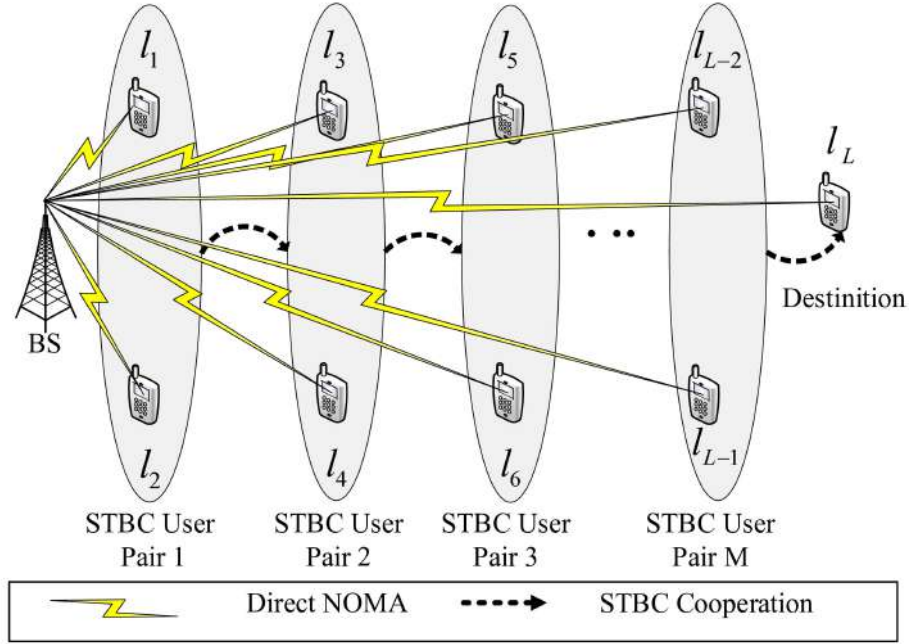
Figure 6.1: An STBC-based cooperation for NOMA network

where n_l is additive white Gaussian noise (AWGN) and $1 \leq l \leq L$. Thereby, the lth user has the SINR as

$$\gamma_{l,noma} = \frac{|g_l|^2 q_l}{\sum\limits_{i=1}^{l-1} |g_l|^2 q_i + \sigma^2}. \tag{6.3}$$

We assume that the transmitted symbol has unit energy and noise power of σ^2. The strongest user l_L, detects the messages of all other users (i.e., $2 \leq l \leq L$) then applies SIC to them and finally detects its own signal with SNR of $\gamma_{1,noma} = \frac{|g_1|^2 q_1}{\sigma^2}$, where q_i is the interference power received at the lth user from the ith interfering user. In the second phase, i.e., the STBC cooperation phase, the first two strong users (l_1 and l_2) make the STBC transmitting user pair, whereas l_3 and l_4 constitute the STBC receiving user pair that receive

the messages by distributed Alamouti STBC transmission scheme and this process continues till the last user, l_L receives its own message. The channel between transmitting user m and the receiving user n is represented as $f_{n,m}$, the SINR at the lth user during the STBC cooperation phase is given by

$$\gamma_{l,STBC} = \frac{(|f_{l-\varepsilon-1,l}|^2 + |f_{l-\varepsilon-2,l}|^2)q_s}{\sigma^2}, \tag{6.4}$$

where $2 < l \leq L$, and q_s is the fraction of power received at the receiving users' pair in STBC cooperation. Also, $\varepsilon \in \{0,1\}$ denotes first and second user of the 2×2 STBC receiving pair.

6.3 Signal Combining Scheme

Each user, in the receiving mode receives two signals. One from BS in direct NOMA phase, which is a composite NOMA signal, and the second is from STBC transmitting users' pair. The SINR at the STBC receiving users' pair with perfect SIC is given by

$$\gamma_l = \frac{|g_l|^2 q_l}{\sum\limits_{i=1}^{l-1} |g_l|^2 q_i + \sigma^2} + \frac{(|f_{l-\varepsilon-1,l}|^2 + |f_{l-\varepsilon-2,l}|^2)q_s}{\sigma^2},$$
$$= \gamma_{l_{NOMA}} + \gamma_{l_{STBC}}. \tag{6.5}$$

The SINR at the STBC receiving user pair with imperfect SICs is given by

$$\gamma_l^\beta = \frac{|g_l|^2 q_l}{\beta|f_\beta|^2 q_\beta + \sum\limits_{i=1}^{l-1} |g_l|^2 q_i + \sigma^2} + \frac{(|f_{l-\varepsilon-1,l}|^2 + |f_{l-\varepsilon-2,l}|^2)q_s}{\sigma^2},$$
$$= \gamma_{l_{NOMA}}^\beta + \gamma_{l_{STBC}}, \tag{6.6}$$

where β denotes the imperfection in SIC, and β=0, and β=1 denotes the absolute perfect and fully imperfect SICs implemented at the receiver, respec-

tively. q_β is the power received along with interfering signal due to imperfect SIC implementation at the lth user. To study the impact of imperfect SIC in STBC-NOMA, we evaluate the ergodic capacity of the system in the next section.

6.4   Ergodic Capacity

In this section, we evaluate the ergodic capacity of each user for perfect and imperfect SICs cases. Ergodic capacity is defined as long term average achievable data rate without considering any delay constraints. By using Jensen's inequalities for (6.5)-(6.6) we get,

$$C_{Erg} \leq \log\left(1 + \mathbb{E}[\gamma_l]\right), \tag{6.7}$$

and

$$C_{Erg}^\beta \leq \log\left(1 + \mathbb{E}[\gamma_l^\beta]\right), \tag{6.8}$$

where C_{Erg}, C_{Erg}^β are the ergodic capacity with perfect and imperfect SICs, respectively, and $\mathbb{E}[.]$ represents the expected value.

In order to find the mean of SINR for different cases, we need the probability density function (PDF) of SINR for different cases. The variables used in (6.5)-(6.6) are redefined as $A = |g_l|^2 q_l$, $B = \sum\limits_{i=1}^{I} |g_l|^2 q_i$, $C = |f_{l,l-2}|^2 q_s$, $D = |f_{l,l-3}|^2 q_s$ and $F = |f_\beta|^2 q_\beta$, where $|g_l|^2$, $|f_\beta|^2$, $|f_{l,l-2}|^2$ and $|f_{l,l-3}|^2$ are the exponential random variable (RVs) with parameters η_g, η_β, $\eta_{f_{l,l-2}}$ and $\eta_{f_{l,l-3}}$, respectively. The variables A, C, D and F are also exponential RVs with parameters μ_g, $\mu_{f_{l,l-2}}$, $\mu_{f_{l,l-3}}$ and μ_β, respectively. We assume $\mu_{f_{l,l-2}} = \mu_{f_{l,l-3}} = \mu_g$. The variable B is hypo-exponential RV with parameters μ_i,

where $i \in \{1, 2, 3, \ldots, I\}$ is a set of users with interferences and $I = l - 1$. We denote $\mu_g = \frac{1}{q_l \eta_g}$, $\mu_i = \frac{1}{q_i \eta_i}$, $\mu_f = \frac{1}{q_s \eta_f}$ and $\mu_\beta = \frac{1}{V_\beta \eta_\beta}$, where V_β is the power of the interfering signal (IS) due to imperfect SICs.

6.4.1 PDF of SINR with Perfect SICs

PDFs of RVs A and B are given as

$$f_A(a) = \mu_g e^{-\mu_g a}, \ a \geq 0 \tag{6.9}$$

For more than one interferer, PDF of B is given as

$$f_B(b) = \prod_{i=1}^{I} \mu_i \left[\sum_{i=1}^{I} \frac{e^{-\mu_i b}}{\prod_{j=1, i \neq j}^{I} (\mu_j - \mu_i)} \right], \ b > 0, \tag{6.10}$$

where I is total number of interferers. The PDF of $V = \frac{A}{B}$ is

$$f_V(v) = \int_0^\infty b f_A(bv) f_B(b) db. \tag{6.11}$$

By substituting (A.1) and (A.3) into (A.4) and doing straight forward mathematical calculations, the PDF of V is given by

$$f_V(v) = \frac{\mu_g \zeta_1 \left[\zeta_2 + v \mu_g \left(\sum_{i=1}^{I} (i+1) v^{i-1} \mu_g^{i-1} \zeta^{I-i-1} \right) \right]}{\prod_{j=1}^{I} (\mu_g v + \mu_j)^2}, \tag{6.12}$$

where $v > 0$ and the mean is given as

$$\mathbb{E}[V] = \frac{\zeta_1 \zeta_3}{\zeta_4}. \tag{6.13}$$

Similarly, for the perfect timing synchronization, let us define $Z = C + D$, which is sum of two exponential RVs, i.e., $Z \sim Gamma(\mu_g)$. As a result, the PDF of Z is the given as,

$$f_Z(z) = \frac{z}{\mu_f^2} e^{-z\mu_f}, \; z > 0. \tag{6.14}$$

For the perfect SICs, suppose $K = V + Z$. By convolving PDF of V and PDF of Z, which are given in (A.5) and (A.6), we obtain the PDF of $K = V + Z$ as

$$f_K(k) = \frac{1}{\mu_f^3 \mu_g^2} \sum_{i=1}^{I} \left[\mho e^{-\frac{\mu_i + \mu_g k}{\mu_f \mu_g}} \left(\mu_i(-\mu_f \mu_g + \mu_i + \mu_g k) \left(\text{Ei}\left(\frac{k\mu_g + \mu_i}{\mu_f \mu_g} \right) \right. \right. \right.$$
$$\left. \left. \left. - \text{Ei}\left(\frac{\mu_i}{\mu_f \mu_g} \right) \right) + \mu_f \mu_g e^{\frac{\mu_i}{\mu_f \mu_g}} \left(\mu_i - \mu_i e^{k/\mu_f} + \mu_g k \right) \right) \right], \tag{6.15}$$

with mean

$$\mathbb{E}[K] = \int_0^\infty K f_K(k) dk$$
$$= \frac{\zeta_1 \zeta_3}{\zeta_4} + \frac{2}{\mu_f}, \tag{6.16}$$

where $k > 0$ and $\textbf{Ei}(x) = \int_{-\infty}^{x} \frac{e^t}{t} dt$.

6.4.2   PDF of SINR with Imperfect SICs

For the imperfect SICs, let us write (6.6) as $K_\beta = \frac{A}{F+B} + Z$. Let A and B be the RVs with the probability distributions defined in (A.1), (A.3) and

$F \sim Exp(\mu_\beta)$ and let $\varpi = F + B$. Then, the PDF of ϖ as

$$
f_\varpi(\varpi) = \mu_\beta \prod_{i=1}^{I} \mu_i \left[\sum_{i=1}^{I} \left(\frac{e^{-\mu_i \varpi}}{\displaystyle\prod_{j=1,i\neq j,\beta\neq j}^{I} (\mu_j - \mu_i)(\mu_j - \mu_\beta)} \right. \right.
$$
$$
\left. \left. + \frac{e^{-\mu_\beta \varpi}}{\displaystyle\prod_{j=1,i\neq j,\beta\neq j}^{I} (\mu_j - \mu_i)(\mu_j - \mu_\beta)} \right) \right],
$$

(6.17)

where $\varpi > 0$. The PDF of $V_\beta = \frac{A}{\varpi}$ is given as

$$
f_{V_\beta}(v) = \int_0^\infty \varpi f_A(\varpi v) f_\varpi(\varpi) d\varpi.
$$

(6.18)

By straightforward mathematical manipulations, we obtain the PDF of V_β

as

$$
f_{V_\beta}(v) = \frac{\zeta_1^\beta \left[\zeta_2^\beta + v\mu_g \left(\sum_{i=1}^{I}(i+2)v^i \mu_g^i \zeta_\beta^{I-i} \right) \right]}{(\mu_g v + \mu_\beta)^2 \prod_{j=1}^{I}(\mu_g v + \mu_j)^2}, \quad v > 0
$$

(6.19)

with mean

$$
\mathbb{E}[V_\beta] = \frac{\zeta_1^\beta \zeta_3^\beta}{\zeta_4^\beta},
$$

(6.20)

By convolving (C.3) and (A.6), we obtain the PDF of K_β as

$$
f_{K_\beta}(k) = \sum_{i=1}^{I} \left[\frac{\Game e^{-\frac{\mu_\beta + \mu_i + \mu_g k}{\mu_f \mu_g}}}{\mu_f^3 \mu_g^2 (\mu_i - \mu_\beta)} \left(e^{\frac{\mu_i}{\mu_f \mu_g}} \left(-\mu_\beta \mu_i \mathrm{Ei} \left(\frac{\mu_\beta}{\mu_f \mu_g} \right) (-\mu_f \mu_g + \mu_\beta + \mu_g k) \right. \right. \right.
$$
$$
\left. \left. \left. + \mu_\beta \mu_i (-\mu_f \mu_g + \mu_\beta + \mu_g k) \mathrm{Ei} \left(\frac{k\mu_g + \mu_\beta}{\mu_f \mu_g} \right) + \mu_f \mu_g^2 k (\mu_\beta - \mu_i) \right. \right. \right.
$$

Table 6.2: Mathematical Notations

Mathematical Notations used in the manuscript
$\zeta_1 = \prod_{j=1}^{I} \mu_j,\ \zeta_1^{\beta} = \mu_g \mu_\beta \prod_{j=1}^{I} \mu_j,\ \zeta_a = \prod_{\substack{j=1,l=1,\\ l>j}}^{I}(\mu_j - \mu_l)$
$\zeta_3 = \sum_{i=1}^{I} \log[\mu_i] \prod_{\substack{j=1,l=1,\\ j\neq i, j\neq l,\\ i\neq l}}^{I}(\mu_j - \mu_l),\ \zeta_4 = \mu_g \zeta_a,$
$\zeta_3^{\beta} = \sum_{j=1}^{I} \log[\mu_i] \prod_{\substack{j=1,l=1,\\ i\neq j, i\neq l,\\ j\neq l}}^{I}(\mu_j - \mu_l) + \log[\mu_\beta] \prod_{\substack{j=1,l=1,\\ i\neq j, i\neq l,\\ j\neq l}}^{I}(\mu_j - \mu_l)$
$\zeta_4^{\beta} = \mu_g \sum_{j=1}^{I} \log[\mu_i] \prod_{j=1,l=1,l>j}^{I}(\mu_j - \mu_l)(\mu_j - \mu_\beta),$

$$\left(-e^{\frac{\mu_\beta}{\mu_f \mu_g}}\right)\right) + \mu_\beta \mu_i \left(-e^{\frac{\mu_\beta}{\mu_f \mu_g}}\right) \text{Ei}\left(\frac{\mu_i}{\mu_f \mu_g}\right)\left(\mu_f \mu_g - \mu_i + \mu_g(-k)\right)$$

$$+ \mu_\beta \mu_i e^{\frac{\mu_\beta}{\mu_f \mu_g}}(\mu_f \mu_g - \mu_i + \mu_g(-k))\text{Ei}\left(\frac{k\mu_g + \mu_i}{\mu_f \mu_g}\right)\right)\bigg], \qquad (6.21)$$

with mean

$$\mathbb{E}[K_\beta] = \int_0^\infty K_\beta f_{K_\beta}(k)dk$$
$$= \frac{\zeta_1^{\beta} \zeta_3^{\beta}}{\zeta_4^{\beta}} + \frac{2}{\mu_f}, \qquad (6.22)$$

where $k > 0$ and $\mho = \sum_{i=1}^{I} \dfrac{\prod_{i=1}^{I} \mu_i}{\prod_{j=1, i\neq j}^{I}(\mu_j - \mu_i)}.$

Plugging in (6.16) and (6.22) into (6.7) and (6.8), we get (6.23) and (6.24), respectively.

$$C_{Erg} \leq \log\left(1 + \mathbb{E}[\gamma_l]\right),$$
$$\leq \log\left(1 + \left\{\frac{\zeta_1 \zeta_3}{\zeta_4} + \frac{2}{\mu_f}\right\}\right), \qquad (6.23)$$

Figure 6.2: PDF of SINR of STBC-NOMA for different values of ipSIC and $L = 4$.

and

$$
\begin{aligned}
C_{Erg}^{\beta} &\leq \log\left(1 + \mathbb{E}[\gamma_l^{\beta}]\right), \\
&\leq \log\left(1 + \left\{\frac{\varsigma_1^{\beta}\varsigma_3^{\beta}}{\varsigma_4^{\beta}} + \frac{2}{\mu_f}\right\}\right).
\end{aligned}
\tag{6.24}
$$

The values of ς_1, ς_3, ς_4, ς_1^{β}, ς_3^{β}, and ς_4^{β} are given in Table 6.2.

6.5   Numerical Results

In this section, we evaluate the performance of the proposed Alamouti-coded cooperative NOMA. We assume frequency-flat Rayleigh fading for both user-
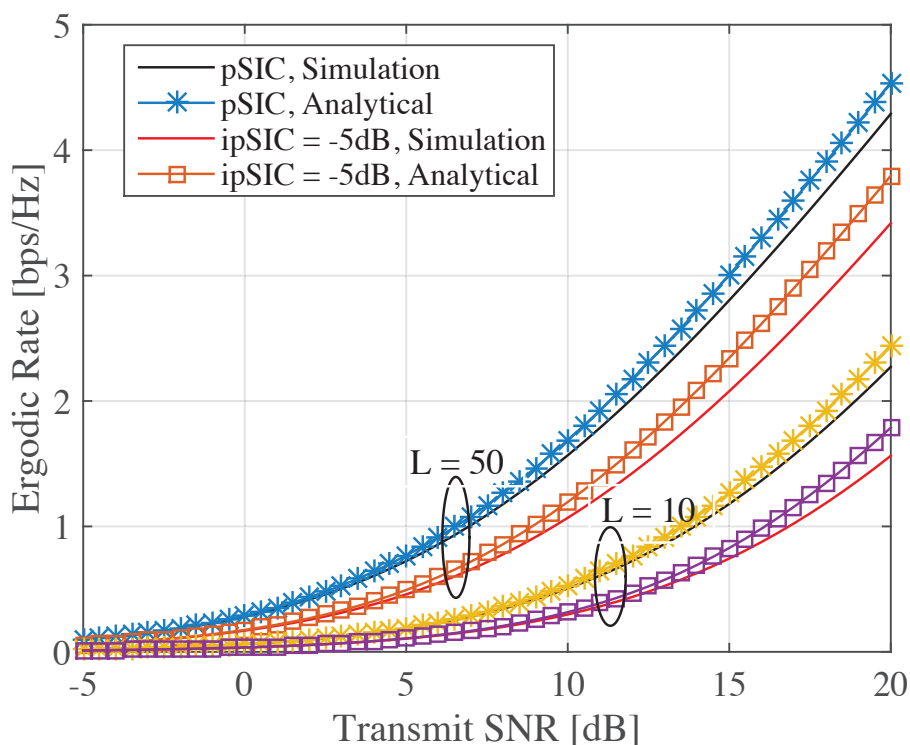
Figure 6.3: Simulation and analytical results for STBC-NOMA for pSIC / ipSIC and different number of users i.e., L = 10, 50.

to-user and BS-to-user channels. The maximum transmit power of the BS is 46dBm, whereas the maximum transmit power of each user is considered as 20dBm.

Fig. 6.2 shows the analytical and simulation results for the PDF of SINR of the STBC-NOMA system for $L = 4$. It can be noticed that simulation and analytical results closely match each other which verifies our analysis. It is obvious from Fig. 6.2 that the mean of SINR shifts towards zero level with the increase in the imperfection level of SICs. The higher the value of the ipSIC, the lower is the SINR value, which ultimately shifts the system towards higher outage probability.

Fig. 6.3 depicts the simulation and analytical results of STBC-NOMA for
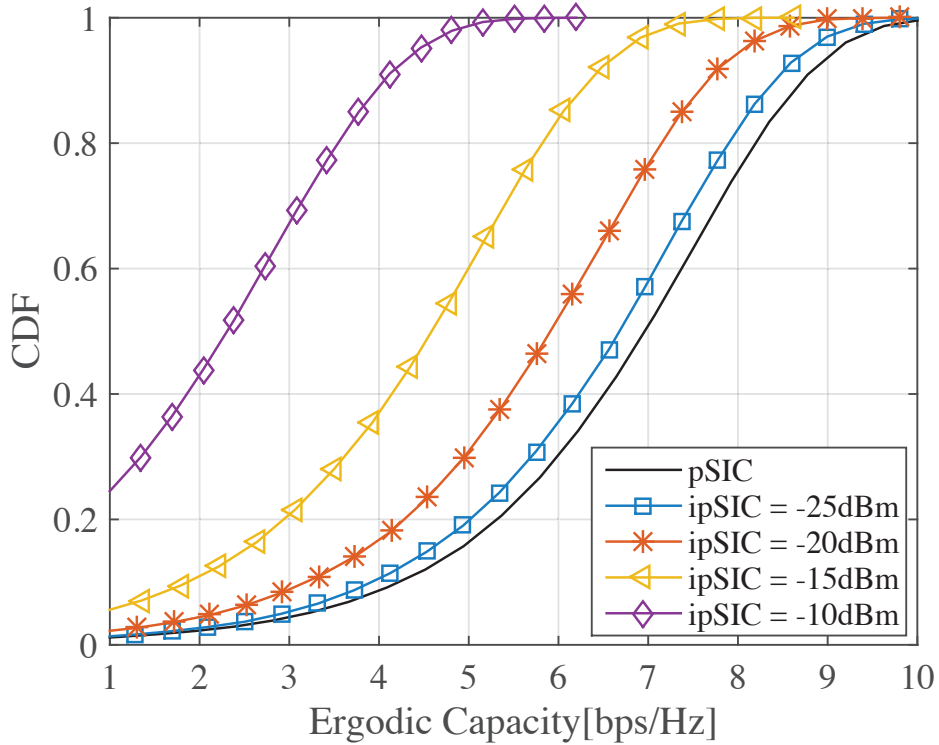
Figure 6.4: CDF of ergodic capacity of STBC-NOMA for different values of ipSIC and $L = 10$.

(6.23) and (6.24). The graph shows that there is a 3 dB SNR loss due to ipSIC = -5dB for $L = 50$ at the 2 bps/Hz of ergodic rate. Similarly, there is a 3 dB SNR loss due to ipSIC = -5dB for $L = 10$ at the ergodic rate of 1 bps/Hz.

Fig. 6.4 shows the cumulative distribution function (CDF) of the ergodic capacity of STBC-based cooperative NOMA, for different values of ipSICs (i.e., -10dBm, -15dBm, -20dBm, and -25dBm), with $L = 10$ and 20dB transmit SNR. It is shown that a lower level of ipSIC gives a higher value of ergodic capacity. It is noted that the system with perfect SICs achieves the maximum ergodic capacity. No user achieves the ergodic rate of greater than 5bps/Hz in STBC-NOMA with ipSIC = -10dBm, 40% of the users achieve
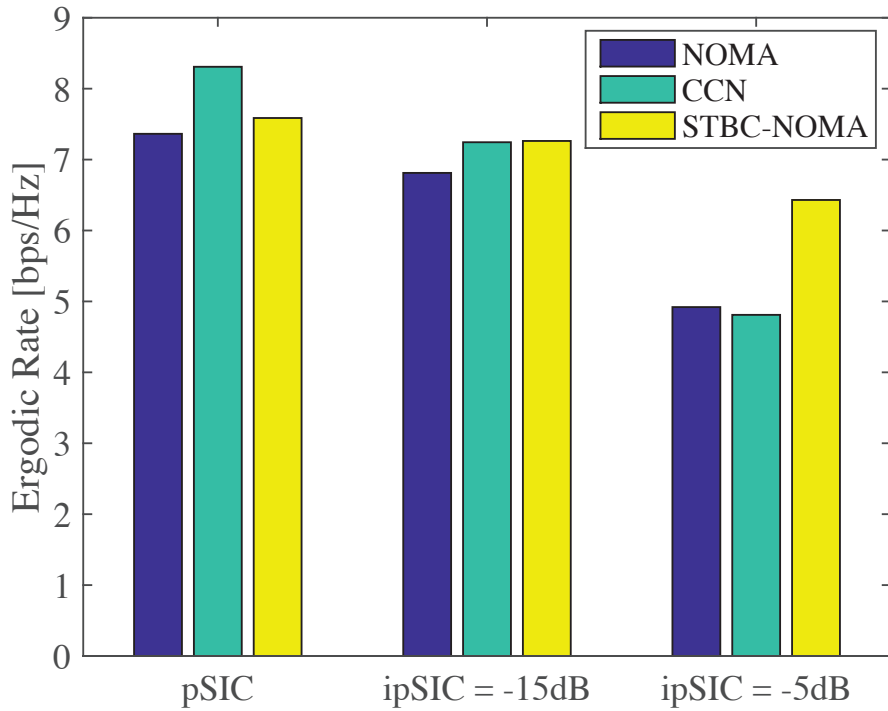
Figure 6.5: Ergodic capacity of conventional non-cooperative NOMA, CCN and STBC-NOMA for $L = 6$.

this rate with ipSIC = -15dBm, 70% of users achieve this rate with ipSIC = -20dBm, 80% with ipSIC=-25dBm, and 83% of the users achieve this rate with perfect SIC.

Fig. 6.5 shows the impact of ipSIC on the ergodic capacity of non-cooperative NOMA, CCN, and STBC-NOMA for $L = 6$. The overall power budget for each system under consideration (i.e., NOMA, CCN, STBC-NOMA) is considered to be the same to have fair comparative analysis between them. The result shows that the performance of non-cooperative NOMA, CCN, and STBC-NOMA decreases with the increase in the value of ipSIC. However, the impact of ipSIC on STBC-NOMA is less as compared to that of non-cooperative NOMA and CCN. In CCN, all of the strong users cooperate

with the weak user by transmitting composite NOMA signal to the weak user which significantly increases the SNR at the weak user, but at the cost of an exponential increase in the number of SICs. However, in the case of STBC-NOMA, only two strong users cooperate with the next two weak users by transmitting the messages of the next two users only by STBC transmission, whereas the number of SICs is not increased in the STBC-cooperation phase. This is the reason that for a higher number of users, a slight imperfection in the SIC implementations may lead to high-performance degradation in CCN, whereas the impact of imperfect SICs on STBC-NOMA is much less as compared to that of CCN. For example, the total number of SICs performed in CCN, for $L = 6$, is 10. However, non-cooperative NOMA and STBC-NOMA require only 6 SICs in this case. This shows that the impact of imperfection in SICs in CCN is much higher than that of STBC-NOMA. It is also shown that for a high value of ipSIC, the performance gap between CCN and STBC-NOMA expands with the increase in the total number of users because of imperfection in a higher number of SICs implemented in CCN.

6.6   Summary

This chapter provided a comprehensive analysis of the effects of imperfect SICs on the performance of STBC-based cooperative NOMA (STBC-NOMA). It is shown that STBC-NOMA outperforms the conventional non-cooperative NOMA as well as conventional cooperative NOMA in terms of complexity reduction and ergodic capacity, respectively, for a smaller number of users. It is also shown that for a high number of users and imperfect SICs, the STBC-NOMA outperforms both CCN and non-cooperative NOMA in

terms of ergodic capacity. Furthermore, the impact of imperfect SICs on the performance of STBC-NOMA is negligible as compared to CCN and conventional NOMA.

Chapter 7

Q-learning Approach for QoS-Aware NOMA

7.1 Introduction

Non-orthogonal multiple access (NOMA) provides an opportunity for multiple users to share the same frequency band simultaneously [89, 90]. In NOMA, a composite signal containing the messages of multiple users, multiplexed in the power domain, is transmitted to the users. Compared to the conventional orthogonal multiple access (OMA) schemes, NOMA enhances the access capabilities of users by allowing multiple users to utilize the resources at the same time. Traditional OMA schemes may not be suitable to handle tens of hundreds of communication devices. On the other hand, conventional NOMA also cannot accommodate devices with multiple service requirements in an efficient manner. In such a scenario, a novel method is required which may have the flexibility to handle multiple devices with different quality-of-service (QoS) requirements. Further, the network archi-

tecture can be intelligent enough to assign resources to the users as per their requirements.

Resource allocation is the key to attain high spectral efficiency (SE) in NOMA systems since the users in NOMA are distributed in the power domain. Prior research on NOMA is focused on assigning fixed values of power coefficient and bandwidth to all users in NOMA. The concern of this scheme is that the QoS of all users may not be assured. In [91], the authors propose a hybrid OMA-NOMA technique, based on successive bandwidth division for a higher number of users in the uplink. Although this technique improves the overall system throughput, it does not guarantee the QoS requirements of users with low data rate requirements along with low channel conditions.

Efficient resource allocation schemes for long-term evolution (LTE) systems are discussed in [92, 93, 94], in which the authors propose an OMA-based resource allocation scheme for delay-tolerant and non-delay tolerant users. The authors in [95] investigate the resource allocation problem in NOMA-based vehicle-to-infrastructure (V2I) network, but at the cost of high complexity. The authors in [96] propose a cascaded Hungarian resource allocation algorithm for high mobility heterogeneous network. However, this algorithm can only perform better in high distinctive channel conditions. An intelligent radio resource allocation framework is proposed to assign the resources to the IoT devices in [97]. In this work, the authors proposed an enhancement in the SE of the NOMA-based IoT network as compared to the OMA scheme. The authors in [98] quantify the performance of NOMA and OMA schemes in non-ideal conditions, i.e., the environment with high inter and intracellular and cluster interference. This work shows that the NOMA scheme cannot always perform better than the OMA scheme in non-ideal environmental conditions. A resource allocation algorithm for the downlink

NOMA-based heterogeneous network is designed in [99], in which vehicular users are assigned with the resources on a priority basis. The concern is of this algorithm is that the cellular user can be affected especially in a network with a high density of vehicular users. The authors in [100, 101], propose a cognitive radio-based NOMA scheme, in which the users with the worst channel conditions are considered as primary users, and therefore are provided with the resources (i.e., power, bandwidth) on a priority basis. The main concern of this scheme is that the users with good channel conditions are more affected and are always served at a later stage.

The above resource allocation schemes either try to optimize the power and/or the bandwidth to enable a robust system. However, to meet the requirements of next-generation communication systems, such as massive machine-type communication, high data rate, high SE, and low latency, there is a need for the development of a robust and intelligent resource allocation scheme that can tune various parameters simultaneously. Therefore, in this work, we propose a novel hybrid scheme based on Q-learning for massive connectivity in future networks. Specifically, a Q-learning-based QoS-aware bandwidth division NOMA, termed QBD-NOMA is proposed which can support a wide range of communication devices with non-uniform service requirements. Thus, the proposed algorithm can be employed in IoT networks with low data rates as well as with high data rates. The users with similar data rate requirements are assigned the same band such that the QoS requirements of all users are fulfilled. The proposed access scheme enhances the sum-rate and increases the number of users to be served with fewer resources (bandwidth, time, and power).
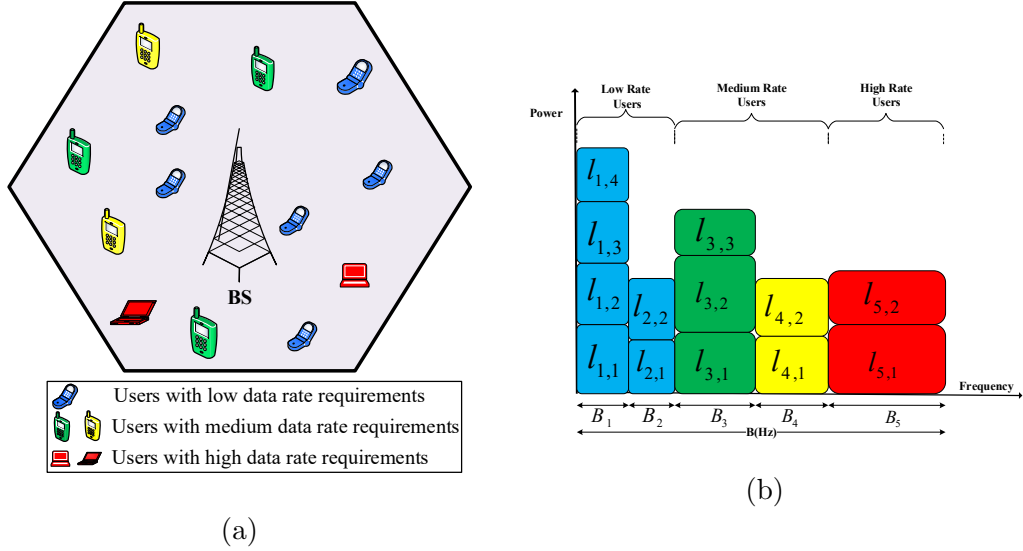
Figure 7.1: A system model with the proposed QBD-NOMA scheme. (a) A system model with a BS and the users with diverse data rate requirements, (b) The proposed QBD-NOMA scheme.

7.2   Scenario Description

Consider a downlink NOMA architecture with a single BS and L single-antenna users as shown in Fig. 7.1a. It is assumed that the users have highly diverse data rate requirements. In Fig. 7.1a, the blue and red colors represent the users with the lowest and the highest data rate requirements, respectively, whereas the yellow and the green colors represent the users with medium data rate requirements.

Fig. 7.1b shows the proposed QoS-aware BD-NOMA (QBD-NOMA), in which the users in each sub-band are accommodated as per their data rate requirements while ensuring the NOMA principle in each sub-band is fulfilled. Lets define the users in the sub-band b as $\Psi_{b,l} = \{l_{b,1}, l_{b,2}, l_{b,3}, \ldots, l_{b,L_b}\}$, where the total number of users in the sub-band b is L_b. Without the loss of generality, the users are arranged according to the power domain NOMA

principle, i.e., $|h_{b,1}|^2 \geq |h_{b,2}|^2 \geq |h_{b,3}|^2 \geq \cdots \geq |h_{b,L_b}|^2$, where the channel between the BS and the user l in the sub-band b, $h_{b,l}$, is a flat fading Rayleigh channel and the power allocated to the user l in the sub-band b is $p_{b,l}$. Let $\Psi_j = \{j_1, j_2, j_3, \ldots, j_J\}$ is a set of data rates, where J is the cardinality of the set Ψ_j. Without the loss of generality, we assume that j_1 is the lowest data rates set, i.e., it represents a range of data rates which have low values, whereas j_J is the highest data rates set. Let B be the available system bandwidth with $\Psi_b = \{B_1, B_2, B_3, \ldots, B_Q\}$ denotes a set of sub-bands, such that $\sum_{b=1}^{Q} B_i = B$, where Q is the total number of sub-bands and $J \leq Q$. We assume that the sum of powers allocated to all users is less than or equal to P_{noma}, i.e., $\sum_{b=1}^{Q} \sum_{l=1}^{L_b} p_{b,l} \leq P_{\text{noma}}$, where P_{noma} is the maximum power of the BS.

The received signal at the user l in the sub-band b is given as

$$y_{b,l} = h_{b,l} \sum_{l=1}^{L_b} \sqrt{p_{b,l}} s_{b,l} + n_{b,l}, \tag{7.1}$$

where $s_{b,l}$ is the message, $p_{b,l} = \phi_{b,l} P_{\text{noma}}$ is the assigned power, and $n_{b,l}$ is the zero mean additive Gaussian noise of user l in sub-band b. In $p_{b,l}$, $\phi_{b,l}$ is the power coefficient and P_{noma} is the total power transmitted by the BS. The instantaneous SINR at the user l in the sub-band b is given by

$$\gamma_{b,l} = \frac{|h_{b,l}|^2 p_{b,l}}{\sum_{i=1}^{l-1} |h_{b,l}|^2 p_{b,i} + \sigma_b^2}, \tag{7.2}$$

where σ_b^2 is the noise power in the sub-band b. The strong users, i.e., $1 \leq l \leq L_b - 1$, in each sub-band, apply the SIC to the composite NOMA signal to subtract the messages of weak users and detect their own message. The

signal-to-noise ratio (SNR) for the strongest user is thus given as

$$\gamma_{b,1} = \frac{|h_{b,1}|^2 p_{b,1}}{\sigma_b^2}. \tag{7.3}$$

The data rate of the user l in the sub-band b in the system is given as

$$C_{b,l} = B_b \log_2(1 + \gamma_{b,l}). \tag{7.4}$$

Consequently, the sum rate of all users is given as

$$C_{\text{sum}} = \sum_{b=1}^{Q} \left(B_b \sum_{l=1}^{L_b} \log_2(1 + \gamma_{b,l}) \right). \tag{7.5}$$

In the next section, we evaluate and the resource allocation and optimization problem.

7.3   Resource Allocation and Optimization Problems

In this section, we focus on the efficient utilization of bandwidth, ultimately accommodating the maximum number of users, with an available power budget. The cumulative target data rate of users in the sub-band b is given by

$$\Omega_b = \sum_{l=1}^{L_b} \Omega_{b,l}, \tag{7.6}$$

where $\Omega_{b,l}$ is the desired/target data rate of the user l in the sub-band b. Similarly, the cumulative target sumrate of users in all sub-bands is given by

$$\Omega_{\text{sum}} = \sum_{b=1}^{Q} \Omega_b. \tag{7.7}$$

The objective of our optimization problem is to assign the power to the user l in sub-band B_b to maximize the SE in that sub-band while providing all users in that sub-band with their required data rates. The bandwidth allocation problem such that the sum-rate of all users in sub-band b is maximized is defined as

$$\max_{\Psi_b} \quad \sum_{l=1}^{L_b} C_{b,l} \tag{7.8a}$$

$$\text{subject to} \quad \sum_{b=1}^{Q} B_b \leq B, \tag{7.8b}$$

$$L_b \geq 1, \forall b \tag{7.8c}$$

$$C_{b,l} \geq \Omega_{b,l}, \forall l = \{1, \ldots, L_b\} \ \ \& \ \ \forall b \in \Psi_b. \tag{7.8d}$$

Here the objective (7.8a) is to find the optimal width of each sub-band and optimal number of sub-bands that maximizes the capacity of users in each sub-band b providing all users in the sub-band b achieve their target data rate. The constraint (7.8b) refers to the sub-band limitations for all users, whereas (7.8c) ensures that each allocated sub-band can have at least one user. The constraint (7.8d) guarantees that the instantaneous data rate of the users in the sub-band b is not less than the required data rate.

Similarly, by defining the vector $\tilde{p} = \{p_1, p_2, p_3, \ldots, p_{L_b}\}$ containing the power assigned to the users in sub-band B_b, the power allocation problem such that sum-rate of all users in sub-band b is maximized, can be redefined

as

$$\max_{\tilde{p}} \quad \sum_{l=1}^{L_b} C_{b,l} \tag{7.9a}$$

$$\text{subject to} \quad \sum_{b=1}^{Q} \sum_{l=1}^{L_b} p_{b,l} \leq P_{\text{noma}}, \tag{7.9b}$$

$$p_{b,l} \geq 0, \forall l, \tag{7.9c}$$

$$C_{b,l} \geq \Omega_{b,l}, l = \{1, \ldots, L_b\}. \tag{7.9d}$$

Here the objective (7.9a) is to find the optimal power that maximizes the capacity of users in the sub-band b providing all users in the sub-band b with their required data rates in (7.9d). The constraint (7.9b) refers to the power limitations for every user in the sub-band b.

It is very difficult to maintain a 100% coverage probability for any algorithm due to limited radio resource availability. However, the proposed algorithm enhances the number of users in coverage by optimizing the inter-user interference at each user at an optimum level and ultimately enhancing the SINR level at each user. We define the outage probability of a user as $\mathbb{P}[C_{b,l} \leq \Omega_{b,l}]$, and its complimentary event, i.e., the success probability is given as

$$\mathbb{P}[C_{b,l} \geq \Omega_{b,l}] = 1 - \mathbb{P}\left[\frac{|h_{b,l}|^2 p_{b,l}}{\sum_{i=1}^{l-1} |h_{b,l}|^2 p_{b,i} + \sigma_b^2} < 2^{\Omega_{b,l}} - 1 \right]$$

$$= 1 - \mathbb{P}\left[\frac{|h_{b,l}|^2 \phi_{b,l}}{\rho\left(\sum_{i=1}^{l-1} |h_{b,l}|^2 \phi_{b,i} \right) + 1} < \frac{2^{\Omega_{b,l}} - 1}{\rho} \right]$$

$$=1 - \mathbb{P}\left[|h_{b,l}|^2 \le \frac{\tilde{\rho}\left(\rho\sum_{i=1}^{l-1}|h_{b,l}|^2\phi_{b,i} + 1\right)}{\phi_{b,l}}\right]$$

$$= \exp\left(-\frac{\lambda_h\tilde{\rho}}{\phi_{b,l} - \left(\sum_{i=1}^{l-1}\phi_{b,i}\right)(2^{\Omega_{b,l}} - 1)}\right)$$

$$\sim 1 - \frac{\lambda_h\tilde{\rho}}{\phi_{b,l} - \left(\sum_{i=1}^{l-1}\phi_{b,i}\right)(2^{\Omega_{b,l}} - 1)}, \tag{7.10}$$

where $\tilde{\rho} = \frac{2^{\Omega_{b,l}}-1}{\rho}$, $\phi_{b,l}$ is the power coefficient assigned to the user l in the sub-band b, and $\rho = \frac{p_{b,l}}{\sigma_b^2}$ is the transmit SNR at the user l in the sub-band b.

The interference term in the denominator of (7.2) reflects that the optimization problems in (7.8) and (7.9) are non-convex. It is very difficult to solve the non-convex problem for a large number of users per sub-band, especially for the low-power IoT devices when the power is highly limited and strong interference from NOMA users affects the QoS requirements of IoT device. It can be noticed that the problems shown in (7.8) and (7.9) are mixed-integer non-linear optimization problems, which are prohibitive to solve analytically. However, (7.8) and (7.9) can be combined and optimized together for the objective of enhancement of the sum rate of the overall network subject to the power and rate constraints. Therefore, in the next section, we propose a Q-learning-based approach to solve these joint problems.
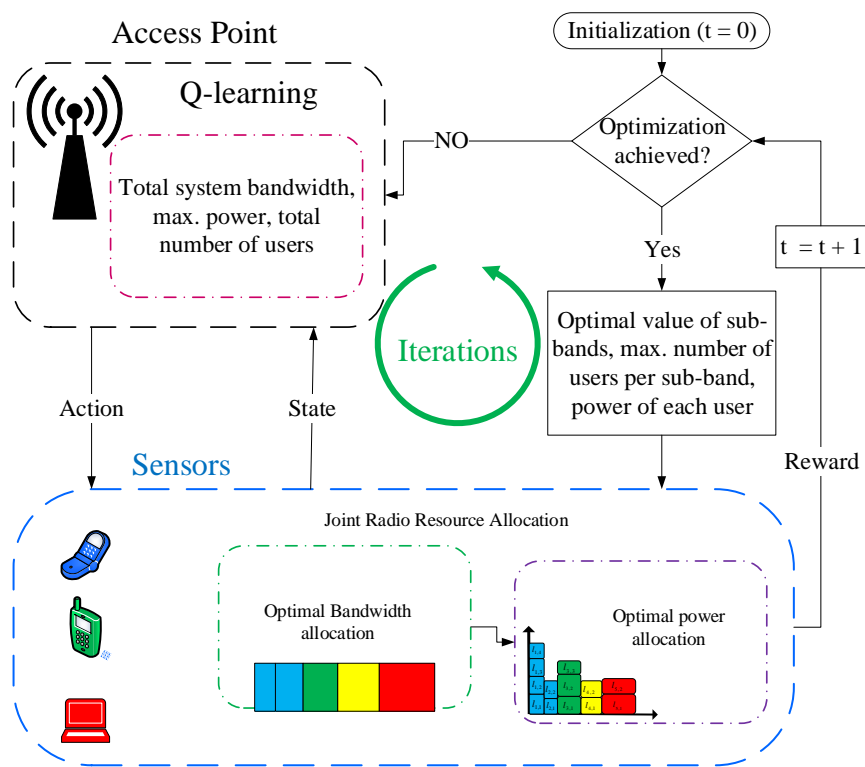
Figure 7.2: Illustration of Q-learning framework.

7.4   *Q*-learning Framework for the Robust Resource Allocation

Reinforcement learning provides a learning framework in which the agent (BS) improves its performance by performing an action in the environment and receiving rewards for achieving the goals and punishment for the failure. In this section, we focus on the learning framework specifically the application of Q-learning at the BS for an optimal allocation of sub-bands and power to the users in the described NOMA network scenario.

7.4.1 Q-Learning Framework

The arrangement of the users in each sub-band can be managed such that the overall sum rate and the SE of the system are enhanced. The QoS requirements of users are changing constantly, which requires the rearrangement of the users in different sub-bands and allocation of respective resources with time. It is generally difficult to design a protocol for the transition from one state to another. Therefore, we adopt the Q-learning algorithm to assign optimum resources to the users, which is illustrated in Fig. 7.2. At each time t, the BS interacts with the users in its coverage area and observes the state s, which is the channel conditions and the required data rate of each user. For each time instant t, the state, action, learning policy, and the reward function are defined as follows

- **State:** State-space is a set of states $s \in \mathbb{S} = \{1, 2, 3, \ldots, \mathcal{S}\}$ indicating key performance indicators (KPIs) of the system, where $\mathcal{S}$ is the total number of states. A state, in our system under consideration, is the channel condition and the target data rate of the user.

- **Action:** Action-space is the set of possible actions $a \in \mathbb{A} = \{1, 2, 3, \ldots, \mathcal{A}\}$ to be taken against the observed state, where $\mathcal{A}$ is the total number of actions. Action is the allocation of power or sub-channel or both. The agent can assign any level of power or sub-band to the users according to the state observed. Further, the agent can also increase or decrease the number of users in each sub-band and/or number of sub-bands allocated to the users.

- **Cost or Reward:** A certain goal is set as a benchmark for each user, and each user must achieve that goal. In this optimization problem, we define the goal in terms of the required data rate of the user (i.e., it

should meet the data rate threshold). If the user achieves the required data rate level, then the user is given a reward by improvement in SE otherwise it is punished by assigning no improvement in SE. The reward function is given as

$$r_{b,l}(s,a) = \frac{\Omega_{\text{sum}}}{C_{\text{sum}}}\Big(C_{b,l} - \Omega_{b,l}\Big), \tag{7.11}$$

where C_{sum}, Ω_{sum}, and $C_{b,l}$ are given in (7.5), (7.7), and (7.4), respectively.

- **Learning Policy:** The BS can learn the optimum action selection policy by properly evaluating its past experience and consequences of actions. The policy or strategy, π, of the BS is a mapping between states $s \in \mathbb{S}$ and the actions $a \in \mathbb{A}$, which is denoted as $\pi : s \to a$. The goal of the BS is to obtain robust and optimum policy $\pi^*(s)$ for all states that can give the maximum reward in terms of enhancement in the overall capacity and reduction in the outage probability of the network. The optimum state transition policy $\pi^*(s)$ is given by

$$W^{\pi}(s) = W^{\pi^*}(s) = \max_{a'}\Big(r_{b,l}(s,a) + \beta \sum_{w \in \mathbb{S}} P_{s,w} W^*(w)\Big), \tag{7.12}$$

where $r_{b,l}(s,a)$ is the reward for taking the action a in the state s, $a' \in \mathbb{A}$ is the next possible action that maximizes the reward and $P_{s,w}$ is the probability of transition from state $s \to w$ given by

$$P_{s,w} = \frac{e^{Q_{b,l(s,a)}}}{\sum_{a \neq a'} e^{Q_{b,l}(s,a')}}. \tag{7.13}$$

The proposed system goes to the new state due to a state-action learning policy [102]. This policy is built during the exploration step and is

exploited during the exploitation stage. In the Q-learning algorithm, a ε-greedy learning policy is adopted. The agent, during the exploitation step, tests all the possible actions for a certain state and observes the reward.

The action, for each state, with the best reward is noted in the state-action lookup table. In such a way, with the help of state-action learning policy, a complete lookup table termed as the Q-table is built for all possible states and actions. At the initial stage, random action is taken with the help of the ε-greedy algorithm, and the corresponding reward is observed. The value of ε is the probability of selecting the random action. A Q-value is updated after applying an action to a certain state as [103]

$$Q_{b,l}(s,a) \leftarrow \cdot Q_{b,l}(s,a) + \alpha \cdot (r_{b,l}(s,a) \quad + \beta \cdot \max_{a'} Q_{b,l}(s',a') - Q_{b,l}(s,a)),$$

$$(7.14)$$

where $\beta \in [0,1]$ is the discount factor, and $0 \leq \alpha \leq 1$ is the learning rate. The value of α in the exploration phase is started by 0 and it approaches 1 with the convergence of the algorithm. A better strategy or policy is made by updating the Q-value attractively by applying different actions at all states.

The BS interacts with the users at any time instant t in its environment in the following procedure

7.4.2   Sub-bands and power swapping strategy for users

As discussed above, the resource allocation problem to the users in QBD-NOMA is a many-to-many matching problem. The SINR of each user in a

sub-band is depending upon the number of users in that sub-band. A higher number of users per sub-band leads to a higher value of interference to strong users and vice versa. Furthermore, the BS considers the association of each user to each sub-band. Also, the BS considers the allocation of powers to each user in each sub-band.

The preference of the users over the sub-band can be formulated as the achievable rate of that user, i.e., $C_{b,l}$. Therefore, the BS formulates the preferences on the set of users Ψ_l as in (7.5). Therefore, for any two users $l \in \Psi_l$ and $l' \in \Psi_l$, where $l \neq l'$, any two sub-band matching $b \in \Psi_b$ and $b' \in \Psi_b$, where $b \neq b'$, we can have following relation

$$(b, l) \succ_{BS} (b', l) \Leftrightarrow C_{b,l}(\Psi_b) > C_{b',l}(\Psi'_b), \qquad (7.15)$$

where Ψ_l is the set of users in all sub-band. Eq. (7.15) shows that the BS prefers the user l in sub-band b to the user l in sub-band b' only if the user l achieves a higher data rate in sub-band b then that of in sub-band b', We define the power matching problem as

$$(p_{b,l}, l) \succ_{BS} (p'_{b,l}, l) \Leftrightarrow C_{b,l}(\Psi_b) > C'_{b,l}(\Psi_b), \qquad (7.16)$$

which indicates that the BS prefers the power $p_{b,l}$ to the $p'_{b,l}$ only if the BS gets higher data rate from the $p_{b,l}$.

Based on these established preferences, we use the Q-learning algorithm to construct the matching state between the users, sub-bands, and the allocated powers. Furthermore, the sub-band swap operation is employed to further enhance the SE and capacity of the network.

Initially, three sub-bands are allocated to the users as per their initial three sets of required data rates, i.e., low, medium, and high. Then, the

algorithm proposes the number of sub-bands and the width of each sub-band based on their priority list. At the acceptance phase, the BS accepts the users in sub-band with prior preferences and rejects the others. Similarly, in each sub-band, initially, fixed power coefficients are assigned to the users in each sub-band and the algorithm proposes the power level for each user as per its preferences list. The BS, in the acceptance phase, accepts the power levels for each user with prior preferences and rejects the other. Finally, the algorithm converges to the optimal power levels for each user in each sub-band, an optimal number of users in each sub-band, the optimal number of sub-bands, and the optimal width of each sub-band. In the next sub-section, we evaluate the complexity of the QBD-NOMA system. Algorithm 1 shows the Q-learning-based algorithm for the proposed QBD-NOMA system based on the above analysis.

7.4.3   Complexity Analysis

The complexity of the Q-learning algorithm is evaluated by the search time. The larger the size of state space $\mathbb{S}$, the longer is the search time. In case of a single BS (single agent) and the set of state-space $\mathbb{S}$, with a finite number of iterations and fixed value of ε for ε-greedy action-selection policy, its complexity is upper bounded by $\mathcal{O}(\mathcal{S} \log(\mathcal{S}) \log(1/\varepsilon)/\varepsilon^2)$, where $\mathcal{S}$ is the cardinality of the set of state-space $\mathbb{S}$ [104]. The optimal exhaustive research, on the other hand, has the complexity of the order $\mathcal{O}(\mathcal{A})$, where $\mathcal{A}$ is the cardinality of the set of possible actions $\mathbb{A}$.

Algorithm 1 Q-Learning algorithm for the sum-rate optimization in a hybrid OMA-NOMA network.

Input: Total number of users L, the total bandwidth of B (Hz), and maximum allowable power P_{noma}.

Output: Total number of sub-bands Q, the width of each sub-band B_b (Hz), and power allocated to each user in sub-bands.

Initialization :

 1: Arrange users as per their data rate requirements, divide the users initially into three categories, i.e., low rate users, medium rate users, and high rate users as shown in Fig. 7.1a.

 2: Assign three sub-bands to the users, each sub-band to one category of the users, and arrange the users in each sub-band as per the NOMA principle.

 3: For each sub-band, start Q value $Q_{b,l}(0,0) = 0$.

 4: **for** each state $s \in \mathbb{S}$ **do**

 5:   **if** $(\mathrm{rand}(.) < \varepsilon)$ **then**

 6:     • Assign fixed power and width of sub-band to the users in each sub-band.

     • Observe the new state $s' \in \mathbb{S}$ due to assignment of power and sub-band as an action a.

     • Take the immediate reward as in (7.11).

     • Change the action, $a \in \mathbb{A}$, i.e., increase or decrease in power assigned to the user, number and width of sub-bands, and number of users in each sub-band according to the new state s' by using (7.15) and (7.16).

     • Transition from state $s \to s'$ leads the change in the Q-value which is required to be updated as in the Q-table according to (7.14).

 7:   **end if**

     • Repeat the process until optimization is achieved and algorithm converges to optimal number of sub-bands Q^*, optimal values of power levels assigned to each user in each sub-band $p_{b,l}^*$, and optimal number of users in each sub-band L_b^*.

 8: **end for**=0

7.4.4 Comparison with OMA and NOMA

To compare the performance of OMA, conventional NOMA, BD-NOMA, and the proposed QBD-NOMA schemes, we formulate the achievable data rates and outage probability constraint for all of these schemes in this section. We denote $\Psi_l = \{l_1, l_2, l_3, \ldots, l_L\}$ a set of all users. The achievable data rate of the user l in the OMA and NOMA schemes is given by

$$C_l^{\text{oma}} = \frac{B}{L} \log_2 \left(1 + \frac{|h_l|^2 p_l}{\sigma_{\text{oma}}^2} \right), \tag{7.17}$$

and

$$C_l^{\text{noma}} = B \log_2 \left(1 + \frac{|h_l|^2 p_l}{\sum\limits_{i=1}^{l-1} |h_l|^2 p_i + \sigma_{\text{noma}}^2} \right), \tag{7.18}$$

respectively, where h_l, p_l, σ_{oma}^2, and σ_{noma}^2 are the channel coefficient, power, the noise power in the OMA scheme, and the noise power in the NOMA scheme for user l, respectively. The achievable data rate of the user l with QBD-NOMA is given in (7.4). Similarly, the outage probability of the user l in the OMA and NOMA is given as

$$P_{out,l}^{\text{oma}} = 1 - P(C_l^{\text{oma}} \geq \Omega_l), \tag{7.19}$$

and

$$P_{out,l}^{\text{noma}} = 1 - P(C_l^{\text{noma}} \geq \Omega_l), \tag{7.20}$$

respectively.
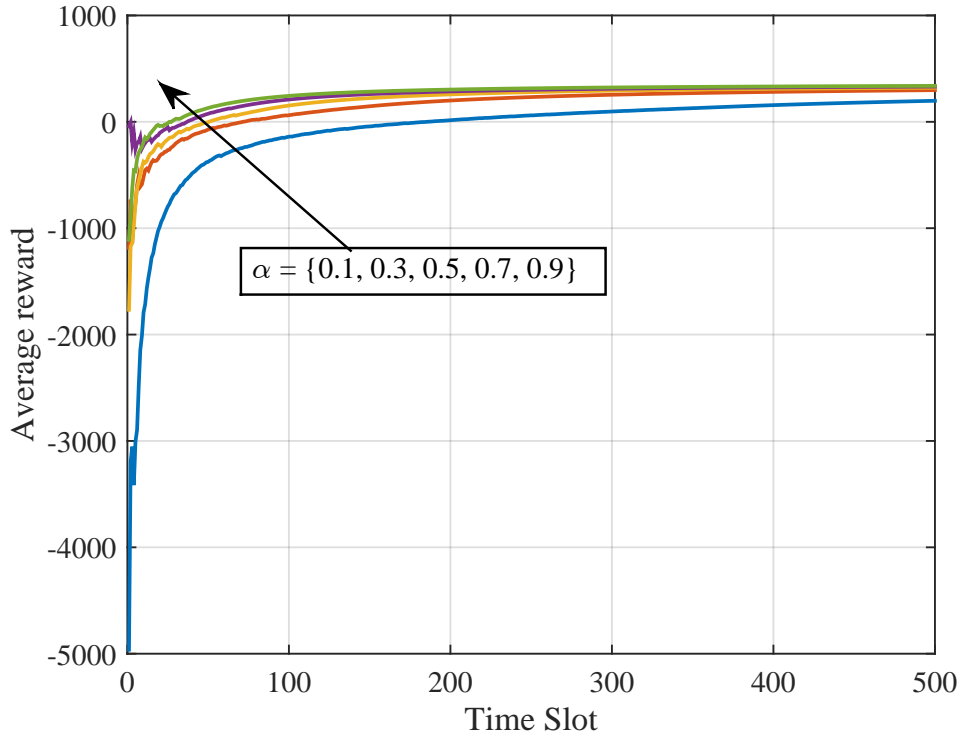
Figure 7.3: Influence of learning rate on allocation of sub-band and power for QBD-NOMA with $L = 20$ and $B = 20$MHz.

7.5   Simulation Environment and Evaluation

In this section, we evaluate our proposed QBD-NOMA scheme by conducting simulations and comparing the results with conventional approaches.

7.5.1   Simulation Environment

Our simulation environment comprises of one BS and L users uniformly distributed in the coverage area. We assume that the data rates of all the users are also uniformly distributed in the interval of [5 kbps 10 Mbps], (i.e., [5 $kbps$, 10 $Mbps$]) unless otherwise stated. The maximum transmit power at the BS is 45dBm and the power spectral density of the noise is considered as
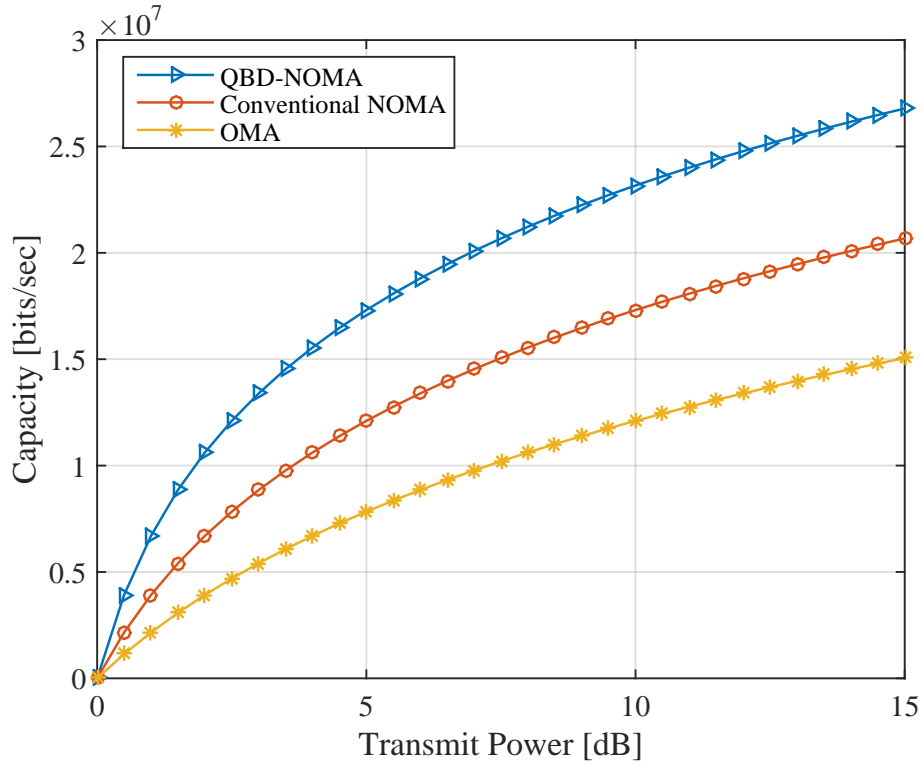
Figure 7.4: Sum-rate comparison between NOMA and QBD-NOMA schemes with $L = 20$ and $B = 1$MHz.

-173 dBm/Hz. We evaluate our system at bandwidth $B = \{20, 40, 60\}$ MHz. The results are averaged over 1e5 Monte Carlo simulations.

7.5.2   Evaluation

Fig. 7.3 depicts the influence of learning rate α on the convergence of QBD-NOMA, where the total bandwidth $B = 20$MHz and the total number of users $L = 20$. It is observed that with $\alpha = 0.1$, the algorithm cannot learn the action selection policy, however, the algorithm learns quickly as α approaches to 1.

Fig. 7.4 shows the comparison of capacity against the transmit power for
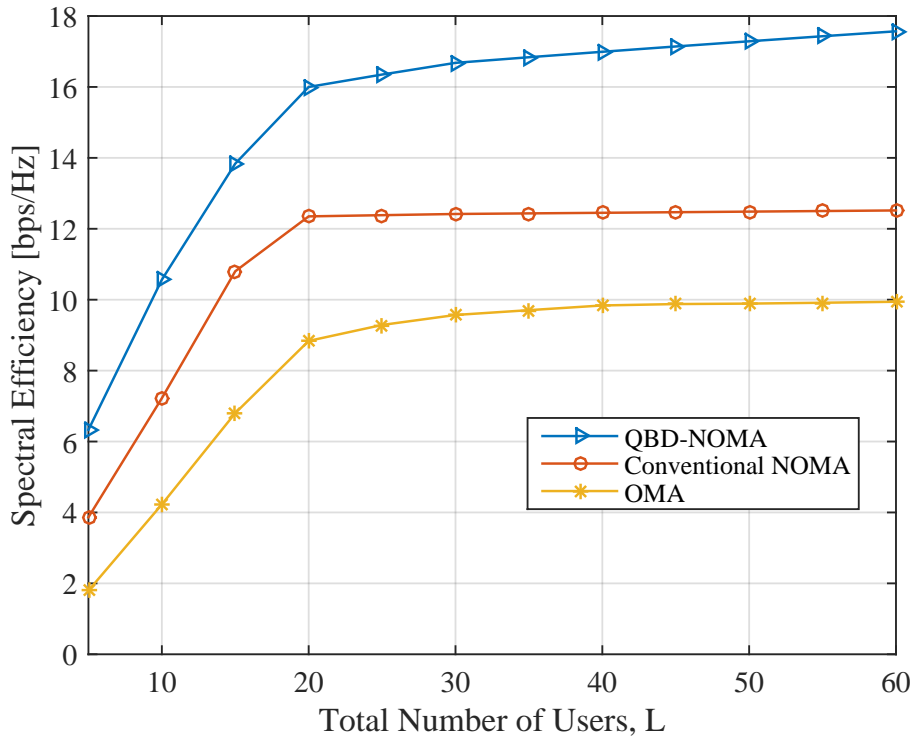
Figure 7.5: Spectral efficiency comparison with increasing number of users for $B = 20$ MHz, $P_{\mathrm{noma}} = 45$ dBm, and the required data rates of the users are in the range [100, 10000] kbps.

different schemes with $L = 20$ and $B = 1$MHz. The complete bandwidth B is allocated to all users in the direct NOMA (or conventional NOMA) scheme. It is noted that QBD-NOMA outperforms conventional NOMA and OMA schemes. The conventional NOMA scheme is less practical for a higher number of users due to the high number of SICs to be performed at each user. Also, low rate users are affected more due to the strong interference from high rate users in the direct NOMA scheme, whereas the QBD-NOMA scheme resolves this issue by arranging the users to the respective sub-bands according to their data rates. A learning algorithm for the

Fig. 7.5 shows the SE comparison of QBD-NOMA, conventional NOMA,
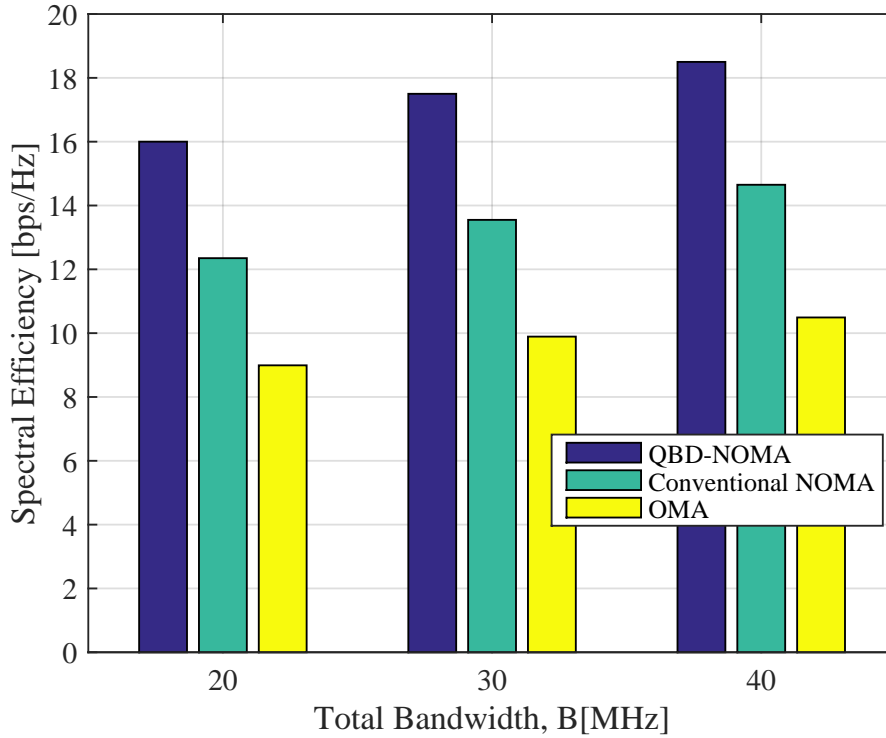
Figure 7.6: Spectral efficiency comparison for $L = 20$ and $B = \{20$ MHz, 30 MHz, 40 MHz$\}$ at $P_{\mathrm{noma}} = 15$ dB.

and OMA schemes for a range of users. The total bandwidth of B allocated for all schemes is 20MHz and transmit power is 45dBm. The required data rates of all users are uniformly distributed in the range of 100kbps to 10Mbps. It can be observed that QBD-NOMA outperforms the conventional NOMA and OMA schemes for all cases. Furthermore, it is observed that the performance gap between QBD-NOMA and conventional NOMA increases with the increase in the total number of users. It is also noted that the increase in SE of conventional NOMA is negligible for a higher number of users due to a decrease in SINR because of a substantial increase in the interference from strong users to weak users.

Fig. 7.6 shows the SE of QBD-NOMA, conventional NOMA, and OMA
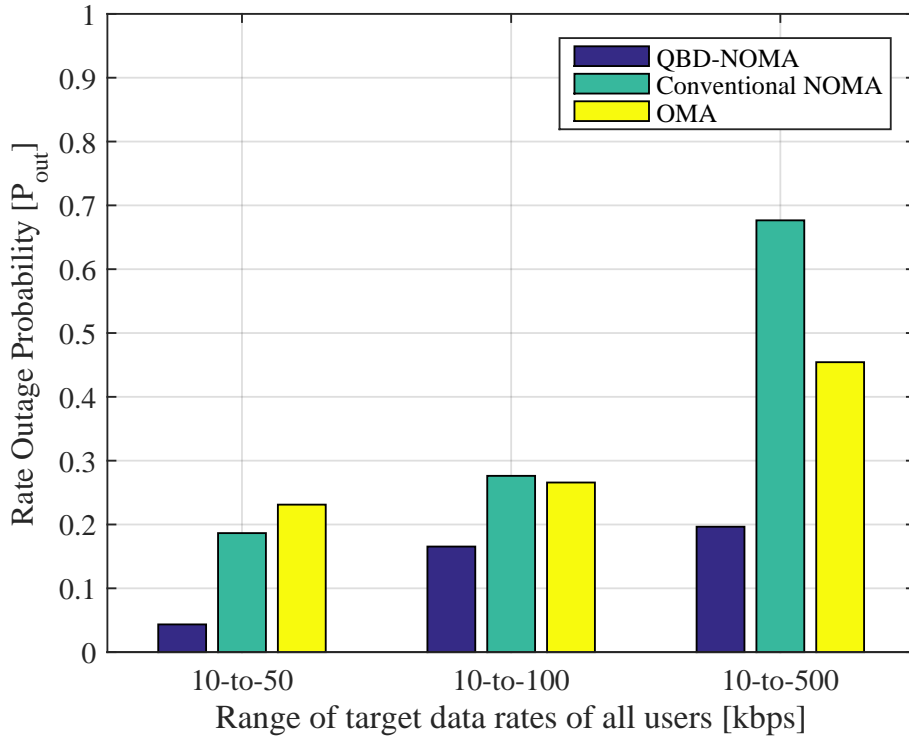
Figure 7.7: System level outage performance of OMA, NOMA, and QBD-NOMA for $L = 60$ and $B = 10$ MHz.

schemes for $L = 20$, transmit power of 45 dBm, and B={20MHz, 30MHz, 40MHz}. It is noted that QBD-NOMA outperforms the QBD-NOMA, conventional NOMA, and OMA schemes for all cases. It is also observed that the performance of the OMA scheme improves significantly with the increase in total bandwidth.

Fig. 7.7 depicts a comparative analysis of the system level outage probability performance of the OMA, the NOMA, and the proposed QBD-NOMA schemes for the users having multiple ranges of target data rates (i.e., 10 kbps-to-50 kbps, 10 kbps-to-100 kbps, and 10 kbps-to-500 kbps) with a bandwidth of 10 MHz and the total number of users is 60. It is observed that for the target data rate range of 10 kbps-to-50 kbps, the outage probability of

Figure 7.8: Average number of users in outage with respect to bandwidth versus total number of users for OMA, NOMA, and QBD-NOMA schemes with data rate range [1, 1000] kbps at $P_{\mathrm{noma}} = 45$ dBm.

QBD-NOMA is 0.05, whereas the outage probability of OMA and NOMA schemes for this range of target data rates is 0.23 and 0.28, respectively. Similarly, with the increase in the range of target data rates of the users, there is an increasing trend in the outage probabilities of all three schemes. However, the QBD-NOMA scheme is least affected by the inculcation of high target data rate users in the system due to the intelligent assignments of resources (sub-bands and powers) to the users. For example, for the range of target data rates of the users of 10 kbps-to-100 kbps, only 17% of the users experience an outage with the QBD-NOMA scheme, whereas OMA and NOMA schemes have 28% and 29% of the users, respectively, in an outage for the

same range of the target data rates of the users. Further, for the range of target data rates of the users of 10 kbps-to-500 kbps, 20% of the users go into outage in QBD-NOMA, whereas in OMA and NOMA schemes 45% and 68% of the users experience an outage, respectively.

Fig. 7.8 depicts a comparison in the number of users in outage versus the total number of users at $B = 10$ MHz and $B = 5$ MHz. In the simulation, we consider the total number of users from 5 to 40 with target data rate requirements from [1, 1000] kbps and transmit power of 45dBm. Fig. 7.8 shows that with the increase in the total number of users, there is an increasing trend in the number of users in an outage. However, the QBD-NOMA scheme has the least number of users in outages as compared to conventional NOMA and OMA schemes. Furthermore, it is observed that with the decrease in the system bandwidth, the number of users in outages increases. For example, for a total of 40 users and with the decrease in system bandwidth to half, there is 15%, 21%, and 23% increase in the number of users in an outage for QBD-NOMA, conventional NOMA, and OMA schemes, respectively.

Fig. 7.9 shows the trend of the number of users in outages by decreasing the transmit power. In the simulation, we consider the system bandwidth of 10MHz and the total number of users from 5 to 40 with target data rate requirements from [1, 1000] kbps. It is observed that for a total number of users of 40, and a transmit power of 30 dBm, there is a 21%, 32%, and 35%, increase in outage with QBD-NOMA, conventional NOMA, and OMA schemes, respectively, as compared to that of at 45 dBm of transmit power.
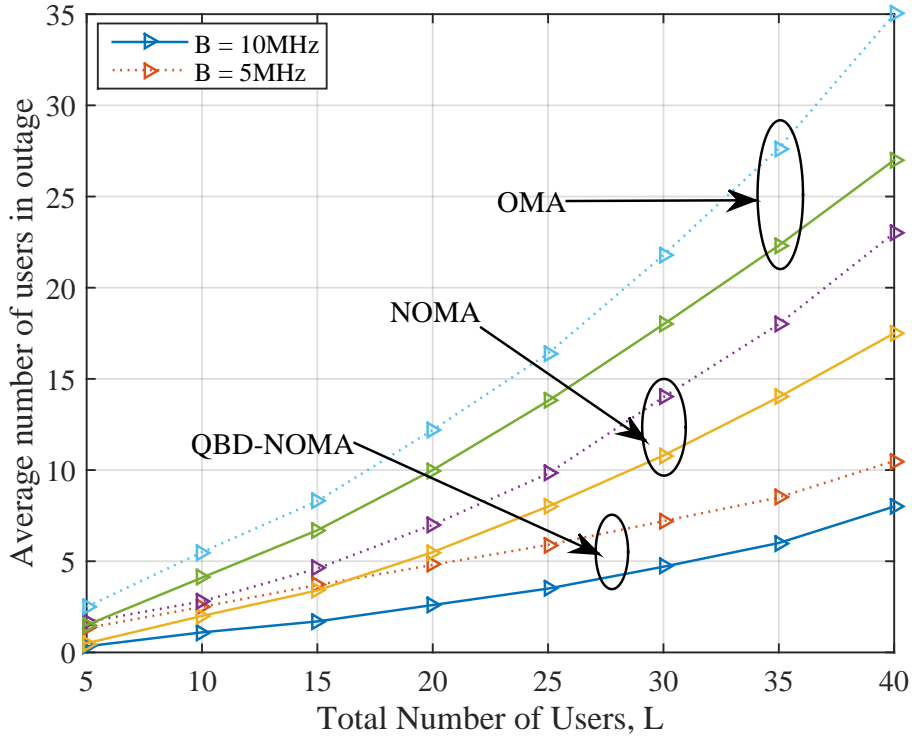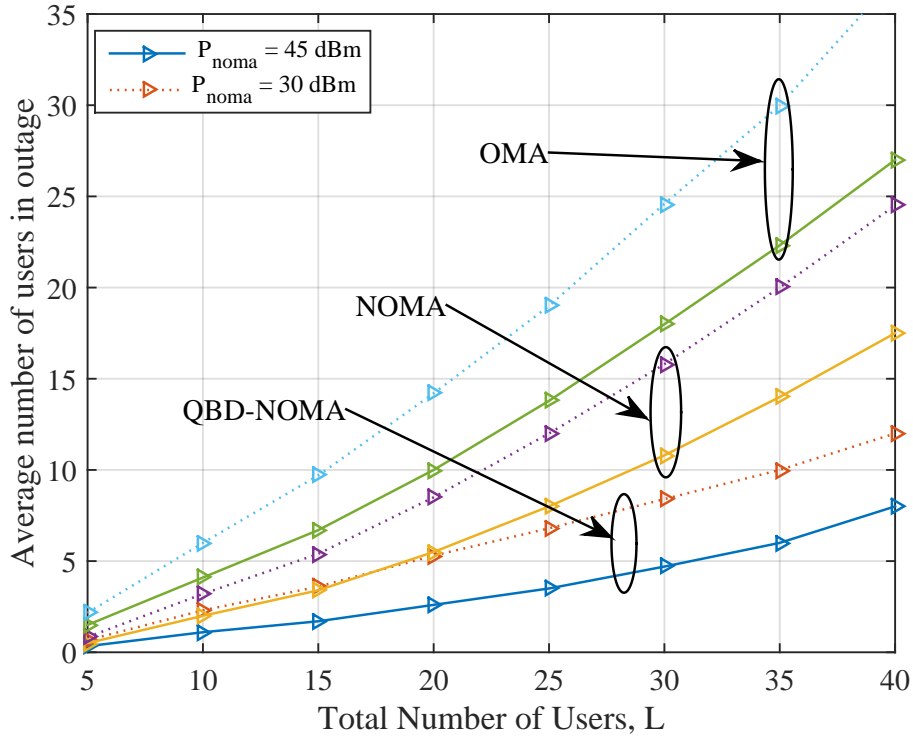
Figure 7.9: Average number of users in outage with respect to power versus total number of users for OMA, NOMA, and QBD-NOMA schemes with data rate range [1, 1000] kbps at $B = 10$ MHz.

7.6   Summary

In this chapter, we proposed a novel Q-learning-based QoS-aware NOMA scheme. In this scheme, we have exploited the interference optimization technique instead of interference mitigation or cancellation. Users are adjusted in different NOMA sub-bands according to their data rate ranges. System parameters such as the number of NOMA sub-bands and maximum allocated power are chosen in such a way that SE and overall throughput of the system are significantly enhanced. Furthermore, the number of devices with diverse data rate requirements can be significantly enhanced with a limited resource budget (i.e., power and bandwidth). It is investigated that the impact of

the number of users with high data rate requirements is more prominent because, with a limited resource budget, it is difficult to maintain the QoS of all users. However, QBD-NOMA with the aid of machine learning can decrease the number of users in an outage and increases the overall system throughput.

Chapter 8

Conclusion and Future Works

8.1 Conclusion and contributions

This research focuses on performance enhancement techniques in NOMA, which is known to be one exciting technology in future 5G/B5G/6G networks. Our main contributions, in this thesis, can be summarized as follows.

- To the best of our knowledge, it is the first comprehensive study on practical impairments in STBC-CNOMA. We present a theoretical framework including a signal model of an arbitrary user under the timing mismatch, imperfect SIC, and channel estimation error.

- We derive the probability distributions of the signal-to-interference-plus-noise ratio (SINR) for different combinations of the three impairments, which can be used in the STBC-CNOMA system design and operation. Based on the derived distributions, we also provide the closed-form expressions of outage probabilities, which are not present in prior arts.

- We also provide asymptotic rate (or capacity) outage probability in the high transmit signal-to-noise ratio (SNR) regime, which offers intuitive insights into how each of the three impairments hurts the performance of STBC-CNOMA.

- For the fair comparison with other cooperative NOMA protocols, we quantify the total number of SIC, the total number of required time slots, and the total number of transmissions of STBC-CNOMA with four existing schemes as functions of the number of user terminals.

- Numerical and simulation results are presented with different degrees of the three impairments. Through the comparison between analysis and simulation, we validate our analysis on the SINR distribution, exact and asymptotic capacity outage probabilities. Also, we compare the outage performance of STBC-CNOMA with CCN and non-cooperative NOMA.

- We intelligently assign the resources such as number of sub-bands, users per sub-band, and power allocated to users of each band in such a way that the versatile QoS requirements in a network are satisfied.

- Our proposed model is based on a hybrid OMA-NOMA scheme that exploits the characteristics of both OMA and NOMA and takes the help of Q-learning, and matching theory to optimize the resources.

- We optimize the inter-user interference by optimizing the number of users per sub-band, power of users in each sub-band, and width of each sub-band such that each user can achieve its target data rate.

- We show that the proposed scheme outperforms the benchmark schemes and also accommodates higher number of users in the system while

meeting their QoS requirements.

8.2   Future Work

We have analyzed the impact of timing offset, ipSIC, and ipCSI in STBC-aided cooperative NOMA. We have also designed a framework for a QoS-aware NOMA system for a higher number of users with versatile data rate requirements. Future research directions can, but not limited to, be as follows

8.2.1   Blockchain-aided D2D communication in NOMA

Security and privacy are the main challenges for future wireless technologies because of the broadcasting nature of wireless channels. In this case, cooperative D2D communication has recently been used as a feasible physical layer security strategy, complementing the conventional cryptographic techniques used in the top layers of a wireless network. Blockchains can improve agility, security, transparency, reliability, and privacy in a wide range of applications, including autonomous systems, the Internet of Things (IoT), and other distributed processes and resource allocation in communication networks. It is also proposed for cloud-based storage and edge computing solutions for distributed cloud services as an advantage of its distributed data storage and security. Ultimate security against malicious threats can be prevented by integrating blockchain with D2D communication, especially in cooperative NOMA systems. Another encouraging application of blockchain technology can be seen in the improvement of software-defined networking data protection and privacy. Also, the blockchain, which is resilient to any unwanted intrusion, is recommended for IoT system monitoring and management.

8.2.2   Power Efficiency in NOMA

In terms of resource management, recent research contributions on NOMA are mainly targeted at optimizing spectral efficiency (SE). However, the power efficiency of NOMA networks, which is to the best of my experience, has not been researched and still in its fancy, as one of the key issues of modern wireless communication systems. The spectral efficiency-power efficiency tradeoff in NOMA structures is therefore crucial to be studied. As a result, a promising future study path is to explore the spectral and power efficiency tradeoff considering the fairness problem and it is my subjects' interest.

8.2.3   Machine learning-aided robust channel estimation in NOMA systems:

The acquisition of channel state information at the transmitter is not a simple problem in a realistic communication system, which involves a pilot training phase. Compressive sensing can be utilized as an efficient method to achieve low-cost channel prediction by reducing the training pilot symbols by using the mutual sparsity of the user channel matrix, as well as reducing the overhead feedback from receivers to the BS. A suitable channel estimation matrix is more than desired in the compressive sensing-based CSI estimate for NOMA, given the universality, and a minimum number of measurements needed and implementation. More explicitly, for channel estimation matrix architecture and sparse domain selection in channel estimation for NOMA, machine learning should be employed, which is yet another useful research area.

8.2.4   Seamless Coexistence of NOMA with other multiple access technologies

With multiple interfaces, next-generation communication systems can incorporate multiple radio access technologies (RATs), such as Wi-Fi, Bluetooth, networks of ad hoc sensors, and IoTs, LTE, CDMA, and GSM, etc. For the change in the user's radio environment, the air interface can dynamically change. Ensuring the Seamless Co-existence of Multiple RATs with NOMA is still an open challenge and there is a need to develop scalable techniques that guarantee interoperability while meeting the KPI requirements of future generation communication systems.

8.2.5   STBC-aided cooperative NOMA in uplink

In the future, we can explore into cooperative NOMA schemes based on STBC. This scheme can also be used in a future industrial internet-of-things (IIoT) sensor environment, where sensors send data to the access point through wireless links.

Appendices

Appendix A

Proof of Lemma 1

Suppose that $A \sim Exp(\lambda_h)$ and B is the sum of exponential RVs resulting in a hypo-exponential RV, i.e., $B \sim hypoexp(\boldsymbol{\lambda_i})$ with $\boldsymbol{\lambda_i}$ is a vector given as $\boldsymbol{\lambda_i} = \{\lambda_1, \lambda_2, \lambda_3, \ldots, \lambda_I\}$, as described in Section IV-A, then the PDF of A is given by

$$f_A(a) = \lambda_h e^{-\lambda_h a}, \ a \geq 0. \tag{A.1}$$

In case of only one interfering user, the PDF of B is given as

$$f_B(b) = \lambda_1 e^{-\lambda_1 b}, \ b \geq 0. \tag{A.2}$$

For more than one interferers, the PDF of B is given as

$$f_B(b) = \left(\prod_{i=1}^{I} \lambda_i \right) \left[\sum_{i=1}^{I} \frac{e^{-\lambda_i b}}{\prod_{j=1, i \neq j}^{I} (\lambda_j - \lambda_i)} \right], \tag{A.3}$$

where $b > 0$ and I is the total number of interferers. The PDF of $Q_1 = \frac{A}{B}$ can be expressed as

$$f_{Q_1}(q) = \int_0^\infty b f_A(bq) f_B(b) db. \tag{A.4}$$

By substituting (A.1) and (A.3) into (A.4), we get the form in (A.5). Then, as in [105], the PDF of $Q_1 = \frac{A}{B}$ is given by

$$f_{Q_1}(q) = \frac{\lambda_h \psi_1 \left[\psi_2 + q \lambda_h \left(\sum_{i=1}^{I} (i+1) q^{i-1} \lambda_h^{i-1} \psi^{I-i-1} \right) \right]}{\prod_{j=1}^{I} (\lambda_h q + \lambda_j)^2}, \tag{A.5}$$

where $q > 0$. Hence, using this PDF, the mean and variance of Q_1 can be obtained as $\mathbb{E}[Q_1] = \frac{\psi_1 \psi_3}{\psi_4}$ and $\mathbb{V}\text{ar}[Q_1] = \frac{\lambda_h \psi_1 (\lambda_h \psi_1 \psi_6^2 + 2\psi_7 \psi_8)}{\psi_9}$, respectively. Similarly, for the perfect timing synchronization, let $Z = C + D$, which is the sum of two exponential RVs. Thus, $Z \sim Gamma(\lambda_g)$, which corresponds to the following PDF of Z

$$f_Z(z) = \frac{z}{\lambda_g^2} e^{-z\lambda_g}, \; z > 0. \tag{A.6}$$

Without any imperfection, we can write (3.1) as $L = Q_1 + Z$, where the PDF of Q_1 is given as (A.5). By convolving the PDFs of Q_1 and Z, we obtain the PDF of $L = Q_1 + Z$, which can be found in [105] as

$$\begin{aligned} f_L(l) = \frac{1}{\lambda_g^3 \lambda_h^2} \sum_{i=1}^{I} \Bigg[& \mho e^{-\frac{\lambda_i + \lambda_h l}{\lambda_g \lambda_h}} \left(\lambda_i (-\lambda_g \lambda_h + \lambda_i + \lambda_h l) \right. \\ & \left(\text{Ei}\left(\frac{l\lambda_h + \lambda_i}{\lambda_g \lambda_h} \right) - \text{Ei}\left(\frac{\lambda_i}{\lambda_g \lambda_h} \right) \right) + \\ & \left. \lambda_g \lambda_h e^{\frac{\lambda_i}{\lambda_g \lambda_h}} \left(\lambda_i - \lambda_i e^{l/\lambda_g} + \lambda_h l \right) \right) \Bigg], \end{aligned} \tag{A.7}$$

where $l > 0$ and $\mathbf{Ei}(x) = \int_{-\infty}^{x} \frac{e^t}{t} dt$. Hence, the outage probability is given as

$$P(L < \gamma_{th}) = \int_{0}^{\gamma_{th}} f_L(l) dl. \tag{A.8}$$

Consequently, based on the PDF of L in (A.7), the outage probability can be derived as (3.18). $\square$

Appendix B

Proof of Proposition 1

Based on (3.1) and (3.17), the rate outage probability for the perfect timing synchronization, perfect SIC, and perfect CSI can be expressed as

$$
\begin{aligned}
\tilde{P}_{out} &= \mathbb{P}[\gamma_k < 2^{\Upsilon} - 1] \\
&= \mathbb{P}\left[\left[\frac{|h_k|^2 p_k}{|h_k|^2 \sum\limits_{i=1}^{k-1} p_i + \sigma^2} + \frac{(|g_{k,k-\iota-1}|^2 + |g_{k,k-\iota-2}|^2) p_s}{\sigma^2} \right] < 2^{\Upsilon} - 1 \right].
\end{aligned}
$$

$$(B.1)$$

As described in Section IV, $|h_k|^2$, $|g_{k,k-\iota-2}|^2$, and $|g_{k,k-\iota-1}|^2$ follow the exponential distributions with parameters λ_h, λ_{g1}, and λ_{g2}, respectively. Therefore, we can rewrite (B.1) in terms of SNR as

$$
\tilde{P}_{out} = \mathbb{P}\left[[\tilde{X} + \tilde{Y}] < g(\texttt{SNR}) \right], \tag{B.2}
$$

where $\tilde{X} = \frac{|h_k|^2 \Phi_k}{\texttt{SNR} |h_k|^2 \sum\limits_{i=1}^{k-1} \Phi_i + 1}$ and $\tilde{Y} = \frac{|g_{k,k-\iota-1}|^2 + |g_{k,k-\iota-2}|^2}{2}$. Because of the independent channel gains, $\mathbb{P}[\tilde{X} + \tilde{Y} < g(\texttt{SNR})] \le \mathbb{P}[\tilde{X} < g(\texttt{SNR})] + \mathbb{P}[\tilde{Y} < g(\texttt{SNR})]$.

116

At high $\mathtt{SNR}$, $\frac{\lambda_h(2^\Upsilon-1)}{\mathtt{SNR}[\Phi_k - \sum\limits_{i=1}^{k-1} \Phi_i(2^\Upsilon-1)]} \to 0$. Using the power series expansion [106], we first have

$$\mathbb{P}[\tilde{X} < g(\mathtt{SNR})] = 1 - \exp\left[- \frac{\lambda_h g(\mathtt{SNR})}{\Phi_k - \sum\limits_{i=1}^{k-1} \Phi_i(2^\Upsilon - 1)} \right]$$

$$= 1 - \exp\left[- \frac{\lambda_h(2^\Upsilon - 1)}{\mathtt{SNR}\left(\Phi_k - \sum\limits_{i=1}^{k-1} \Phi_i(2^\Upsilon - 1)\right)} \right]$$

$$\sim \frac{\lambda_h}{\Phi_k - \sum\limits_{i=1}^{k-1} \Phi_i(2^\Upsilon - 1)} \left(\frac{2^\Upsilon - 1}{\mathtt{SNR}} \right). \tag{B.3}$$

In addition, based on Fact-1 and Fact-2 in Appendix-I and Eq. (26) of [107] to find the outage behavior when $\mathtt{SNR} \to \infty$, we obtain

$$\mathbb{P}[\tilde{Y} < g(\mathtt{SNR})] \sim 2\lambda_g^2 \left(\frac{2^\Upsilon - 1}{\mathtt{SNR}} \right)^2. \tag{B.4}$$

By substituting (B.3) and (B.4) into (B.2), we have the asymptotic rate outage probability in (3.19). $\qquad\square$

Appendix C

Proof of Lemma 2

For the imperfect SIC, perfect timing synchronization and perfect CSI, we can rewrite (4.2) as $L_\eta = \frac{A}{F+B} + Z$. Let A and B be the RVs as defined in (A.1) and (A.3). Also, suppose $F \sim Exp(\lambda_\eta)$ and $\varpi = F + B$. Then, the PDF of ϖ is given as

$$f_\varpi(\varpi) = \lambda_\eta \prod_{i=1}^{I} \lambda_i \left[\sum_{i=1}^{I} \left(\frac{e^{-\lambda_i \varpi}}{\prod_{j=1, i\neq j, \eta\neq j}^{I}(\lambda_j - \lambda_i)(\lambda_j - \lambda_\eta)} \right. \right. $$
$$\left. \left. + \frac{e^{-\lambda_\eta \varpi}}{\prod_{j=1, i\neq j, \eta\neq j}^{I}(\lambda_j - \lambda_i)(\lambda_j - \lambda_\eta)} \right) \right], \qquad (C.1)$$

where $\varpi > 0$. The PDF of $Q_\eta = \frac{A}{\varpi}$ is given as

$$f_{Q_\eta}(q) = \int_0^\infty \varpi f_A(\varpi q) f_\varpi(\varpi) d\varpi. \qquad (C.2)$$

118

Table C.1: K-S Test Results for Lemma 3

Distrns.	Mean and Variance		Estimated Para.		MSE	
	μ	Var.	$\hat{\kappa_1}$	$\hat{\kappa_2}$	e_{κ_1}	e_{κ_2}
Gamma	5.9834	23.87	1.498	3.9893	0.0061	0.0192
Wei-bull	6.0164	24.9705	6.4089	1.2095	0.0177	0.0028
Exponential	5.9834	35.8037	5.9834		0.0189	
Rayleigh	7.2006	14.1672	5.7452		0.0092	
Rician	7.2010	14.1687	0.1753	5.7442	0.3146	0.0102
Nakagami	6.4162	24.8484	0.4744	66.016	0.0017	0.3030

By substituting (A.1) and (C.1) into (C.2), we obtain the PDF [105] of $Q_\eta = \frac{A}{F+B}$ is given as

$$f_{Q_\eta}(q) = \frac{\psi_1^\eta \left[\psi_2^\eta + q\lambda_h \left(\sum_{i=1}^{I}(i+2)q^i\lambda_h^i\psi_\eta^{I-i} \right) \right]}{(\lambda_h q + \lambda_\eta)^2 \prod_{j=1}^{I}(\lambda_h q + \lambda_j)^2}, \tag{C.3}$$

where $q > 0$. Thus, the mean and variance of Q_η are given by $\mathbb{E}[Q_\eta] = \frac{\psi_1^\eta \psi_3^\eta}{\psi_4^\eta}$, and $\mathbb{V}\mathrm{ar}[Q_\eta] = \frac{\psi_1^\eta(\psi_1^\eta(\psi_7^\eta)^2 + 2\psi_8^\eta\psi_9^\eta)}{\psi_{10}^\eta}$, respectively. By convolving (C.3) and (A.6) [105], We get the PDF [105] of $L_\eta = \frac{A}{F+B} + Z$ given as

$$f_{L_\eta}(l) = \sum_{i=1}^{I} \left[\frac{\mho e^{-\frac{\lambda_\eta + \lambda_i + \lambda_h l}{\lambda_g \lambda_h}}}{\lambda_g^3 \lambda_h^2 (\lambda_i - \lambda_\eta)} \left(e^{\frac{\lambda_i}{\lambda_g \lambda_h}} \left(-\lambda_\eta \lambda_i \mathrm{Ei}\left(\frac{\lambda_\eta}{\lambda_g \lambda_h} \right)(-\lambda_g \lambda_h + \lambda_\eta + \lambda_h l) \right. \right. \right.$$

$$+ \lambda_\eta \lambda_i(-\lambda_g \lambda_h + \lambda_\eta + \lambda_h l)\mathrm{Ei}\left(\frac{l\lambda_h + \lambda_\eta}{\lambda_g \lambda_h} \right) + \lambda_g \lambda_h^2 l(\lambda_\eta - \lambda_i)\left(-e^{\frac{\lambda_\eta}{\lambda_g \lambda_h}} \right) \right)$$

$$+ \lambda_\eta \lambda_i \left(-e^{\frac{\lambda_\eta}{\lambda_g \lambda_h}} \right)\mathrm{Ei}\left(\frac{\lambda_i}{\lambda_g \lambda_h} \right)\left(\lambda_g \lambda_h - \lambda_i + \lambda_h(-l) \right)$$

$$+ \lambda_\eta \lambda_i e^{\frac{\lambda_\eta}{\lambda_g \lambda_h}}(\lambda_g \lambda_h - \lambda_i + \lambda_h(-l))\mathrm{Ei}\left(\frac{l\lambda_h + \lambda_i}{\lambda_g \lambda_h} \right) \right) \right], \tag{C.4}$$

where $l > 0$. By substituting (A.7) into (A.8), we get the outage probability [105] as shown in (4.5). □

Appendix D

Proof of Proposition 2

Based on (4.2) and (3.17), the rate outage probability for the perfect timing synchronization, imperfect SIC, and perfect CSI can be rewritten as

$$
\begin{aligned}
\tilde{P}_{out}^{\eta} &= \mathbb{P}[\gamma_k^{\eta} < 2^{\Upsilon} - 1] \\
&= \mathbb{P}\left[\frac{|h_k|^2 \Phi_k}{\mathtt{SNR}(\eta |g_\eta|^2 \Phi_\eta + \sum\limits_{i=1}^{k-1} |h_k|^2 \Phi_i) + 1} \right. \\
&\quad \left. + \frac{|g_{k,k-\iota-1}|^2 + |g_{k,k-\iota-2}|^2}{2} < \frac{2^{\Upsilon} - 1}{\mathtt{SNR}} \right].
\end{aligned}
\tag{D.1}
$$

If $\tilde{Z} = \frac{|h_k|^2 \Phi_k}{\mathtt{SNR}(\eta |g_\eta|^2 \Phi_\eta + \sum\limits_{i=1}^{k-1} |h_k|^2 \Phi_i) + 1}$, using power series expansion, we have

$$
\mathbb{P}[\tilde{Z} < g(\mathtt{SNR})] = 1 - \exp\left[-\tilde{g}(\mathtt{SNR}) \right] \sim \tilde{g}(\mathtt{SNR}).
\tag{D.2}
$$

By substituting (D.2) and (B.4) into (D.1), we can approximate the outage behaviour when $\mathtt{SNR} \to \infty$ as in (3.20). $\qquad\square$

Appendix E

Proof of Lemma 3

For the perfect SIC, imperfect timing synchronization, and perfect CSI, we can rewrite (3.15) as $V = Q_1 + R$. Further, the second part of (3.13) can be expressed as $R = \frac{v}{\Lambda}$, where $v = \frac{(C+\varepsilon_1 D)^2}{C+D}$ and $\Lambda = \frac{|\aleph|^2}{C+D}$ with $|\aleph|^2 = |(1 - \varepsilon_1)g_{4,1}g_{4,2}^* - \varepsilon_2 g_{4,1}g_{4,2}^*|^2$. It can be shown from [108] that v is the Generalized Gamma distribution. Whereas, let Λ be a Gamma distribution. Then, the PDF of Λ is Gamma distribution [109]. Also, R is a ratio of Generalized Gamma Distribution and Gamma Distribution [108]. Thus, the PDF of R is given as in (E.1). Similarly, suppose $C \sim Exp(\lambda_g)$, $D \sim Exp(\lambda_g)$, $0 < \varepsilon_1 \leq 1$, and $0 < \varepsilon_2 \leq 1$. Then, the PDF of $R = \frac{(C+\varepsilon_1 D)^2}{(1-\varepsilon_1)^2 CD + \varepsilon_2^2 CD + C + D}$ is

$$
f_R(r) = \frac{1}{4(\varepsilon_1 - 1)} \lambda_g \left[\frac{1}{\sqrt{\lambda_g r}} \left(\sqrt{\pi} \text{erf} \left(\sqrt{\lambda_g} r \right) \right. \right.
$$
$$
\left. \left. - \text{erf} \left(\frac{\sqrt{\lambda_g} r}{\varepsilon_1} \right) \right) + \frac{2e^{-\frac{\lambda_g r}{\varepsilon_1^2}}}{\varepsilon_1} - 2e^{\lambda_g(-r)} \right], \qquad \text{(E.1)}
$$

where $r > 0$. Also, using this PDF, we can obtain the mean and variance as

$$\mathbb{E}[R] = \frac{2(1 + \varepsilon_1 + \varepsilon_1^2)}{3\lambda_g}, \tag{E.2}$$

and

$$\mathbb{V}\text{ar}[R] = \frac{2(17 + 7\varepsilon_1 - 3\varepsilon_1^2 + 7\varepsilon_1^3 + 17\varepsilon_1^4)}{45\lambda_g^2}, \tag{E.3}$$

respectively. By applying the Kolmogorov–Smirnov test (K-S test) [110, 111] on the distribution of $V = Q_1 + R$, it is determined that $V \sim \Gamma(\alpha, \beta)$. Further, the PDF of $V = Q_1 + R$ is given as

$$f_V(v) = \frac{\beta^{-\alpha} v^{\alpha-1} e^{-\frac{v}{\beta}}}{\Gamma(\alpha)}, \ v > 0, \tag{E.4}$$

where $\alpha = \frac{\mathbb{E}[V]^2}{\mathbb{V}\text{ar}[V]}$ and $\beta = \frac{\mathbb{V}\text{ar}[V]}{\mathbb{E}[V]}$ are the parameters of Gamma distribution. Also, $\Gamma(x)$ is the gamma function given as $\Gamma(x) = (x - 1)!$. By applying the mathematical operation [105] and [112], as given in (A.8) on the PDF of V in (E.4), we obtain the outage probability as shown in (3.21). $\quad\square$

Appendix F

Proof of Proposition 3

Based on (3.15) and (3.17), the rate outage probability for the imperfect timing synchronization, perfect SIC, and perfect CSI can be expressed as

$$
\begin{aligned}
\tilde{P}^{\epsilon}_{out} &= \mathbb{P}[\gamma^{\epsilon}_k < 2^{\Upsilon} - 1] \\
&= \mathbb{P}\left[\frac{|h_k|^2 \Phi_k}{\mathtt{SNR} \sum\limits_{i=1}^{k-1} |h_k|^2 \Phi_i + 1} + \frac{(|\varphi_1|^2 + \varepsilon_1 |\varphi_2|^2)^2}{\mathtt{SNR}\, |\varphi_\varepsilon|^2 + 2(|\varphi_1|^2 + |\varphi_2|^2)} < \frac{2^{\Upsilon} - 1}{\mathtt{SNR}} \right],
\end{aligned}
$$

$$(F.1)$$

where $|\varphi_1|^2 = |g_{k,k-\iota-1}|^2$, $|\varphi_2|^2 = |g_{k,k-\iota-2}|^2$, and $|\varphi_\varepsilon|^2 = |(1-\varepsilon_1)g_{k,k-\iota-2}g^*_{k,k-\iota-1} - \varepsilon_2 g_{k,k-\iota-2}g^*_{k,k-\iota-1}|^2$. Letting $\tilde{W} = \frac{(|\varphi_1|^2 + \varepsilon_1|\varphi_2|^2)^2}{\mathtt{SNR}\,|\varphi_\varepsilon|^2 + 2(|\varphi_1|^2 + |\varphi_2|^2)}$, based on Fact-1 and Fact-2 in Appendix-I of [107], we can obtain

$$
\mathbb{P}[\tilde{W} < g(\mathtt{SNR})] \sim g^{\varepsilon}(\mathtt{SNR}), \tag{F.2}
$$

where $g^{\varepsilon}(\mathtt{SNR}) = 2\varepsilon_1 \lambda_g^2 \left(\frac{2^{\Upsilon}-1}{\mathtt{SNR}} \right)^2$. By substituting (F.2) and (B.3) into (F.1), we can approximate the outage behaviour when $\mathtt{SNR} \to \infty$ as in (3.22). $\quad\square$

Appendix G

Proof of Lemma 4

For the imperfect SIC, imperfect timing synchronization, and perfect CSI, we first rewrite (4.4) as $V_\eta = Q_\eta + R$, where the PDFs of Q_η and R are given in (C.3) and (E.1), respectively. Applying the Kolmogorov–Smirnov test (K-S test) [110, 111] on the distribution of $V_\eta = Q_\eta + R$, it is determined that $V_\eta \sim \Gamma(\theta, \phi)$, which corresponds to the following PDF

$$f_{V_\eta}(v) = \frac{\phi^{-\theta} (v)^{\theta-1} e^{-\frac{(v)}{\phi}}}{\Gamma(\theta)}, \tag{G.1}$$

where $v > 0$. In addition, $\theta = \frac{(\mathbb{E}[V_\eta])^2}{\mathbb{V}\mathrm{ar}[V_\eta]}$ and $\phi = \frac{\mathbb{V}\mathrm{ar}[V_\eta]}{\mathbb{E}[V_\eta]}$ are the parameters of Gamma distribution, where the mean and the variance of the V_η are given by

$$\mathbb{E}[V_\eta] = \int_0^\infty v f_{V_\eta}(v) dv = \frac{\psi_1^\eta \psi_3^\eta}{\lambda_h \psi_a^\eta} + \frac{2(\varepsilon_1^2 + \varepsilon_1 + 1)}{3\lambda_g} \tag{G.2}$$

and

$$\mathbb{V}\mathrm{ar}[V_\eta] = \int_0^\infty v^2 f_{V_\eta}(v) dV - \mathbb{E}[V_\eta]^2$$

$$= \frac{\psi_1^\eta(\psi_1^\eta(\psi_3^\eta)^2 + 2\psi_7^\eta\psi_8^\eta)}{\psi_9^\eta} + \frac{2\left(17\varepsilon_1^4 + 7\varepsilon_1^3 - 3\varepsilon_1^2 + 7\varepsilon_1 + 17\right)}{45\lambda_g^2}, \qquad \text{(G.3)}$$

respectively. By substituting (G.1) into (A.8), as in [105], we can derive the outage probability as shown in (3.23). $\qquad\square$

Appendix H

Proof of Proposition 4

With (4.4) and (3.17), the rate outage probability for the imperfect timing synchronization, imperfect SIC, and perfect CSI can be found as (4.4) is less than γ_{th}, which can be written as

$$
\begin{aligned}
\tilde{P}_{out}^{\eta,\epsilon} =\ & \mathbb{P}[\gamma_k^{\eta,\epsilon} < 2^{\Upsilon} - 1] \\
=\ & \mathbb{P}\left[\left[\frac{|h_k|^2 \Phi_k}{\mathtt{SNR}(\eta|g_\eta|^2 \Phi_\eta + \sum\limits_{i=1}^{k-1} |h_k|^2 \Phi_i) + 1} \right.\right. \\
& \left.\left. + \frac{(|\varphi_1|^2 + \varepsilon_1|\varphi_2|^2)^2}{\mathtt{SNR}\,|\varphi_\varepsilon|^2 + 2(|\varphi_1|^2 + |\varphi_2|^2)} \right] < \frac{2^{\Upsilon} - 1}{\mathtt{SNR}} \right].
\end{aligned}
\tag{H.1}
$$

By substituting (B.4) and (F.2) into (H.1), we can obtain (3.24). $\qquad\square$

Appendix I

Proof of Lemma 5

For the perfect SIC, perfect timing synchronization, and imperfect CSI given in (5.9), let $A_\varrho = \varrho_{n,n-3}$, $A_g = g_{n,n-3}$, $B_\varrho = \varrho_{n,n-2}$, $B_g = g_{n,n-2}$, $C_\chi = |A_\chi|^2 p_s$, and $D_\chi = |B_\chi|^2 p_s$, where $A_\chi = A_\varrho + \rho A_g$ and $B_\chi = B_\varrho + \rho B_g$. As described in Section III-C, $A_\varrho \sim CN(0, \sigma_\varrho^2)$, $A_g \sim CN(0, \sigma_g^2)$, $B_\varrho \sim CN(0, \sigma_\varrho^2)$, $B_g \sim CN(0, \sigma_g^2)$. Therefore, we can find out that $A_\chi \sim CN(0, \sigma_\varrho^2 + \rho^2 \sigma_g^2)$ and $B_\chi \sim CN(0, \sigma_\varrho^2 + \rho^2 \sigma_g^2)$. We model A_χ and B_χ as mutually independent complex Gaussian RVs with variance σ_χ^2. Then, their magnitudes (i.e., $|A_\chi|$ and $|B_\chi|$) follow the Rayleigh distribution, and their squared magnitudes (i.e., $|A_\chi|^2$ and $|B_\chi|^2$) follow the exponential distributions with the parameter λ_χ, where $\lambda_\chi = 1/\sigma_\chi^2 = 1/(\sigma_\varrho^2 + \rho^2 \sigma_g^2)$ [56, 57]. The PDFs of C_χ and D_χ are given as $f_{C_\chi}(c) = \frac{e^{-\frac{c}{\lambda_\chi}}}{\lambda_\chi}$, $c > 0$, and $f_{D_\chi}(d) = \frac{e^{-\frac{d}{\lambda_\chi}}}{\lambda_\chi}$, $d > 0$, respectively. If we define another variable $Z_\chi = C_\chi + D_\chi$, it follows a Gamma distribution, and its PDF is obtained by convolving $f_{C_\chi}(c)$ and $f_{D_\chi}(d)$ as

$$f_{Z_\chi}(z) = \frac{z e^{-\frac{z}{\lambda_\chi}}}{\lambda_\chi^2}, \ z > 0. \tag{I.1}$$

For the perfect SIC, perfect timings and imperfect CSI, (5.9) can be written as $L_\chi = Q_1 + Z_\chi$ and the PDF of L_χ is obtained by convolving (A.5) and (I.1), which is given as

$$
\begin{aligned}
f_{L_\chi}(l) = \frac{1}{\lambda_\chi^3 \lambda_h^2} \sum_{i=1}^{I} \Bigg[& \mho e^{-\frac{\lambda_i + \lambda_h l}{\lambda_\chi \lambda_h}} \bigg(\lambda_i(-\lambda_\chi \lambda_h + \lambda_i + \lambda_h l) \\
& \left(\mathrm{Ei}\left(\frac{l\lambda_h + \lambda_i}{\lambda_\chi \lambda_h} \right) - \mathrm{Ei}\left(\frac{\lambda_i}{\lambda_\chi \lambda_h} \right) \right) + \\
& \lambda_\chi \lambda_h e^{\frac{\lambda_i}{\lambda_\chi \lambda_h}} \left(\lambda_i - \lambda_i e^{l/\lambda_\chi} + \lambda_h l \right) \bigg) \Bigg], \quad l > 0.
\end{aligned}
\tag{I.2}
$$

As a result, the corresponding outage probability is obtained as (5.10). $\square$

Appendix J

Proof of Proposition 5

From (5.9) and (3.17), the rate outage probability for the perfect timing synchronization, perfect SIC, and imperfect CSI can be expressed as

$$
\begin{aligned}
\tilde{P}_{out}^{\chi} &= \mathbb{P}[\gamma_k^{\chi} < 2^{\Upsilon} - 1] \\
&= \mathbb{P}\left[\left[\frac{|h_k|^2 \Phi_k}{\mathtt{SNR} \sum\limits_{i=1}^{k-1} |h_k|^2 \Phi_i + 1} + \frac{(|A_\chi|^2 + |B_\chi|^2)}{2} \right] < \frac{2^{\Upsilon} - 1}{\mathtt{SNR}} \right].
\end{aligned} \tag{J.1}
$$

Following the same procedure as in (B.4), we obtain the PDF of Z_χ as

$$
\mathbb{P}[\tilde{Z}_\chi < g(\mathtt{SNR})] \sim 2\lambda_\chi^2 \left(\frac{2^{\Upsilon} - 1}{\mathtt{SNR}} \right)^2. \tag{J.2}
$$

Replacing (B.4) and (J.2) into (J.1), we have the asymptotic rate outage probability in (5.11). $\qquad \square$

Bibliography

[1] Ding, Z., Yang, Z., Fan, P., & Poor, H. V. (2014). On the performance of non-orthogonal multiple access in 5G systems with randomly deployed users. *IEEE Signal Process. Lett.*, *21*(12), 1501–1505.

[2] Ding, Z., Liu, Y., Choi, J., Sun, Q., Elkashlan, M., Chih-Lin, I., & Poor, H. V. (2017). Application of non-orthogonal multiple access in LTE and 5G networks. *IEEE Commun. Mag.*, *55*(2), 185–191.

[3] Mohjazi, L., Al-Qutayri, M., Barada, H., Poon, K., & Shubair, R. (2011). Deployment challenges of femtocells in future indoor wireless networks, In *Ieee gcc conference and exhibition*.

[4] Singh, A. P., Nigam, S., & Gupta, N. K. (2007). A study of next generation wireless network 6G. *Int. J. of Innovative Research in Computer and Communication Engineering*, *4*(1), 871–874.

[5] Holma, H., Toskala, A., & Reunanen, J. (2016). *Lte small cell optimization: 3GPP evolution to release 13*. John Wiley & Sons.

[6] Kiani, A. Y., Hassan, S. A., Su, B., Pervaiz, H., & Ni, Q. (2020a). Minimizing the transaction time difference for noma-based mobile edge computing. *IEEE Communications Letters*, *24*(4), 853–857.

[7] Amjad, M., Qureshi, H. K., Hassan, S. A., Ahmad, A., & Jangsher, S. (2020). Optimization of MAC frame slots and power in hybrid VLC/RF networks. *IEEE Access*, *8*, 21653–21664.

[8]   Nawaz, S., Hassan, S. A., & Jung, H. (2020). Auxiliary beam pair
        enabled initial access for mmwave D2D networks. *Physical Commu-
        nication, 39*, 101039.

[9]   Abbas, Q., Zeb, S., Hassan, S. A., Mumtaz, R., & Zaidi, S. A. R.
        (2020). Joint optimization of age of information and energy efficiency
        in iot networks, In *2020 ieee 91st vehicular technology conference
        (vtc2020-spring)*. IEEE.

[10]   Ghunney, E., Hassan, S. A., & Weitnauer, M. A. (2020). Impact of
        wrong beam selection on beam pair scanning method for user dis-
        covery in mmwave systems, In *2020 ieee 91st vehicular technology
        conference (vtc2020-spring)*. IEEE.

[11]   Akram, M. U., Saeed, U., Hassan, S. A., & Jung, H. (2020). Uav-based
        air-to-ground channel modeling for diverse environments, In *2020 ieee
        wireless communications and networking conference (wcnc)*. IEEE.

[12]   Jan, M. A., Hassan, S. A., & Jung, H. (2019). Qos-based performance
        analysis of mmwave uav-assisted 5G hybrid heterogeneous network,
        In *2019 ieee global communications conference (globecom)*. IEEE.

[13]   Zia-ul-Mustafa, R., & Hassan, S. A. (2019). Machine learning-based
        context aware sequential initial access in 5G mmwave systems, In *2019
        ieee globecom workshops (gc wkshps)*. IEEE.

[14]   Ijaz, A., Hassan, S. A., Zaidi, S. A. R., Jayakody, D. N. K., & Zaidi,
        S. M. H. (2017). Coverage and rate analysis for downlink hetnets using
        modified reverse frequency allocation scheme. *IEEE access, 5*, 2489–
        2502.

[15]   Mushtaq, E., Ali, S., & Hassan, S. A. (2017). On low complexity
        ml decoder for quaternion orthogonal designs. *IEEE Communications
        Letters, 21*(5), 1087–1090.

[16] Hussain, M., & Hassan, S. A. (2016). Impact of intra-flow interference on the performance of 2-d multi-hop cooperative network. *IEEE Communications Letters*, *21*(4), 869–872.

[17] Raja, A. A., Jamshed, M. A., Pervaiz, H., & Hassan, S. A. (2020). Performance analysis of uav-assisted backhaul solutions in thz enabled hybrid heterogeneous network, In *Ieee infocom 2020-ieee conference on computer communications workshops (infocom wkshps)*. IEEE.

[18] Bint Saleem, A., & Hassan, S. A. (2020). On the performance of spatial modulation schemes in large-scale MIMO under correlated nakagami fading, In *2020 ieee 91st vehicular technology conference (vtc2020-spring)*. IEEE.

[19] Zhang, H., Qiu, Y., Long, K., Karagiannidis, G. K., Wang, X., & Nallanathan, A. (2018). Resource allocation in NOMA-based fog radio access networks. *IEEE Wireless Communications*, *25*(3), 110–115.

[20] Saleem, U., Jangsher, S., Qureshi, H. K., & Hassan, S. A. (2018). Joint subcarrier and power allocation in the energy-harvesting-aided D2D communication. *IEEE Transactions on Industrial Informatics*, *14*(6), 2608–2617.

[21] Mushtaq, M. T., Hassan, S. A., Saleem, S., & Jayakody, D. (2018). Impacts of k-fading on the performance of massive MIMO systems. *Electronics Letters*, *54*(1), 49–51.

[22] Ansari, R. I., Chrysostomou, C., Hassan, S. A., Guizani, M., Mumtaz, S., Rodriguez, J., & Rodrigues, J. J. (2017). 5g D2D networks: Techniques, challenges, and future prospects. *IEEE Systems Journal*, *12*(4), 3970–3984.

[23] Naqvi, S. A. R., Hassan, S. A., Pervaiz, H., & Ni, Q. (2018). Drone-aided communication as a key enabler for 5G and resilient public safety networks. *IEEE Communications Magazine*, *56*(1), 36–42.

[24] Ansari, R. I., Hassan, S. A., Ali, S., Chrysostomou, C., & Lestas, M. (2017). On the outage analysis of a D2D network with uniform node distribution in a circular region. *Physical Communication*, *25*, 277–283.

[25] Qureshi, S., Hassan, S. A., & Jayakody, D. N. K. (2018a). Divide-and-allocate: An uplink successive bandwidth division noma system. *Transactions on Emerging Telecommunications Technologies*, *29*(1), e3216.

[26] Munir, H., Hassan, S. A., Pervaiz, H., Ni, Q., & Musavian, L. (2017). Resource optimization in multi-tier hetnets exploiting multi-slope path loss model. *IEEE Access*, *5*, 8714–8726.

[27] Rahman, M. A., Hossain, M. S., Alrajeh, N. A., & Guizani, N. (2020). B5G and explainable deep learning assisted healthcare vertical at the edge: COVID-19 perspective. *IEEE Network*, *34*(4), 98–105.

[28] Lai, C., Chang, Y., Chao, H., Hossain, M. S., & Ghoneim, A. (2017). A buffer-aware QoS streaming approach for SDN-enabled 5G vehicular networks. *IEEE Communications Magazine*, *55*(8), 68–73.

[29] Ullah, S. A., Khalid, I., Saleem, S., & Hassan, S. A. (2018). On the estimation of modulation index for binary full responseCPM signals. *IEEE Communications Letters*, *22*(5), 918–921.

[30] Jameel, F., Javed, M. A., Jayakody, D. N., & Hassan, S. A. (2018). On secrecy performance of industrial internet of things. *Internet Technology Letters*, *1*(2), e32.

[31] Nawaz, F., Hassan, S. A., Aissa, S., & Saleem, S. (2018). Outage probability for a decode-and-forward SWIPT relaying system in nakagami fading. *Internet Technology Letters*, *1*(1), e13.

[32] Munawar, T., Saleem, S., Hassan, S. A., & Zaidi, S. M. H. (2018). Estimation of modulation index for partial responseCPM signal. *IEEE Access*, *6*, 7664–7674.

[33] Omar, M. S., Hassan, S. A., Pervaiz, H., Ni, Q., Musavian, L., Mumtaz, S., & Dobre, O. A. (2017). Multiobjective optimization in 5G hybrid networks. *IEEE Internet of Things Journal*, *5*(3), 1588–1597.

[34] Mahmood, A., Sisinni, E., Guntupalli, L., Rondón, R., Hassan, S. A., & Gidlund, M. (2018). Scalability analysis of a lora network under imperfect orthogonality. *IEEE Transactions on Industrial Informatics*, *15*(3), 1425–1436.

[35] Mushtaq, E., Ali, S., & Hassan, S. A. (2018). On decoupled decoding of quasi-orthogonal stbcs using quaternion algebra. *IEEE Systems Journal*, *13*(2), 1580–1586.

[36] Jamal, M. N., Hassan, S. A., Jayakody, D. N. K., & Rodrigues, J. J. (2018a). Efficient nonorthogonal multiple access: Cooperative use of distributed space-time block coding. *IEEE Vehicular Technology Magazine*, *13*(4), 70–77.

[37] Solaija, M. S. J., Saleem, S., Khurshid, K., Hassan, S. A., & Kamboh, A. M. (2018). Dynamic mode decomposition based epileptic seizure detection from scalp eeg. *IEEE Access*, *6*, 38683–38692.

[38] Munir, H., Pervaiz, H., Hassan, S. A., Musavian, L., Ni, Q., Imran, M. A., & Tafazolli, R. (2018). Computationally intelligent techniques for resource management in mmwave small cell networks. *IEEE Wireless Communications*, *25*(4), 32–39.

[39] Naqvi, S. A. R., Pervaiz, H., Hassan, S. A., Musavian, L., Ni, Q., Imran, M. A., Ge, X., & Tafazolli, R. (2018). Energy-aware radio resource management in D2D -enabled multi-tier hetnets. *IEEE Access*, *6*, 16610–16622.

[40] Qureshi, S. S., Ali, S., & Hassan, S. A. (2018). Optimal polarization diversity gain in dual-polarized antennas using quaternions. *IEEE Signal Processing Letters*, *25*(4), 467–471.

[41] Umer, A., Hassan, S. A., Pervaiz, H., Musavian, L., Ni, Q., & Imran, M. A. (2019). Secrecy spectrum and energy efficiency analysis in massive MIMO -enabled multi-tier hybrid hetnets. *IEEE Transactions on Green Communications and Networking*, *4*(1), 246–262.

[42] Chaoudhry, B. B., Hassan, S. A., Speidel, J., & Jung, H. (2019). Energy efficiency of a decode-and-forward multiple-relay network with rate adaptive LDPC codes. *Sensors*, *19*(21), 4793.

[43] Shafi, U., Mumtaz, R., García-Nieto, J., Hassan, S. A., Zaidi, S. A. R., & Iqbal, N. (2019). Precision agriculture techniques and practices: From considerations to applications. *Sensors*, *19*(17), 3796.

[44] Aslam, M. S., Khan, A., Atif, A., Hassan, S. A., Mahmood, A., Qureshi, H. K., & Gidlund, M. (2019). Exploring multi-hop lora for green smart cities. *IEEE Network*, *34*(2), 225–231.

[45] Ansari, R. I., Pervaiz, H., Hassan, S. A., Chrysostomou, C., Imran, M. A., Mumtaz, S., & Tafazolli, R. (2019). A new dimension to spectrum management in iot empowered 5G networks. *IEEE Network*, *33*(4), 186–193.

[46] Ansari, R. I., Pervaiz, H., Chrysostomou, C., Hassan, S. A., Mahmood, A., & Gidlund, M. (2019). Control-data separation architec-

ture for dual-band mmwave networks: A new dimension to spectrum management. *IEEE Access*, *7*, 34925–34937.

[47] Ding, Z., Lei, X., Karagiannidis, G. K., Schober, R., Yuan, J., & Bhargava, V. K. (2017). A survey on non-orthogonal multiple access for 5G networks: Research challenges and future trends. *IEEE Journal on Selected Areas in Communications*, *35*(10), 2181–2195. https://doi.org/10.1109/JSAC.2017.2725519

[48] Dai, L., Wang, B., Ding, Z., Wang, Z., Chen, S., & Hanzo, L. (2018). A survey of non-orthogonal multiple access for 5G. *IEEE Communications Surveys Tutorials*, *20*(3), 2294–2323. https://doi.org/10.1109/COMST.2018.2835558

[49] Vaezi, M., Aruma Baduge, G. A., Liu, Y., Arafa, A., Fang, F., & Ding, Z. (2019). Interplay between NOMA and other emerging technologies: A survey. *IEEE Transactions on Cognitive Communications and Networking*, *5*(4), 900–919. https://doi.org/10.1109/TCCN.2019.2933835

[50] Wan, D., Wen, M., Ji, F., Yu, H., & Chen, F. (2018). Non-orthogonal multiple access for cooperative communications: Challenges, opportunities, and trends. *IEEE Wireless Communications*, *25*(2), 109–117. https://doi.org/10.1109/MWC.2018.1700134

[51] Ding, Z., Peng, M., & Poor, H. V. (2015a). Cooperative non-orthogonal multiple access in 5G systems. *IEEE Communications Letters*, *19*(8), 1462–1465. https://doi.org/10.1109/LCOMM.2015.2441064

[52] Jamal, M. N., Hassan, S. A., & Jayakody, D. N. K. (2017a). A new approach to cooperative NOMA using distributed space time block coding, In *2017 ieee 28th annual international symposium on personal, indoor, and mobile radio communications (pimrc)*. https://doi.org/10.1109/PIMRC.2017.8292344

[53] Avendi, M. R., Poorkasmaei, S., & Jafarkhani, H. (2014). Differential distributed space-time coding with imperfect synchronization, In *2014 ieee global communications conference*. https://doi.org/10.1109/GLOCOM.2014.7037296

[54] Hussain, M., & Hassan, S. A. (2014). Analysis of bit error probability for imperfect timing synchronization in virtual MISO networks, In *2014 ifip wireless days (wd)*. https://doi.org/10.1109/WD.2014.7020806

[55] Cheng, H. T., Mheidat, H., Uysal, M., & Lok, T. M. (2005). Distributed space-time block coding with imperfect channel estimation, In *Ieee international conference on communications, 2005. icc 2005. 2005*. IEEE.

[56] Gu, D., & Leung, C. (2003). Performance analysis of transmit diversity scheme with imperfect channel estimation. *Electronics letters*, *39*(4), 402–403.

[57] Laneman, J. N. (2003). Limiting analysis of outage probabilities for diversity schemes in fading channels, In *Globecom '03. ieee global telecommunications conference (ieee cat. no.03ch37489)*.

[58] Usman, M. R., Khan, A., Usman, M. A., Jang, Y. S., & Shin, S. Y. (2016). On the performance of perfect and imperfect sic in downlink non orthogonal multiple access (NOMA), In *2016 international conference on smart green technology in electrical and information systems (icsgteis)*. https://doi.org/10.1109/ICSGTEIS.2016.7885774

[59] Jamal, M. N., Hassan, S. A., & Jayakody, D. N. K. (2017b). A new approach to cooperative NOMA using distributed space time block coding, In *2017 ieee 28th annual international symposium on personal, indoor, and mobile radio communications (pimrc)*. IEEE.

[60] Liu, Y., Ding, Z., Elkashlan, M., & Poor, H. V. (2016). Cooperative non-orthogonal multiple access with simultaneous wireless information and power transfer. *IEEE Journal on Selected Areas in Communications*, *34*(4), 938–953.

[61] Zhong, C., & Zhang, Z. (2016). Non-orthogonal multiple access with cooperative full-duplex relaying. *IEEE Communications Letters*, *20*(12), 2478–2481.

[62] Zhang, Z., Ma, Z., Xiao, M., Ding, Z., & Fan, P. (2017). Full-duplex device-to-device-aided cooperative non-orthogonal multiple access. *IEEE Transactions on Vehicular Technology*, *66*(5), 4467–4471. https://doi.org/10.1109/TVT.2016.2600102

[63] Ding, Z., Dai, H., & Poor, H. V. (2016a). Relay selection for cooperative NOMA. *IEEE Wireless Communications Letters*, *5*(4), 416–419. https://doi.org/10.1109/LWC.2016.2574709

[64] Kim, J., & Lee, I. (2015). Capacity analysis of cooperative relaying systems using non-orthogonal multiple access. *IEEE Communications Letters*, *19*(11), 1949–1952. https://doi.org/10.1109/LCOMM.2015.2472414

[65] Liu, H., Ding, Z., Kim, K. J., Kwak, K. S., & Poor, H. V. (2018). Decode-and-forward relaying for cooperative noma systems with direct links. *IEEE Transactions on Wireless Communications*, *17*(12), 8077–8093.

[66] Liang, X., Wu, Y., Ng, D. W. K., Zuo, Y., Jin, S., & Zhu, H. (2017). Outage performance for cooperative NOMA transmission with an AF relay. *IEEE Communications Letters*, *21*(11), 2428–2431. https://doi.org/10.1109/LCOMM.2017.2681661

[67] Toka, M., & Kucur, O. (2018). Non-orthogonal multiple access with alamouti space–time block coding. *IEEE Communications Letters*, *22*(9), 1954–1957. https://doi.org/10.1109/LCOMM.2018.2849387

[68] Kader, M. F., & Shin, S. Y. (2016). Cooperative relaying using space-time block coded non-orthogonal multiple access. *IEEE Transactions on Vehicular Technology*, *66*(7), 5894–5903.

[69] Alamouti, S. M. (1998). A simple transmit diversity technique for wireless communications. *IEEE Journal on Selected Areas in Communications*, *16*(8), 1451–1458. https://doi.org/10.1109/49.730453

[70] Mheidat, H., & Uysal, M. (2007). Non-coherent and mismatched-coherent receivers for distributed stbcs with amplify-and-forward relaying. *IEEE Transactions on Wireless Communications*, *6*(11), 4060–4070.

[71] Ganesan, G., & Stoica, P. (2001). Space-time block codes: A maximum snr approach. *IEEE Transactions on Information Theory*, *47*(4), 1650–1656.

[72] Lv, L., Chen, J., & Ni, Q. (2016). Cooperative non-orthogonal multiple access in cognitive radio. *IEEE Communications Letters*, *20*(10), 2059–2062.

[73] Zhang, Z., Ma, Z., Xiao, M., Ding, Z., & Fan, P. (2016). Full-duplex device-to-device-aided cooperative nonorthogonal multiple access. *IEEE Transactions on Vehicular Technology*, *66*(5), 4467–4471.

[74] Lv, L., Chen, J., Ni, Q., & Ding, Z. (2017). Design of cooperative non-orthogonal multicast cognitive multiple access for 5G systems: User scheduling and performance analysis. *IEEE Transactions on Communications*, *65*(6), 2641–2656.

[75] Xu, M., Ji, F., Wen, M., & Duan, W. (2016). Novel receiver design for the cooperative relaying system with non-orthogonal multiple access. *IEEE Communications Letters*, *20*(8), 1679–1682. https://doi.org/10.1109/LCOMM.2016.2575011

[76] Yang, Z., Ding, Z., Wu, Y., & Fan, P. (2017). Novel relay selection strategies for cooperative NOMA. *IEEE Transactions on Vehicular Technology*, *66*(11), 10114–10123. https://doi.org/10.1109/TVT.2017.2752264

[77] Kader, M. F., Shahab, M. B., & Shin, S. Y. (2017). Exploiting non-orthogonal multiple access in cooperative relay sharing. *IEEE Communications Letters*, *21*(5), 1159–1162. https://doi.org/10.1109/LCOMM.2017.2653777

[78] Kiani, A. Y., Hassan, S. A., Su, B., Pervaiz, H., & Ni, Q. (2020b). Minimizing the transaction time difference for NOMA-based mobile edge computing. *IEEE Communications Letters*, *24*(4), 853–857.

[79] Ding, Z., Dai, H., & Poor, H. V. (2016b). Relay selection for cooperative NOMA. *IEEE Wireless Communications Letters*, *5*(4), 416–419.

[80] Ding, Z., Peng, M., & Poor, H. V. (2015b). Cooperative non-orthogonal multiple access in 5G systems. *IEEE Communications Letters*, *19*(8), 1462–1465.

[81] Chen, J., Yang, L., & Alouini, M.-S. (2018). Physical layer security for cooperative NOMA systems. *IEEE Transactions on Vehicular Technology*, *67*(5), 4645–4649.

[82] Qureshi, S., Hassan, S. A., & Jayakody, D. N. K. (2018b). Divide-and-allocate: An uplink successive bandwidth division NOMA system.

Transactions on Emerging Telecommunications Technologies, 29(1), e3216.

[83] Xu, P., Yang, Z., Ding, Z., & Zhang, Z. (2018). Optimal relay selection schemes for cooperative NOMA. *IEEE Transactions on Vehicular Technology, 67*(8), 7851–7855.

[84] Zeb, S., Abbas, Q., Hassan, S. A., Mahmood, A., Mumtaz, R., Zaidi, S. H., Zaidi, S. A. R., & Gidlund, M. (2019). NOMA enhanced backscatter communication for green IoT networks, In *2019 16th international symposium on wireless communication systems (iswcs)*. IEEE.

[85] Yue, X., Liu, Y., Kang, S., Nallanathan, A., & Ding, Z. (2018). Exploiting full/half-duplex user relaying in noma systems. *IEEE Transactions on Communications, 66*(2), 560–575. https://doi.org/10.1109/TCOMM.2017.2749400

[86] Jamal, M. N., Hassan, S. A., Jayakody, D. N. K., & Rodrigues, J. J. (2018b). Efficient nonorthogonal multiple access: Cooperative use of distributed space-time block coding. *IEEE Vehicular Technology Magazine, 13*(4), 70–77.

[87] Ding, Z., Peng, M., & Poor, H. V. (2015c). Cooperative non-orthogonal multiple access in 5G systems. *IEEE Communications Letters, 19*(8), 1462–1465.

[88] Liu, Y., Qin, Z., Elkashlan, M., Ding, Z., Nallanathan, A., & Hanzo, L. (2018). Non-orthogonal multiple access for 5G and beyond. *arXiv preprint arXiv:1808.00277*.

[89] Zeng, J., Lv, T., Liu, R. P., Su, X., Peng, M., Wang, C., & Mei, J. (2018). Investigation on evolving single-carrier NOMA into multi-carrier NOMA in 5G. *IEEE Access, 6*, 48268–48288. https://doi.org/10.1109/ACCESS.2018.2868093

[90] Ding, Z., Fan, P., & Poor, H. V. (2016). Impact of user pairing on 5G nonorthogonal multiple-access downlink transmissions. *IEEE Trans. Veh. Technol.*, *65*(8), 6010–6023.

[91] Qureshi, S., Hassan, S. A., & Jayakody, D. N. K. (2018c). Divide-and-allocate: An uplink successive bandwidth division NOMA system. *Transactions on Emerging Telecommunications Technologies*, *29*(1), e3216.

[92] Malik, H., Alam, M. M., Pervaiz, H., Le Moullec, Y., Al-Dulaimi, A., Parand, S., & Reggiani, L. (2019). Radio resource management in NB-IoT systems: Empowered by interference prediction and flexible duplexing. *IEEE Network*, *34*(1), 144–151.

[93] Mwakwata, C. B., Alam, M. M., Le Moullec, Y., Malik, H., & Pärand, S. (2020). Cooperative interference avoidance scheduler for radio resource management in NB-IoT systems, In *Eucnc*.

[94] Liang, J.-M., Wu, K.-R., Chen, J.-J., Liu, P.-Y., & Tseng, Y.-C. (2018). Energy-efficient uplink resource units scheduling for ultra-reliable communications in NB-IoT networks. *Wirel Commun. Mob. Comput.*, *2018*.

[95] Zheng, H., Li, H., Hou, S., & Song, Z. (2018). Joint resource allocation with weighted max-min fairness for NOMA-enabled V2X communications. *IEEE Access*, *6*, 65449–65462.

[96] Guo, S., & Zhou, X. (2018). Robust resource allocation with imperfect channel estimation in NOMA-based heterogeneous vehicular networks. *IEEE Trans. Commun.*, *67*(3), 2321–2332.

[97] Abozariba, R., Naeem, M. K., Patwary, M., Seyedebrahimi, M., Bull, P., & Aneiba, A. (2019). NOMA-based resource allocation and mo-

bility enhancement framework for IoT in next generation cellular networks. *IEEE Access, 7*, 29158–29172.

[98] Celik, A., Tsai, M.-C., Radaydeh, R. M., Al-Qahtani, F. S., & Alouini, M.-S. (2018). Distributed cluster formation and power-bandwidth allocation for imperfect NOMA in DL-HetNets. *IEEE Trans. Commun., 67*(2), 1677–1692.

[99] DinTrabelsi, A., Marouane, H., Bouhamed, E., & Zarai, F. (2019). NOMA based on dynamic scheduling algorithm with priority assignment for V2X communications, In *Ieee/acs international conference on computer systems and applications (aiccsa).*

[100] Liu, Y., Qin, Z., Elkashlan, M., Gao, Y., & Hanzo, L. (2017). Enhancing the physical layer security of non-orthogonal multiple access in large-scale networks. *IEEE Trans. Wireless Commun., 16*(3), 1656–1672.

[101] Liu, Y., Ding, Z., Elkashlan, M., & Yuan, J. (2016). Nonorthogonal multiple access in large-scale underlay cognitive radio networks. *IEEE Trans. Veh. Technol., 65*(12), 10152–10157.

[102] Doan, K. N., Vaezi, M., Shin, W., Poor, H. V., Shin, H., & Quek, T. Q. (2019). Power allocation in cache-aided NOMA systems: Optimization and deep reinforcement learning approaches. *IEEE Trans. Commun., 68*(1), 630–644.

[103] Akhtar, M. W., Ghaffar, R., & Rashid, I. (2016). A Q learning and fuzzy Q learning approach for optimization of interference constellations in femto–macro cellular architecture in downlink. *Wireless Personal Communications, 88*(4), 797–817.

[104] Kearns, M. J., & Singh, S. P. (1999). Finite-sample convergence rates for Q-learning and indirect algorithms, In *Advances in neural information processing systems*.

[105] Walpole, R. E., Myers, R. H., Myers, S. L., & Ye, K. (1993). *Probability and statistics for engineers and scientists* (Vol. 5). Macmillan New York.

[106] Gradshteyn, I. S., & Ryzhik, I. M. (2014). *Table of integrals, series, and products*. Academic press.

[107] Laneman, J. N., Tse, D. N., & Wornell, G. W. (2004). Cooperative diversity in wireless networks: Efficient protocols and outage behavior. *IEEE Transactions on Information theory, 50*(12), 3062–3080.

[108] Coelho, C. A., & Mexia, J. T. (2007). On the distribution of the product and ratio of independent generalized gamma-ratio random variables. *Sankhyā: The Indian Journal of Statistics (2003-2007), 69*(2), 221–255. http://www.jstor.org/stable/25664553

[109] Wiener, N. (1988). *The fourier integral and certain of its applications*. CUP Archive.

[110] Chakravarti, I. M., Laha, R. G., & Roy, J. (1967). Handbook of methods of applied statistics. *Wiley Series in Probability and Mathematical Statistics (USA) eng.*

[111] Glen, A. G., Leemis, L. M., & Barr, D. R. (2001). Order statistics in goodness-of-fit testing. *IEEE Transactions on Reliability, 50*(2), 209–213. https://doi.org/10.1109/24.963129

[112] Bettstetter, C., Hartenstein, H., & Pérez-Costa, X. (2004). Stochastic properties of the random waypoint mobility model. *Wireless Networks, 10*(5), 555–567. https://doi.org/10.1023/B:WINE.0000036458.88990.e5